THEORETICAL AND EXPERIMENTAL INVESTIGATION OF THE PUNCHING PROCESS OF DP-AI PLATE COMPOSITES BY USING DIFFERENT PUNCH TIPS

2023
PhD. THESIS
MECHANICAL ENGINEERING

Khalil Abubaker BELRAS ALI

Thesis Advisors
Prof. Dr. Bilge DEMİR
Assoc. Prof. Dr. Hakan GÜRÜN

THEORETICAL AND EXPERIMENTAL INVESTIGATION OF THE PUNCHING PROCESS OF DP-AL PLATE COMPOSITES BY USING DIFFERENT PUNCH TIPS

Khalil Abubaker BELRAS ALI

Thesis Advisors
Prof. Dr. Bilge DEMİR
Assoc. Prof. Dr. Hakan GÜRÜN

T.C.
Karabük University
Institute of Graduate Programs
Department of Mechanical Engineering
Prepared as
PhD Thesis

KARABUK
May 2023

I certify that, in my opinion, the thesis submitted by Khalil Abubaker BELRAS ALI titled "THEORETICAL AND EXPERIMENTAL INVESTIGATION OF THE PUNCHING PROCESS OF DP-AL PLATE COMPOSITES BY USING DIFFERENT PUNCH TIPS" is fully adequate in scope and in quality as a thesis for the degree of Ph.D of Science.

Prof. Dr. Bilge DEMİR ....
Thesis Advisor, Department of Mechanical Engineering Department of Mechanics

Assoc. Prof. Dr. Hakan GÜRÜN ....
Thesis Advisor, Department of Department of Manufacturing Engineering

This thesis is accepted by the examining committee with a unanimous vote in the Department of Mechanical Engineering as a PhD of Science thesis. 09/06/2023

Examining Committee Members (Institutions)   Signature

Chairman : Prof. Dr. Mustafa ACARER (SU) ....

Member   : Prof. Dr. Bilge DEMİR (KBU) ....

Member   : Prof. Dr. Hakan DİLİPAK (GU) ....

Member   : Assoc. Prof. Dr. Gökhan SUR (KBU) ....

Member   : Assoc. Prof. Dr. Hakan GÜRÜN (GU) ....

Member   : Prof. Dr. Ahmet DURGUTLU (GU) ....

Member   : Assoc. Prof. Dr. Ömer ASAL (GU) ....

The degree of PhD by the thesis submitted is approved by the Administrative Board of the Institute of Graduate Programs, Karabük University.

Prof. Dr. Müslüm KUZU ....
Director of the Institute of Graduate Programs

"I declare that all the information within this thesis has been gathered and presented in accordance with academic regulations and ethical principles and I have according to the requirements of these regulations and principles cited all those which do not originate in this work as well."

Khalil Abubaker BELRAS ALI

iii

ABSTRACT

Ph.D. Thesis

THEORETICAL AND EXPERIMENTAL INVESTIGATION OF THE PUNCHING PROCESS OF DP-AL PLATE COMPOSITES BY USING DIFFERENT PUNCH TIPS

Khalil Abubaker BELRAS ALI

Karabük University
Institute of Graduate Programs
Department of Mechanical Engineering

Thesis Advisors:
Prof. Dr. Bilge DEMİR
Assoc. Prof. Dr. Hakan GÜRÜN
May 2023, 163 pages

Although there has been a great development in laser, water jet and similar sheet metal cutting processes, cutting/drilling processes continue to gain more importance as drilling and cutting are the most used applications in the industrial field. On the other hand, a major challenge when using punching/punching sheet metal is overcoming the shear force required for high-strength and bonded sheets. Increased cutting forces lead to higher performance requirements expected from the press machine and cause increased wear on the punch tool and die. The quality and condition of the cut area are also very important as a separate phenomenon. One of the techniques used to reduce the punch cutting force needed is to change the punch type, which is done by changing the punch shape, especially the cutting angle. This study aimed to produce laminated composites of three different Dual Phase steels and Al sheets with enhanced strength

by explosive welding and then to examine the punch-cutting process of these three quality laminated composite sheets and the shear effects on the material. Sheet steels were commercial grades DP600, DP1000 and DP1200. The Al plate was commercial Al 1100 grade Al alloys. Base metals were used to produce laminated Al-DP steel composite by explosive welding. Cutting tests were conducted in punching operations using five punch slip angles, 0°, 16°, R1, R2 and V16°.

The force graphs corresponding to the procedure times were obtained thanks to the load-cell computer system in Punching operations. Experimental studies meaning shear analyses have also been evaluated via finite element method simulations. Besides, the punching results showed good agreement between modelling and experimental punching forces. The highest cutting forces were observed when the punch was "0" (flat-punch, 0°). The other punch forms obtained the lowest cutting forces using punch R2, V16, R1, and 16, respectively. Moreover, the punched surfaces have been observed by comparing the force-time graphs. In addition, this study is a pioneer in the literature on its concepts, such as explosive weld materials and their punch process.

Keywords : Explosive Welding, Punching, Dual-phase steels, Cutting surface characterisation, Finite element analysis, Microstructure, Tensile Properties

Science code : 91417

ÖZET

Yüksek Lisans Tezi

DP-AL PLAKA KOMPOZITLERIN ZIMBA ILE DELME IŞLEMLERININ, FARKLI TIPTE ZIMBA KULLANILARAK TEORIK VE DENEY ILE İNCELENMESİ

Khalil Abubaker BELRAS ALI

Karabük Üniversitesi
Lisansüstü Eğitim Enstitüsü
Makina Mühendisliği Anabilim Dalı

Tez Danışmanları:
Prof. Dr. Bilge DEMİR
Doç. Dr. Hakan GÜRÜN
Mayıs 2023, 163 sayfa

Lazer, su jeti ve benzeri sac metal kesme işlemlerinde büyük gelişme olmasına rağmen, delme ve kesme endüstriyel alanda en çok kullanılan uygulamalar olduğu için kesme/delme işlemleri halen daha fazla önem kazanmaya devam ediyor. Diğer taraftan metal sacı makinede zımba ile kesme/delme kullanırken karşılaşılan önemli bir zorluk, yüksek mukavemetli ve birleştirilmiş saclar için gereken kesme kuvvetinin üstesinden gelmektir. Artan kesme kuvvetleri, pres makinesinden beklenen daha yüksek performans gerekliliğine yol açar ve zımba takımında ve kalıpta aşınmanın artmasına neden olur. Kesilen bölge de oluşan kalitede ve durum da ayrı bir olgu olarak oldukça önemlidir. İhtiyaç duyulan zımba kesme kuvvetini azaltmak için kullanılan tekniklerden biri zımba tipinin değiştirilmesi ve bunun zımba şeklini özellikle de kesme açısını değiştirerek yapılmasıdır. Bu çalışma, gelişmiş mukavemetli üç farklı

Çift Fazlı çelik ve Al sacların patlama kaynağı ile lamine kompozitlerinin üretilmesini ve ardında, bu üç kalite lamine kompozit levhanın punç ile kesme sürecini ve oluşan kesme etkilerini malzeme üzerinden incelemeyi hedef edinmiştir. Sac çelikler, DP600, DP1000 ve DP1200 ticari kaliteleriydi. Al levha, ticari Al 1100 dereceli Al alaşımlarıydı. Patlayıcı kaynak yoluyla lamine Al-DP çelik kompoziti üretmek için baz metaller kullanıldı. 0°, 16°, R1, R2 ve V16° olmak üzere beş zımba kayma açısı kullanılarak zımbalama operasyonlarında kesme deneyleri gerçekleştirilmiştir.Punch ile kesme deneylerinde bilgisayar sistemine bağlanan load cell ile işlem sürelerine karşılık gelen zımba kuvveti-işlem süresi veri ve grafikleri elde edilmiştir. Kesme-kayma analizleri anlamına gelen deneysel çalışma sonuçları sonlu elemanlar yöntem simülasyonları ile değerlendirilmiştir.

Punch ile kesme-delme Deneysel ve simulasyon sonuçları punch kesme kuvvetleri arasında oldukça iyi bir iyi bir uyum göstermiştir. En yüksek kesme kuvveti düz zımba "0" (0°) kullanılan işlemlerde gözlendi. Diğer taraftan, sırasıyla olmak üzere R2, V16, R1 ve 16 punch tipleri kullanılarak yapılan punc ile delme işlemlerinde elde edilmiştir. Bu çalışmada elde edilen punch ile delme deneyleri kesme yüzeyleri ve ortaya çıkan kesme sonuçları kuvvet-zaman grafikleri ile karşılaştırılarak da bazı değerlendirmeler yapılmıştır. Genel bir değerlendirme olarak, bu çalışma, patlamalı kaynak ile clading-kompozit metaller ve bunların zımbalama prosesi gibi kavramları konusunda kullanılan metallerde ayrıca değerlendirildiği, literatürde bir öncü niteliğindedir.

Anahtar kelimeler **:** Patlatma kaynağı, Punc ile delme, Çift-afzlı çelik, kesilmiş yüzey analizi, Finite element analizi, Mikroyapı, Çekme Özellikleri

Bilim kodu   **:** 91417

ACKNOWLEDGMENT

CONTENTS

LIST OF FIGURES

SYMBOLS AND ABBREVIATIONS INDEX

ABBREVIATIONS

AHSS   : Advanced High Strength steels

TWIP   : Twinning Induced Plasticity

CP   : Complex Phase

DP   : Dual Phase

TRIP   : Transformation Induced Plasticity

BiW   : Body-In-White

HSLA   : High Strength Low Alloyed

HSS   : High Strength Steel

TRIP   : Transformation Induced Plasticity

TWIP   : Twinning-Induced Plasticity

CP   : Complex Phase

MS   : Martensitic Steel

FB   : Ferritic Bainitic

HF   : Hot Forming

LA   : Low Alloy

FCC   : Face center cubic

PART 1

INTRODUCTION

1.1. BACKGROUND INFORMATION

The punching of Al 1100 sheets, various grades of (DP) steel plates, and the explosively welded limited composite of Al-DP steel sheets are all the subjects of this study's extensive research. Essentially, sheet metal punching operations are an efficient, modern, and useful production technique. Recent years have seen a substantial advancement in our understanding of the technological aspects of punching, particularly concerning punching instruments[1, 2]. However, AHSS sheets have substantially aided in producing structural components with reduced thickness, resulting in weight reduction. As a result, they contributed to the development of lighter automobiles at the expense of reduced fuel use and greenhouse gas emissions [1]. Due to their resilience to weathering, and corrosion, being more lightweight, etc., sheet materials such as AHSS may also need to be clad using substitute sheet metals. However, working with sheet steel coated with different metals is difficult. However, explosive welding is direct welding of a wide range of equivalent and dissimilar metal combinations, which is impossible with conventional techniques [3]. Given the preceding, this study seeks to benefit from every phenomenon.

This study focuses on aluminium-steel composite plates bonded by explosive welding, which show promise for usage in chemical industries, certain reactors, or automobiles [4]. Like solid-state welding, explosive welding can unite disparate metal components directly where other methods cannot. One of them, the topic of this work, Utilizing explosive welding to join aluminium-steel composite plates, could be an excellent choice for the automotive industry, nuclear power plants, and the chemical industry [5, 6].

1

Iron and steel corrosion develop colour changes and flaking, whereas aluminium does not[7]. In corrosive settings like the sea and weather, aluminium resists corrosion. In its normal state, aluminium (Al), the third most common metal in the earth's crust, reacts with oxygen and other substances. Compared to other engineering metals, it is relatively simple to process at room temperature, is highly ductile and has Face center cubic (FCC) [8]. Today's advanced aluminium alloys are widely used in many structural components, especially in aviation, railway vehicles, automotive, structural materials and many other fields and industries, with their high specific strength, cost-effectiveness and relatively good wear resistance [9]. The ductile-brittle transition phenomena in BCC metals are typically not seen in aluminium alloys. When the yield strength rises, this poses a challenge for increasing the ductile fracture resistance [10]. Aluminium alloys are the second-most popular metals used as engineering metals after steel. As is common knowledge, the specific density of aluminium alloys is roughly one-third that of steel materials.

DP steel, alternatively, is the most well-liked and frequently utilized variety of advanced high-strength steel (AHSS) [11-13]. Commercially, DP steels range in strength from 400 MPa to 1400 MPa [14]. Dual-phase steel is a class of materials with special economic and technological qualities, including continuous yielding behaviour [15], reduced yield strength, high standard and overall elongation, quick work hardening, and lower yield ratio [16], *etc*

When two materials must be linked, the problem becomes more difficult [17]. However, in industrial applications, in particular, good mechanical characteristics, corrosion resistance, and resistance to wear, etc., Welded composite materials made of two different metals are crucial. Current advancements in material technologies are driven by new materials with greater properties. Therefore, novel plate composite materials are being developed by researchers for a variety of other purposes. Steel materials can be blended with other metals using composite techniques. Since ferritic-perlitic-martensitic steels have minimum corrosion resistance, They must be clad using welding and materials that resist corrosion, such as titanium, stainless steel, and aluminium, which is possible [18]. The joint of explosive welding is a large range of

combinations of similar and different metals that cannot be connected using normal methods, just like another solid-state welding [19].

Furthermore, due to its capacity to disperse the high energy density produced by the explosion, the process can connect over a large surface area and sheet such as Related metals (plain carbon steel, steel to steel) [20], stainless steel to steel, Al-Al [21], different metals (aluminium with steel [21, 22], Also aluminium alloys and nickel, titanium and steel [23], Al-Mg and copper, aluminium, steel, and titanium, magnesium, copper, aluminium, copper, iron and copper[24]. Vehicles, some reactors, and the chemical industry may benefit from explosion-bound composite materials such as aluminium steel [25, 26].

1.2. THE OBJECTIVE OF THE STUDY

One of the best combinations of technology and economic benefits can be found in DP-Al metal plate composite [27]. However, the sheet metal sector relies heavily on the manufacturing processes of blanking and piercing, which have both practical and technological advantages [28, 29]. It is not easy to provide the required shearing power for thick, high-strength stock when utilizing the blanking/piercing of plate composites and sheet metals. Due to larger shearing forces, the press machine must operate at a higher level, which causes the punch and die to wear out faster. [30]. Utilizing the punch shear angle is one method for lowering the necessary force. Punches with formed ends are another tactic [31].

More reliable data about force and friction processes in the industry is urgently needed. These phenomena cause a multitude of annoyances, including excessive and unexpected machining pressures, tool life, poor precision, and workpiece surface quality, and are frequently poorly understood [32-34]. One of the most frequently used sheet metal processes is punching particularly punch-piercing shaping. These circumstances also apply to dual-phase, all AHSS, and composite plate piercings [28, 35]. The literature contains many practical and theoretical investigations on sheet metal cutting. For cutting various sheet materials, this research [36, 37]. There are numerous studies on DP steel, including one that examined the common edges for the

DP600, DP780, and DP980 [38]. It stated that being able to predict and minimize punch wear in terms of efficiency, cost and product quality are the major issues when the sheet metal of AHSS is cutting. Metal punching methods are straightforward, highly effective, and inexpensive, making them popular in mass manufacturing. The punching process involves several elements that affect the final product's quality, such as the sheet material's characteristics, the punching conditions, the punching and die materials' qualities, and tool wear.[39, 40].

In spirit, sheet metal punching operations are a widely utilized economic, technological, and useful manufacturing cutting process in various applications, including electronics, communication, automotive, and other manufacturing applications. Today much more is known about the technological components of the punching process [41, 42].

The piercing procedure that was the subject of this investigation is carried out by punching a blank from a sheet in extra production steps. In sheet metal blanking, the punching process results in holes of various sizes and shapes [43, 44]. Both situations involve a punch tool on a shear piece not attached to a sheet. Figure 1 depicts an illustration of a punching operation. That is widely used to industrialize sheet metal components from different materials. Usually, the chopped components go through additional elastomeric and plastic processing [45].

The mechanical characteristics of the material, its thickness, and punching-piercing parameters-elements, such as tool geometry, The quality of the cutting edge and punch process is mostly determined by factors such as die clearance, cutting edge radius, tool materials and wear, shear cutting technique (single-stage, two-stage), etc. [46, 47]. Punch-shear edges each have a distinctive cutting surface. Part quality, process efficiency, and fertility are all greatly impacted by metal punching (piercing & blanking) [38, 48]. Burr height, cutting/punching force, gap effects, punch tips angle, punching and die tool geometries, punching and die material properties, and tool wear impact process effectiveness and component quality [48, 49].
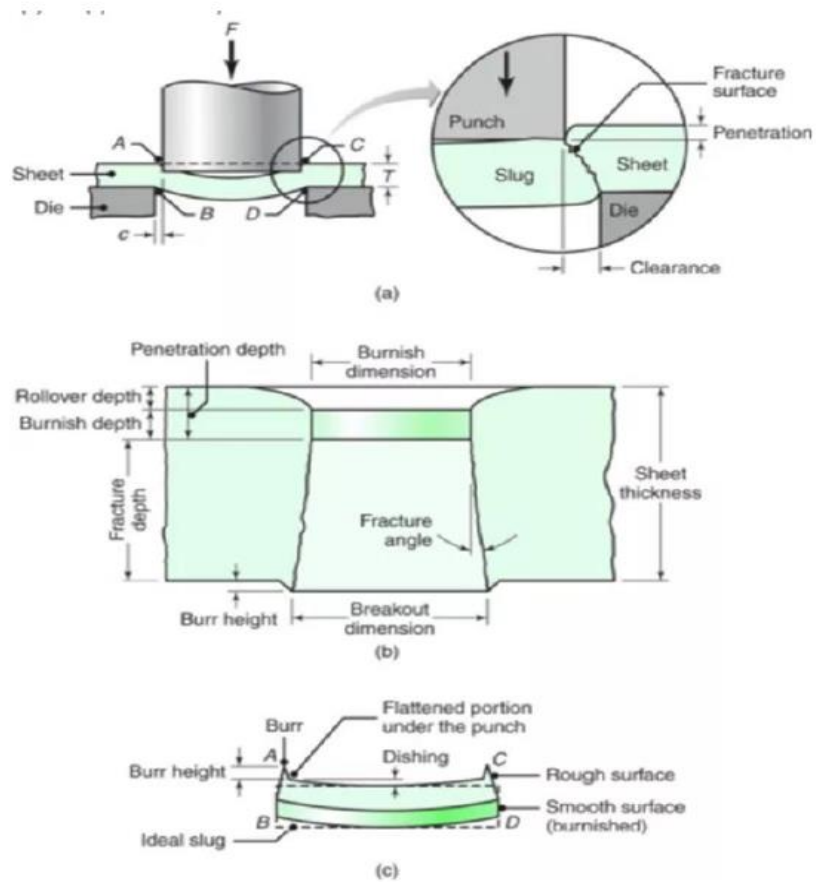
Figure 1.1. Distinguishing properties of (a) a punched hole and pierced part, (b) a blanked part, and (c) a schematic depiction of shearing utilizing a punch and die to demonstrate numerous process factors. [45].

It is known that during punching procedures, material fractures occur inside the between the tool and die, which denotes the metal sheet is divided into the four zones of fracture, bur area, burnishes, and rollover in the thickness direction [50]. The clearance between the die and the punch and the cutting angle of the punch are important factors in the cutting forces and the edge quality of the pieces [51]. Increased punch angles significantly lower the amount of power needed for shearing. Furthermore, the shearing force would rise if the clearance values were low. Increased clearance values, however, degrade the product's edge quality [30]. The location where the parts are used determines the punch tip form used throughout production. In cutting activities, flat-ended punches are typically preferred. Concave, convex, angled, and other punch forms can be employed for piercing operations [52]. Initial to other cutting procedures, the blanking process results in some ductility loss and gains in hardening, brittleness, and strength. Use the Finite Element Method (FEM) to specify the process

parameters throughout the length of the sheared surface, forces, and part characteristics, such as beginning compression, punch, and die shapes.

Particularly in the automotive business, the modern industrial practice strives to minimize material use while concurrently improving product qualities. The most important attributes are strength, crashworthiness, dynamic properties, and bending resistance. The proper part design and forming process make these characteristics possible. However, the improvement in sheet metal strength and the formability of manufactured parts has accelerated dramatically during the past ten years due to the discovery of innovative materials [53, 54]. Furthermore, most punched components are cut or punctured to eliminate extra material or combine other components. The part's great strength causes high contact pressure and stress on the cutting tool and materials [55, 56]. As a result, research and improvement represent a substantial and diverse effort. The literature contains no known works on explosive-welded DP sheet steels and DP-Al 1100 sheet composite. These foundational components and the piercing punching of this composite sheet allow for punching and estimating the characteristics of punched edges. Also new and distinct to the pertinent literature is an understanding of the punching operations involved in these composite sheet materials' fabrication process.

The stability of the interface and the production of the shear forces necessary for high-strength and thick stock might be considered the main challenges in punching sheet metal and metal-to-metal high-strength composites. The conventional approach's higher cutting pressures result in higher performance expectations for the machine of the press, and the punch and die experience increased wear. Punch tip varieties may be crucial for cutting force optimization and reduction. An automated model was also created to represent explosive welded sheets' punch pounding. This model was used to simulate 3D models while numerically analyzing the drilling process. When their consistency is guaranteed, numerical models are valid for experimental studies and offer several benefits. Its objectives are to ascertain the material characterizations, distributions of strain and stress when cutting these materials. This research aimed to identify the optimal punch to produce the best result with the least shear force.

According to a literature survey, no studies on piercing-cutting explosively welded materials have been conducted.

PART 2

ADVANCED HIGH-STRENGTH STEEL (AHSS)

Due to rising fuel efficiency standards, passenger safety, and vehicle performance, intense competition existed between low-density and steel metal sectors. Advanced strength steels are important structural elements used in many industries, particularly the automobile industry [57, 58]. Global players propose more complex targets for future years while enacting harsher car emissions standards by 2020 [59]. In response to growing concerns over anthropogenic greenhouse gases. In order to meet demands, automotive industrialists frequently hunt for novel materials and engineering capabilities. For instance, materials for structural purposes must be strong and rigid, which is frequently accomplished with higher thicknesses. However, Fuel economy and emissions are improved when the component's thickness is reduced [60]. Complex geometries in new vehicle designs are visually appealing but challenging to form and assemble. Thickness reduction to fulfil mass reduction goals further compromises these designs. The worldwide steel industry constantly creates new steel grades with ever-increasing strength and formability. In order to satisfy these conflicting expectations, it constantly reinvents this heterogeneous material. The specific microstructures and metallurgical properties of these advanced high-strength steels (AHSS) enable OEMs to meet the different functional requirements of today's automobiles. Advanced high strength steels (AHSS) have been created as a result of the steel industry's swift response to the new problems [61].

Today's AHSS steels are categorized. Examples of "First Generation" steels include DP, TRIP, complex phase (CP), and martensitic (MART) steels. "Second Generation" are austenitic steels with important manganese and occasionally aluminium content. A few secondary steels have a close relationship with austenitic stainless steels. The potential to produce new steels that outperform the First Generation of AHSS, or the so-called "3rd Generation" of AHSS, " generates growing interest. Better strength and

ductility combinations than those reached in first-generation AHSS are projected to be developed without the pricey processing expenses and stabilizing components required for austenitic second-generation AHSS steels [62, 63]. Combinations of microstructure and alloy. Microstructural characteristics must be controlled simultaneously and independently to produce materials with the right final properties. These include the constituents' amount, mechanical characteristics, and volume proportion (such as the number of phases). The potential for material development and desired microstructure and property combinations are contrasted in Figure 2.1.

Figure 2.1 illustrates the anticipated effects of systematic microstructural fluctuations caused by increasing the martensite volume fraction (up to 70%) in two imaginary two-component composite materials from ferrite (plus martensite or stable austenite) [62, 63]. Figure 2.1 shows that the properties of a variety of steel sheet families, including First Generation AHSS steels, can be reasonably predicted by a two-component system based on ferritic steels and that steels in the Third Generation band can be created using a variety of martensite and stable austenite mixtures. Austenitic mixtures that turn into martensite at low loads have properties similar to those shown in Figure 2.1 for the ferrite/martensite combination. In contrast, austenitic composites more resistant to deformation have properties in the Third Generation AHSS band [63].
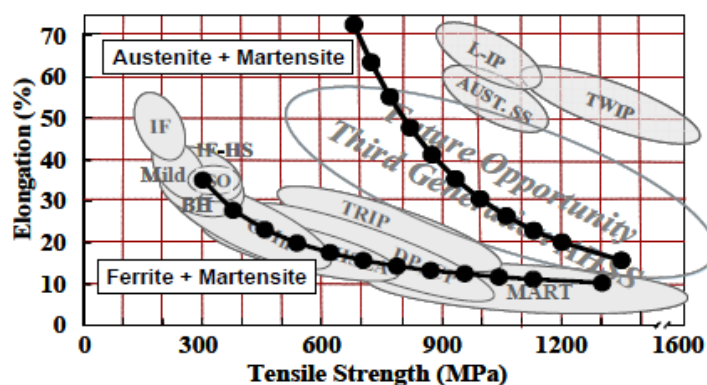
Figure 2.1. Shows predictions for two hypothetical steel groups' strength and ductility with different martensite component volumes and property areas for various conventional and AHSS steel classes. Ferrite and martensite, or stable austenite and martensite, comprise composites [62, 63].

Commercial Advanced steel grades are shown in Table.2.1.

Table 2.1. Commercial grades of AHSS.

No	Steel Grade	Min Yield Strength Mpa	Min Tensile Strength Mpa
1	mild 140/270	140	270
2	BH170/340	170	340
3	Bh210/340	210	340
4	DP210/440	210	440
5	BH260/370	260	370
6	IF260/410	260	410
7	BH280/400	280	400
8	IF300/420	300	420
9	DP300/500	300	500
10	FB330/450	330	450
11	H8LA350/450	350	450
12	DP350/600	350	600
13	TRIP350/600	350	600
14	TRIP400/700	400	700
15	H8LA420/500	420	500
16	FB450/600	450	600
17	TRIP450/800	450	800
18	H8LA490/600	490	600
19	CP 500/800	500	800
20	DP 500/800	500	800
21	TWIP 500/900	500	900
22	TWIP500/980	500	980
23	H8LA 550/650	550	650
24	CP 600/900	600	900
25	TWIP 600/900	600	900
26	DP 600/980	600	980
27	TRIP 600/980	600	980
28	Q8P 650/980	650	980
29	CP 680/780	680	780
30	TPN 680/780	680	780
31	HSLA 700/780	700	780
32	DP700/1000	700	1000
33	CP 750/900	750	900
34	TPN750/900	750	900
35	DP750/980	750	900
36	TRIP750/980	750	980
37	TWIP750/1000	750	1000
38	CP 800/1000	800	1000
39	DP 800/1180	800	1180
40	CP850/1180	850	1180
41	MS950/1200	950	1200
42	TWIP950/1200	950	1200
43	CP1000/1200	1000	1200
44	MS1050/1470	1050	1470
45	CP1050/1470	1050	1470
46	HF1050/1500	1050	1500
47	DP1150/1270	1150	1270
48	MS1150/1400	1150	1400
49	HF1200/1900	1200	1900
50	MS1250/1500	1250	1500

As can be observed in Table 2.1, AHSS are crashworthy due to their enhanced formability and high strength-ductility. Tensile strength > 600 MPa and yield strength > 300 MPa are roughly defined strength qualities used to distinguish between AHSS. Formability/ductility and high strength combined with modern AHSS, in contrast to the conventional high strength steel, where ductility diminished with strength. For dynamic loading that occurs during auto accidents [61].

High-strength steel with a high capacity for energy absorption, such as DP and TRIP steels with UTS 1000 MPa, is advised, are suggested. As a result of more stringent laws around the world requiring better auto safety and fuel economy restrictions, advanced high-strength steel (AHSS) is being used more frequently in vehicle body construction. 30% AHSS may be present in a conventional vehicle body structure. Five years ago, the World Auto Steel organization predicted extensive usage of AHSS and high-strength steel- which accounts for 97 % of the structure mass of the vehicle body. Modern high-strength steel was a crucial component of the body bulk reduction and safety performance improvement of automobiles. The failure condition for some AHSS materials is edge cracking during forming, but it cannot be anticipated using traditional failure criteria (such as forming limit curves-FLCs). Another local formability concern is shear fracture during tight-radius stretch bending, where failure happens distant from [64].

2.1. ADVANCED HIGH-STRENGTH STEEL CLASSIFICATION (AHSS)

The main phase ferrite's strength and hardening reaction is the primary source of AHSS strength and ductility bands, even in DP and "traditional" TRIP steels. One can alter the characteristics of ferrite by using solid solutions, alloys, grain size management, cold working, and precipitation. There is strong evidence in the literature that when ferrite, There is little room for these steels to considerably improve their strain hardening behaviour at high strains since they have stable microstructures, which makes their strain hardening behaviour at high strains mainly independent of them [65].

Utilizing strain-dependent control, Steel TRIP The austenite-to-martensite transition offers more potential for modification. Ferritic steels' high-strain work-hardening behaviour. Figure 2.2 illustrates this benefit [65].
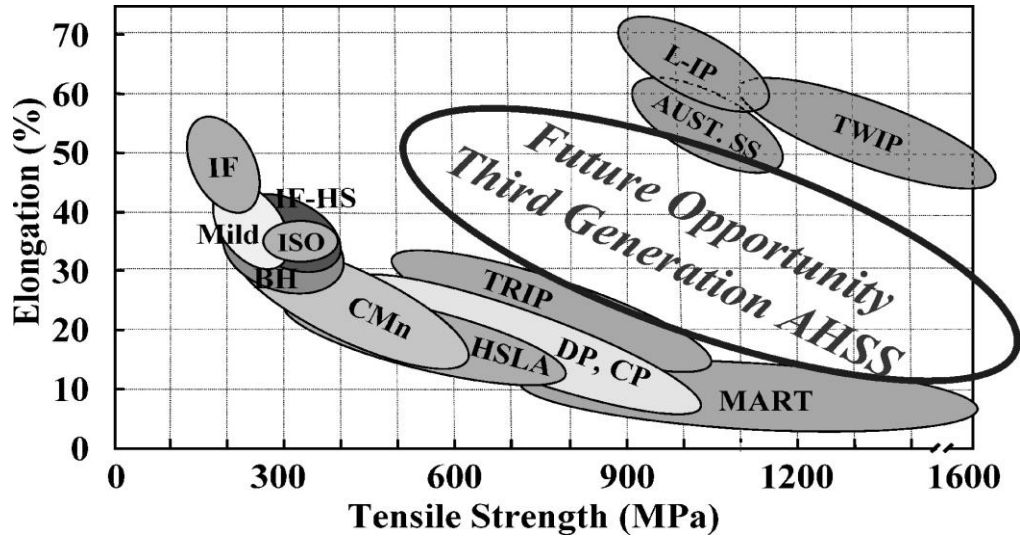
Figure 2.2. Data on tensile strength and elongation for several classes of traditional and modern high-strength sheet steels (AHSS) are summarized [65].

Compared to conventional high-strength steel, AHSS dramatically increased high tensile strength (HSS). High-strength steel's exceptional strength and ductility are two of its most important and prized qualities. Groups of advanced high-strength steel (AHSS) types can be created based on the material's processing and mechanical properties. High-strength low alloy (HSLA), dual-phase (DP), complex phase (CP), martensite steel (MS), transformation-induced plasticity (TRIP), ferrite bainite (FB), and martensite (MART) twinning-induced plasticity (TWIP) are the varieties that are currently most frequently utilized [66]. Enhanced formability and high strength are two features of the equipped 590R used in large automotive applications. This novel steel was created using a good weld alloy that contains little carbon [67]. The performance of TRIP steel ranks first in the first generation of the AHSS property band due to improved strain hardening at high strain. Few other processing methods can change the ferrite dislocation structure (and hence the strain-hardening behaviour).

Few other processing techniques can change the ferrite dislocation structure, which causes strain-hardening behaviour. According to certain research, ferrite deformation

12

in the dynamic strain ageing (DSA) range causes It might be advantageous to have a larger dislocation density than what would be generated by equivalent cold working at room temperature [68]. However, Li and Leslie [69] demonstrated that in their investigation of 0.22 wt. pct., this was not the case. At DSA temperatures (such as 200 to 400°C), a pre-strain of 3% or 5% in carbon steel results in a significant decrease in ductility at room temperature, which, together with an increase in room temperature, lowers yield stress.

A complex microstructure with strength-enhancing elements like martensite and enhanced strain hardening must be incorporated into materials with much greater strength/ductility combinations than first-generation AHSS. (e.g. austenite). The mechanical properties of each element are closely regulated in AHSS steel, a new development procedure that uses a significant percentage of metastable austenite. The use of controlled strain hardening is another option. Heavy-duty temper rolling (or other methods) might be used to boost yield strength. Austenite stability is another significant issue, as illustrated below. As austenite declines, so does its resistance to transformation. The addition of stabilizing elements for austenite like C, Ni, Mn, etc., the increase in test temperature, the larger particle size [70], and these three factors. However, maximizing uniform strain by regulating the austenite transition may also decrease uniform strain [4, 65, 71]. Additionally important are austenite's strain-hardening characteristics and martensite's strength [71]. When Austenite is stabilized, and TRIP is inhibited, austenitic characteristics are very crucial.

2.2. DUAL-PHASE STEELS (DP)

DP steels are promising for the automobile industry because of their high strength and excellent formability. According to several reports, DP steel is utilized in upcoming automobiles. These characteristics of DP steel are brought about by its distinctive microstructure [72, 73]. The DP microstructure comprises hard martensite islands scattered throughout a soft ferrite matrix [74]. Martensite and ferrite phases have volume fractions of about 0.2 and 0.8, respectively. Davies claims that the desirable characteristics of dual-phase steel resulted from hard martensite dispersion at the strength, very ductile ferrite matrix [75, 76]. In addition to the ferrite and martensite

properties, dual-phase steels can deform based on the shape and volume percentage of the martensite particles [77]. Ferrite's composition and particle size, in general, dictate its strength. In dual-phase steel, the initial dislocation density, which is produced Via the stress and strain like the martensite during the cooling produced from the austenite, gives extra ferrite strength [78, 79]. The carbon at martensite concentration has a significant impact on its strength. As the carbon concentration of martensite rises, so does its yield strength. Leslie has demonstrated that martensite's yield strength rises linearly with its carbon concentration. It stated that they were linearly increasing the yield stress starting at 1000 MPa and going up to 1265 MPa by increasing the carbon concentration of martensite by 0.2 to 0.3 wt% [75, 80, 81]. Although Mn, Si, and other substitutional alloying metals enhance martensite, their impact pales in comparison to that of carbon. Many scientists are presently concentrating on developing models that forecast flow behavior the dual-phase steels of their microstructure, The research seek to link modeling the evolution of microstructure to regard the advance high strength steel. To get the optimal mechanical qualities, these investigations aid in the optimization of the processing settings [80]. By accurately modeling the microstructure of dual-phase steel, dislocation-based modelling may be utilized to quantify the flow characteristics of ferrite and martensite.

However, the constituent properties of dual-phase steels are not well understood enough to predict their behaviour. To describe dual-phase steel, it is also required to consider how stress and strain are distributed between the two phases during deformation [75]. Micromechanical modelling is used to anticipate dual-phase steels from the flow behaviour of the various elements. To do this, RVEs dual-phase steel has been developed by Abaqus [75, 82]. An FE solver is used to resolve this.

The band-like martensite structure of industrial DP steels evolved into a dual-phase structure during stress and strain, which is favourable for establishing a uniform distribution of martensite islands in the ferrite matrix. One of two causes for the banded dual-phase microstructure may exist. Due to the segregation of alloying elements during casting, the hot-rolled microstructure, which forms before the cold-rolling and annealing process to generate dual-phase steel, may have a banded microstructure.

After intercritical annealing, segregated portions rich in alloying elements create martensite after cooling; that martensite had banded structures.

Cold rolling bands the microstructure even if heat rolling equiaxed the steel. In this case, If the right heat treatment is not used to produce the dual-phase material, pearlite bands change into martensite bands.

DP steel's microstructure was examined using two different martensite morphologies. They altered the microstructure by varying the heating rate to the intercritical temperature [75]. They investigated the deformation behaviour of the martensite islands under tensile strain in numerous dual-phase steel samples by examining photographs of the deformed steel microstructures. This study outlines a modelling approach for estimating the initial flow curve for DP steels from their microstructure and contrasts DP microstructures with and without bands. The dislocation strengthening theory is applied to simulate the flow curves in a 2D RVE framework. The dislocation-strengthening parameters are derived from earlier research [75].
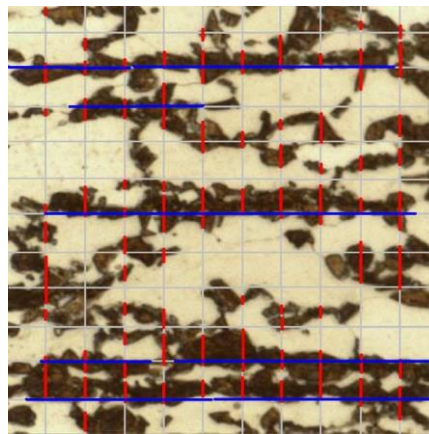
Figure 2.3. Measurement grids for the martensitic aspect ratio [75].
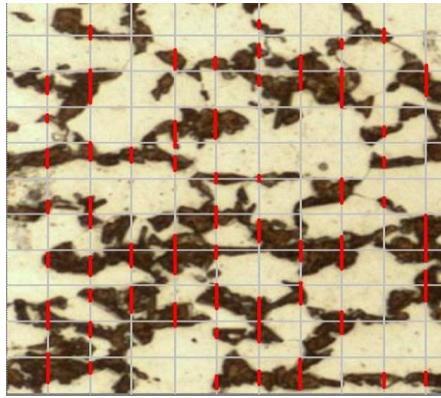
Figure 2.4. measuring grids for martensitic height [75].

Table 2.2. Effect of alloying elements on DP steels[61].

Alloying element	Effect and reason for adding
C (0.06–0.15%)	stabilizer for austenite Martensite is strengthened; phase distribution is determined.
Mn (1.5–2.5%)	Austenite stabilizer Solid solution strengtheners of ferrite Retards ferrite formation
Si	Promotes ferritic transformation
Cr, Mo (up to 0.4%)	Austenite stabilizers Retards pearlite and bainite formation
V (up to 0.06%)	Austenite stabilizer Precipitation strengtheners Refines microstructure
Nb (up to 0.04%)	Austenite stabiliser Reduces M_s temperature Refines microstructure and promotes ferrite transformation from non-recrystallized austenite

Advanced high-strength steels (AHSS), especially dual-phase (DP) steels, have been widely employed for automobile body-in-white and chassis applications because of their high strength and excellent formability. The microstructure of multiphase DP steels, which contains a high-strength martensitic phase from a hard ferritic matrix, is what gives them their strength and ductility. These steels, for instance, have good in-plane formability, demonstrated via a forming limit diagram technique. However, during commercial stretch-flanging operations, They frequently exhibit failure strains at the sheared edge lower than the forming limit strain and are prone to early failure. Because strong stretch-flange capabilities are necessary to create complicated press-formed elements like chassis, suspension arms, and control arm components, DP steels are less suited for edge stretching operations. There is hence a lot of interest in creating

materials that potentially enhance AHSS's functionality in stretch-flange operations in the industrial setting [83].

2.2.1. Classification of Dp Steels

Islands of high-hardness martensite are present in the ferritic matrix of DP steels in levels ranging from 85 to 90%. As martensite content rises, the steel's mechanical strength usually follows suit. the same as FB steels; These steels are made using a multistage cooling process that regulates the cooling rate from the austenitic field (for hot-rolled steels) or the ferritic-austenitic field (for cold-rolled steels and other types of steel) to achieve the transformation of some austenite into ferrite (at intermediate temperatures within the ferritic field) before rapid cooling causes the transformation of the remaining austenite into martensite. Martensite originates at lower temperatures and has a high hardness due to the progressive carbon enrichment that occurs in the remaining austenite at higher temperatures during the ferritic transition. Depending on the size of the austenitic grain, interim homogenization phases lasting around 15 seconds are used to facilitate homogenous diffusion of the carbon into the material. The center of an austenitic grain typically contains less carbon than the perimeter due to the solubility limit, whereas the periphery typically has greater localized carbon levels. According to Figure 2.4 [84]. The presence of self-tempered martensite or even bainite grains within larger grains is common.
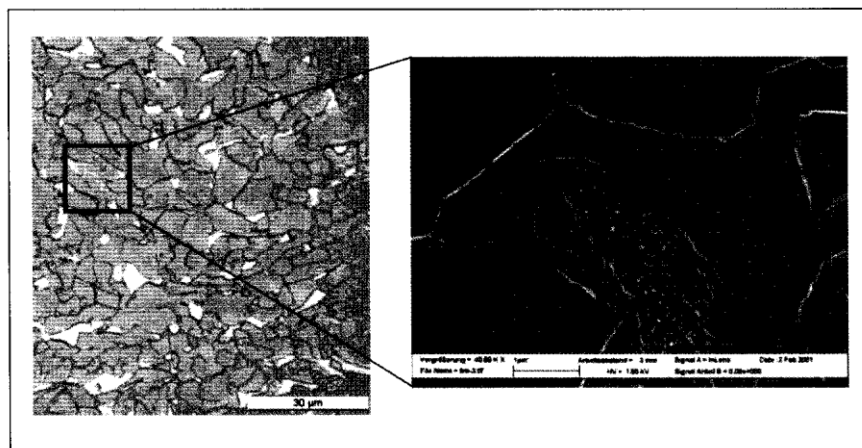
Figure 2.5.   Self-tempering martensite with a formed grain center (DP600 steel, courtesy of Voestalpine Stahl GmbH) [84].

Depending on the manufacturing process and chemical composition, these may also contain sizable amounts of bainite. Figure 2.5 provides a schematic representation of the microstructure of these steels. Low-hardness ferrite is typically continuous and contributes to the steel's optimal ductility. When the material is deformed, it concentrates in the ferritic phase, close to the martensitic grains, using the typical work-hardening phenomenon of such materials. Such steels have better attributes than traditional HSLA steels due to this characteristic and the high rupture strength (DP600 grade steel has a minimum elongation of 22%), as well as a transverse Rp0.2 consisting of between 300 and 470 MPa and an Rm between 580 and 670 MPa. If carbon permits martensitic transformation during cooling, adding manganese, chromium, molybdenum, vanadium, and nickel—singly or in combination—promotes the matrix hardening process. All alloy components are also carefully balanced to maintain suitable weldability by the resistance process, and in any case, the strongest grades (DP 700 and 1000) require ad hoc welding procedures. In Figure 2.6, a photomicrograph of such steels is displayed. The DP steels also have a significant bake-hardening effect [84].
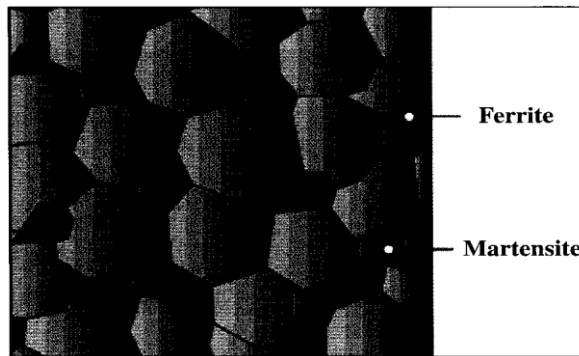
Figure 2.6. Schematic depiction of the microstructure of a DP Steel [84].
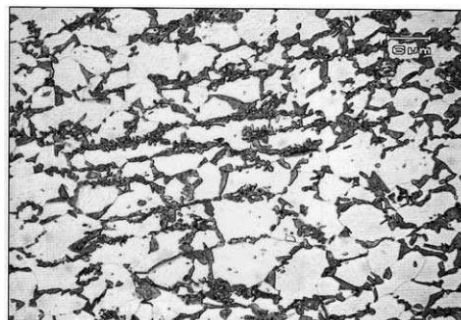
Figure 2.7. Microstructure of DP steel (metallographic fixer 4% Picral, C = 0.15%, Mn=l.5%, Si = 1.5%, tempered in water at 775°C) [84].

2.2.2. DP600

The DP600 is one of the most advanced dual-phase high-strength steels, with a tensile strength of 600 MPa. It is used in the automotive industry to lighten car bodies and improve fuel efficiency. Due to its composition of ferrite and martensite, DP600 has high strength, good elongation, and a high initial work-hardening rate[79]. It can improve the vehicle's crash performance and resist stronger collision forces without adding additional weight [85, 86].

2.2.3. DP1000

The minimum yield and minimum tensile strengths for DP 1000 steel sheets are 700 MPa and 1000 MPa, respectively [87].

2.2.4. DP1200

Usage of fuel. In this regard, enhanced high-strength steels (AHSS) and aluminium alloys are being investigated as potential replacements for the low-carbon and HSLA steels already in use; despite having a density one-third that of steel, aluminium alloys are rarely used in automobiles. Its application is constrained by its higher cost and the difficulty of manufacturing procedures like shaping and welding [88].

To provide energy conservation, safety enhancement, and crash-resistance properties for light vehicle design methods, AHSS; are essential materials [89, 90].

Steels with tensile strengths greater than 1 GPa are necessary for structural applications.

In the vehicle safety cage, reinforcing parts included pillars, side sills, rocker arms, door reinforcement beams, roof rails, and the floor. For these components, AHSS is one of the most promising steels [91, 92]. According to the material's microstructure, mechanical characteristics, and applied method, AHSS is classified into several classes. Dual-phase (DP), TRIP, and ferritic-bainitic (FB) steels are the three

classifications that are most frequently employed [93]. AHSS provides better yield strength, a lower yield/tensile strength ratio, good formability compared to conventional high-strength steels, a higher working hardness ratio, and a higher capacity to absorb strain energy [94]. In this context, AHSS is utilized in the automobile sector for its benefits, including weight reduction, improved safety, and cost savings [95]. By cooling after annealing austenite, AHSS is created by austenite transition at low temperatures. AHSS has various microstructures influenced by various alloying components and cooling techniques [94, 96]. The low-alloy steels utilized by automakers most frequently among AHSS are DP steels [97]. The carbon to manganese ratio in DP steels typically ranges from 0.05-0.2%, and the manganese to carbon ratio is greater than 1.5% [98]. Because of their great ductility and strength, Automobile components, including bumpers, wheels, and chassis, typically use DP steels. The ferrite and martensite structure was created using the cooling procedure following critical annealing possesses these qualities [79, 99]. Volumetric diffusion causes mobile dislocations in the ferritic matrix during the change from austenite to martensite. Due to their contact and phase boundaries, high strain hardening rate and continuous deformation behaviour are seen in this direction [100-102]. It has better overall elongation, good tensile strength, and a lower yield strength/tensile strength ratio than conventional or HSLA steels. These advantages make DP steels appealing for automotive applications [5].

2.3. THEORY OF DP STEEL PRODUCTION

Before heat treatment or rolling, most DP steel microstructure contains ferrite, pearlite and iron carbide at the grain boundaries [103].

The cooling process is the same whether cold rolling, hot rolling, continuous annealing, or batch annealing are used in production. According to Fig. 2.7, the DP steel is heated to the interlayer temperature range in the Fe-C phase scheme's + field. Consequently, austenite rapidly cools and transforms into martensite as the temperature reaches Ms. The unusual cooling method illustrates the black colour of C-Mn DP steel.
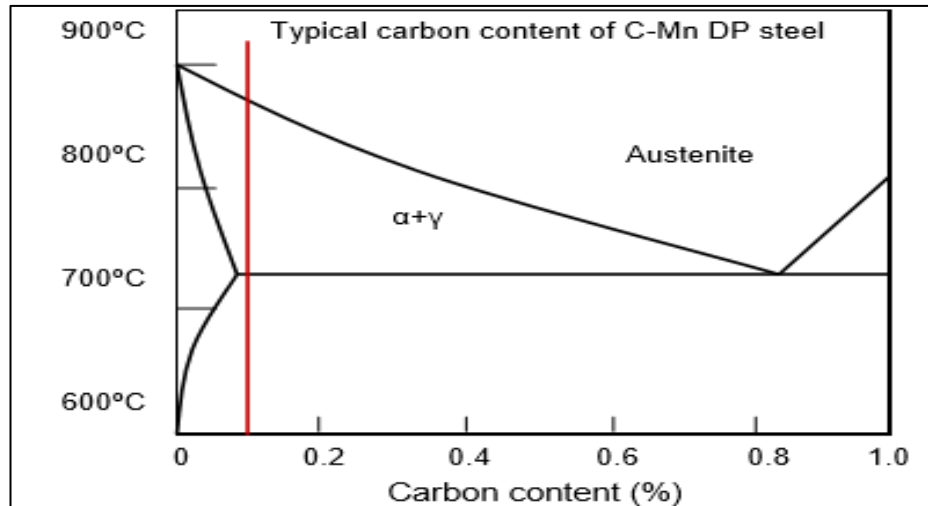
Figure 2.8. The iron-carbon stage plan, in part [104].
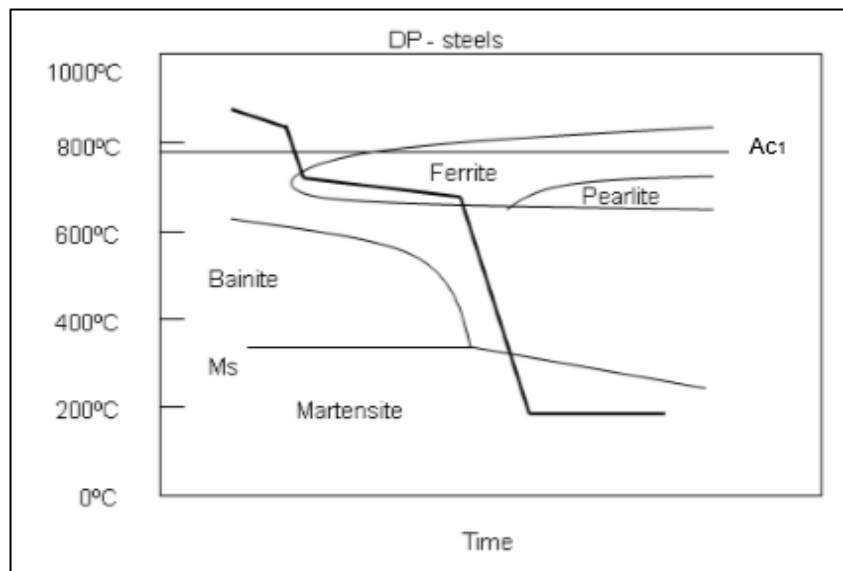
Figure 2.9. DP steel CTT diagram [105].

It should be remembered that Ac1 denotes the heating temperature at which austenite transformation initiation occurs, and Ms denotes the heating temperature at which martensitic transformation initiation occurs.

The three common stages in the complete theory of DP steel production are as follows:

- Increase the intercortical temperature and maintain it there for a short while. The austenite volume fraction is described here.

21

- Cooling encourages austenite conversion to martensite by lowering the martensite initiation temperature (Ms). The austenite's strength should grow as the concentration of carbon in the material increases due to the cooling ratio.

- Some procedures also incorporate an averaging stage to lower the martensite initiation temperature after cooling from the intercortical annealing temperature to boost the steel's durability and ductility above the tensile.

During manufacturing, various factors, including the cooling ratio, annealing temperature, and soaking time, impact the volume fraction and composition of the austenite and ferrite. [105].

Si in ferrite encourages the transmigration the carbon from ferrite up to austenite in C-Mn DP steels, but Mn diffuses into austenite differently and boosts its strength. [106, 107]. The transition temperature has been calculated using a variety of empirical equations that depend on the chemical composition of DP steel, as shown in the following list: [108]:

$A_{c1}=723-10.7Mn-16.9Ni+29.1Si+16.9Cr$
$M_s=539-423C-30.4Mn-17.7Ni-12.1Cr-7.5Mo$

According to Fig. 2.9 (a), Body-centered cubic (bcc) ferrite and body-centred tetragonal martensite comprise most of the DP microstructure. Even if opposed to (a), (b) partial austenitization in HAZ results in ferrite and micro-component martensite-grained austenite is formed and thinner than FZ and BM. As a result, lath martensite should occur, potentially with some lower bainite and very thin laths or retained austenite between laths, as shown in Fig. 2.9(c).

With increasing absolute strength, the microstructure of DP steel changes substantially. Furthermore, as illustrated in Fig, The martensitic transformation substructure in DP steels, which is crucial for mechanical properties, may differ from the martensitic lath substructure typical of low-carbon martensite. A distinct martensite twin substructure with significant carbon content. In line with Figure 2.10.B.

This shape change demonstrates how the amount of carbon in the austenite phase is affected by the chemical composition and annealing temperature, affecting the MS temperature [109].
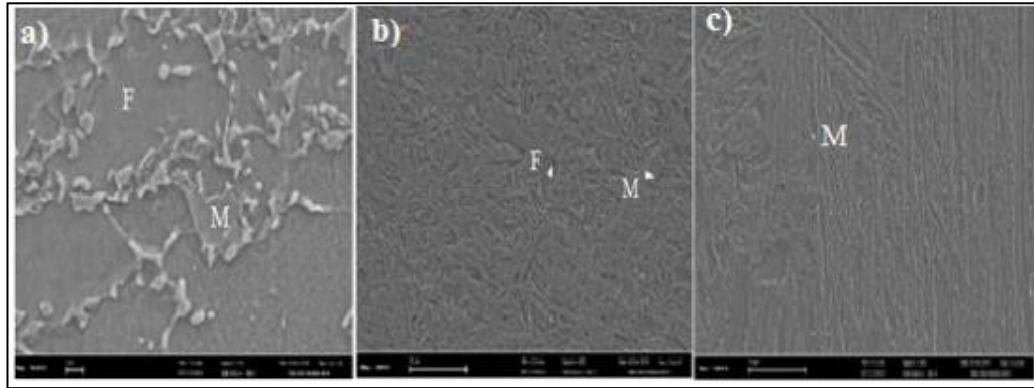
Figure 2.10. The microstructure of DP600 a) BM, b) HAZ, and c) FZ [110].
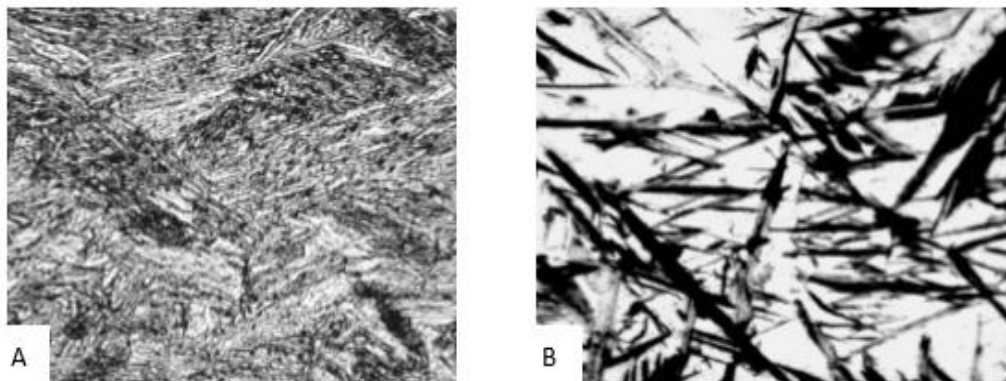
Figure 2.11. A (Lath martensite), B (Twinned martensite) [111].

2.4. MECHANICAL PROPERTIES

The automobile sector wants high tensile elongation with grade steel to guarantee survival, high tensile to create crashes, and resistance to fatigue and low alloy materials to guarantee weldability without compromising cost-effectiveness in manufacturing[112]. The martensitic phase content significantly influences dual-phase steels' mechanical properties[113]. For instance, High tensile strength (up to 1000 MPa), general greater homogeneity, overall elongation, continuous yielding behaviour (no yield point), low yield strength (i.e., 0.2%) offset, and high work hardening rate are only a few of the distinctive properties of DP steels [114]. For many years to come,

DP steel is still be in demand. Materials with great strength and good sustainability also contribute less weight to cars and other items, which has numerous positive effects on the economy and environment. Figure 2.10 shows how the performance of DP steel surpasses that of other high-strength low-alloy steel (HSLA). Automobile manufacturers are encouraged to examine novel materials and other tactics by growing consumer demand for vehicles with higher fuel efficiency [115]. The new material has been determined to be either lightweight or stronger, reducing the car's weight and perhaps lowering fuel consumption. The residual austenite during deformation slows the transformation to martensite, allowing TRIP steels to theoretically absorb more energy during collisions. Through careful microstructure design, TRIP steel can have excellent ductility, formability, and strength balance compared to normal steel. Tuning the TRIP steel mechanical properties requires considering the volume, size, chemical composition, and form of microstructural components, particularly retained austenite [116]. Figure 2.10 demonstrates how the microstructure of TRIP steels, which have the same strong values as DP steel and traditional, high-strength low-alloys, causes them to exhibit higher uniform elongation and overall elongation.
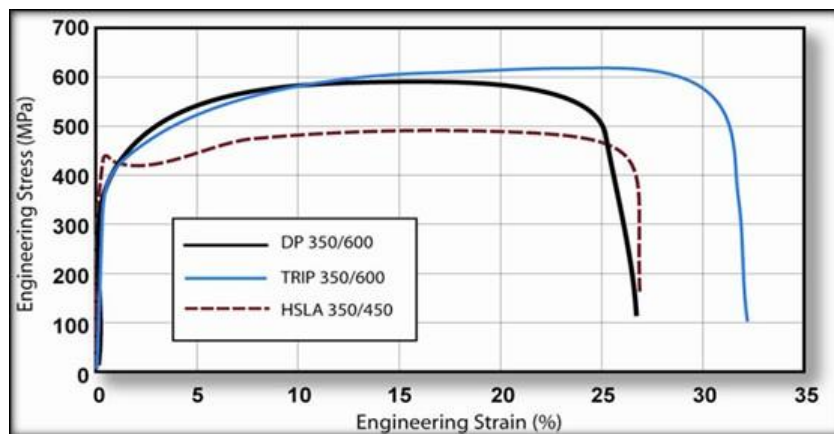
Figure 2.12. HSLA, DP350/600, and TRIP350/600 steel tensile curves [116].

Most recent research has focused on characterizing the response to a particular steel grade and the microstructure, nugget formation, and mechanical characteristics of AHSS welding resistance. In addition, Maria et al. [117]. Tensile testing assessed how the RSW process parameters affected the way DP steel failed. Similar to this, Tong et al. [118]. Testing was done on the mechanical characteristics of DP-speckled steel and how they affected failure behaviour. However, the existing literature does not offer a

thorough evaluation of the mechanical characteristics and microstructure of speckles in various AHSS classes.

2.5. DUAL-PHASE STEEL'S IMPORTANCE IN MICROSTRUCTURE

In typical DP steel microstructure, polygonal soft ferrite islands are 10–40% hard martensitic islands. The steel is given, respectively, ductility and strength. This fabrication method contributes to a final tensile strength of 500–1200 MPa. When martensite makes up more than 20% of the volume, the material is typically referred to as DP steel or partial martensite. Ferrite-bainite-martensite is needed to satisfy customs regulations. Ferritic-bainitic steels have also been developed to adjust mechanical characteristics; studies reveal that bainite, as opposed to martensite, improves formability while marginally lowering strength and progress [119-121]. The effects of ferrite fraction, grain size, martensite fraction, broadening, and martensite size on the mechanical performance of DP steels have all been extensively studied [122].

A very clear illustration of a two-phase microstructure can be found in Figure 2.11. The soft ferrite phase appears white in the microstructure, but the hard martensite appears black regions.
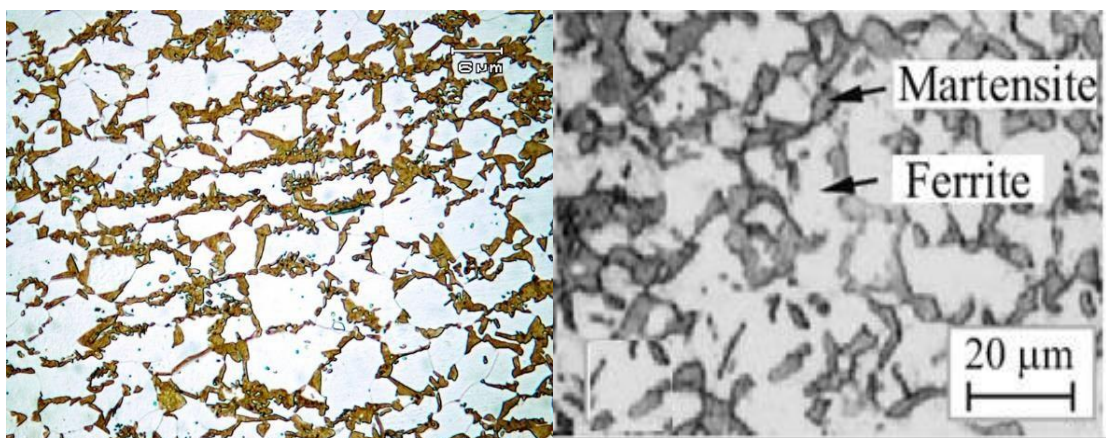
Figure 2.13. DP steel's microstructure [123].

Technically, low- and medium-carbon steel that has been cooled continuously from a temperature higher than the A1 temperature but lower than the A3 temperature was

used to make dual-phase. But this result features a microstructure with a second phase in a ductile martensite ferrite matrix. Martensite increases tensile strength. Furthermore, the carbon concentration, morphology, particle size, and volume fraction all influence the inclusion behaviour of DP steels. To generate these microstructures, which improve the martensite and stabilize the austenite phase, DP steels frequently contain 0.06 to 0.15% C.

Adding 1.5–3% Mn reinforces the ferrite, and the austenite phase is stabilized. It is believed that chromium and molybdenum hinder the formation of bainite or pearlite. Si encourages ferrite transition. (V and Nb) elements accomplish precipitation strengthening and microstructural refinement. In addition, the mechanical behaviour of DP steel was affected via the martensite dispersion [124-126].

Within the ferrite matrix is a distinct zone known as the martensite region. Its strength and ductility are greater than those of the martensite region, which, adjacent to the ferrite, creates a network structure like a chain [124].

Ferrite and martensite that have been refined increase ductility and strength [127-129].

PART 3

THE EXAMINATIONS OF HIGH-STRENGTH TWO-PHASE STEEL SHEARING

Generally, the manufacturing process for sheet metal forming and cutting has been seen as being dominated by the automotive sector. As a result, sheet metal forming and shearing development is significantly influenced by the needs of the growth of the automotive sector. Numerous contradicting demands, such as less hazardous emissions, reduced consumption, improved performance, and more comfort and safety, are placed on the car industry. It is not easy to meet these objectives using conventional materials and manufacturing techniques. Meeting these seemingly contradictory demands has traditionally been seen as a key driving force in the development of materials, Automotive sector production processes and sheet metal shaping

Applications for high-strength steel have changed significantly in recent years. One of the best instances of this is DP steel [106].

However, manufacturing and forming issues with various kinds of steel have always existed. After the sheet metal is formed, the spring return is one of the formability-related issues.

Draw beads are passed through during deformations like straightening and bending on the tool radius. Another issue is that the hardening behaviour differs significantly between forward and reverse loading, such as the reverse loading condition, because the well-known Dr Inge impact invariably happens in similar forming scenarios.

The following is a summary of the difficulties in AHSS formation:

- Because of the multiphase structure and complicated production process:

1) New test techniques are necessary for the accurate determination of material properties.

2) Variation from batch such batch was frequent.

- Accordingly outcome, high strength and depressed formability:

1) In many forming surgeries, when fractures need to be examined, first fractures are noticed.

2) Blanking or forming demands a larger press capacity.

3) Equipment degrades quickly. It's important to choose lubricants, tool materials, and coatings wisely.

4) A significant problem requiring further research is the large spring back (leading to erroneous dimensions).

As illustrated in Figure 3.1, during the sheet-forming process, the sheet metal's stress-strain curve or flow stress considerably affects the product quality and metal flow. It is essential to precisely calculate the flow stress when using FEM to simulate operations [130].

The main technological difficulties are in designing. It is challenging to create sheet metal elements with the necessary precision due to the increased springback generated by the forming of high-strength steels and the significant change in formability with increasing strength.
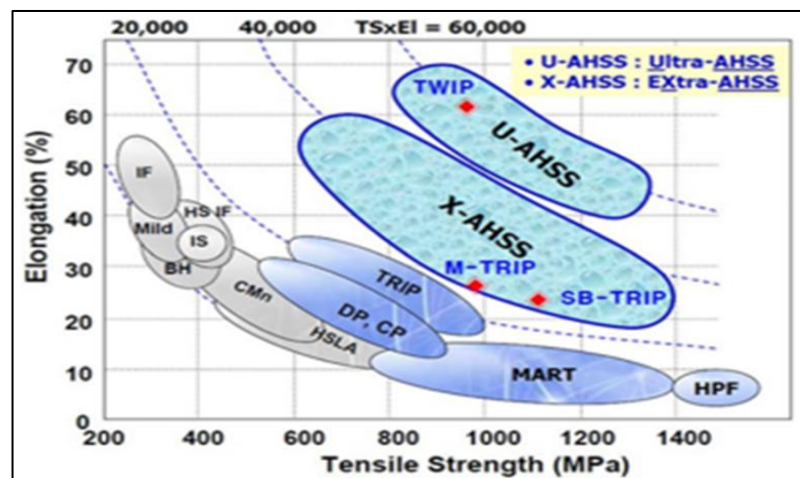
Figure 3.1. Tensile strength against elongation of conventional and AHSS materials [131].

3.1. METAL FORMING PROCESSES

Trimming, fine blanking, punching, and blanking are just a few sheet metal cutting procedures that use controlled breaking and shearing at the cut contour to separate substantial amounts of material from the remaining sheet. The characteristics of the resulting cut surface are determined by the ratio of the fracture and shear areas [132]. The material's properties determine the cut surface's characteristics and parameters, such as the punch, die radius, sheet thickness, and gap. It is generally known that the cut blank's edge geometry and microstructural properties significantly affect the subsequent punching processes. That is especially true for sheets with high strength and limited formability characteristics. For instance, it is important to define sheared edges more thoroughly and examine how they affect punchings' formability because AHSS is susceptible to edge cracking. Many nations worldwide have created unique case studies and application manuals for the steel sector [38].

The thermomechanical processing of DP steel produces fine-grained martensitic particles embedded in a ferritic matrix, giving it low-cost mutual strength and ductility. This material was regarded such the most sophisticated high-strength steel. Numerous manufacturing and cutting activities, including trimming, punching, and blanking, are used during the punching of an automotive body. Most of these actions near the intended cutting line occur in a production setting where mechanical shearing separates sheets at high cut rates or efficiency. In contrast, laser cutting is frequently employed when producing or fabricating sample parts due to its tremendous geometric flexibility. Benefits shorter lead times and lower tool costs [132], the study on trimming, blanking, and perforation is important in the literature. The materials in this group are often the same. This material's microscopically non-uniform DP microstructure contains martensitic components that are finite microns in size or less. Various strengths could obtain good forming than standard high-strength steel by varying the volume fraction in the martensitic stage. Few researchs, however, have focused on cutting AHSS, especially edge features and how they relate to edge cracking in DP steels. AHSS's flanging is an older body of work still relevant today [133].

If the staging interface is where the microcracks are mostly propagating, DP steel's edge stretch formability is low. In contrast, the formability is high if the fracture passes through the ferrite and martensite stages. The difference in hardness is the main factor affecting tensile flanges' crack path and formability. The phase volume fraction also impacts formability. High-edge strain gradients help single-phase martensitic steels to become more formable. It is vital to grasp the edge morphological characteristics and associated fracture mechanisms to comprehend the mechanisms that lead to edge cracking in AHSS and offer a qualitative explanation for the supply of restraint at the sheared edge during cutting operations. [134].

3.2. PUNCHING

Shearing is a fast and economical way to cut sheet metal compared to laser and plasma cutting. Shear cutting is frequently employed in the sheet metal industry throughout several processing stages, such as cutting the length, cropping, and slitting. Increased forces are put on the tools and equipment of shear due to the continuous development of sheet metal toward increased strength and formability. A refined process and in-depth expertise are crucial to sustain and accomplishing tool existence and acceptable sheet tolerance. To model, validate numerical models and comprehend shear mechanism, experimental data is required.

The experimental shear force is rarely documented, and virtually never is the force separating the two shear tools included. While the blanking process might be limited to punch and die, force is delivered through the straight cutting at similar tools to the surrounding structure, Crane (1927) [135], Oldenburg 1980 [136] and hambli et al. 2003 [137] correlating forces to edge geometries and researching the impacts of sheet clamping, respectively.

Several noteworthy studies report force measurements on the rotationally symmetric blanking procedure. Additionally, the majority of studies in the equipment into account throughout the shear process do not take tool clearance fluctuations or friction forces concentration on the shortcomings above. This work aimed to quantify shear forces without friction losses accurately and to measure changes in clearance during the

shearing process. The Gustafsson et al. (2014) [138] method and setup, briefly discussed in the next section, were used to record the measurements. This study used shear trials to examine how clamping and clearance affected the tool forces.

Punching creates cuts by applying pressure until a workpiece reaches its elastic limit. Punching makes coins, bone graft implant plates, rings, and small and large industrial components. An implant frequently utilized in skull transplants is the Keychain Skull Plate.

Cutting by pressing a workpiece past its elastic limit is known as punching [139]. Punching makes coins, plates for bone graft implants, rings, and both large and small designed components. The Keychain Skull Plate is a common implant for replacing the skull. The punched product has two completely smooth surfaces. As shown in Figure 3.2 [140], the shear edge surface of blanking and punching contains four different types of areas: tumbling, shearing area, fracture, and burr. Punching die and design punching the material chosen for the die and punch process, the punch design, and the appropriate clearance after to avoid product burrs; accurate calculation, burrs, and material type, thickness, and size are crucial factors that must be taken into account to create a smooth surface [141].
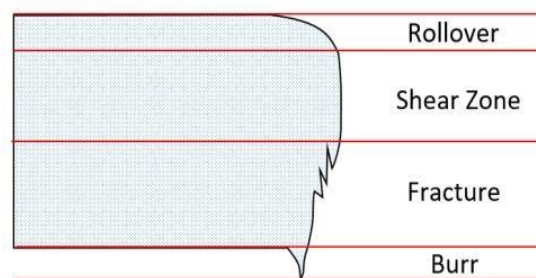
Figure 3.2. Sheared edge characteristics from the punching process[140].

Metal parts are typically created from sheet metal during the fabrication of panels. They utilize processes like blanking, punching, and bending. Additionally, metal can be punctured for cutting and sheared for blanking.

Sheets are available as needed. The drilling process entails feeding the punctured sheet metal through the scrap. It's interesting to look at the discs being cut throughout the bleaching process. A scrap is a metal plate with a hole [142], as shown in Fig. 3.3.
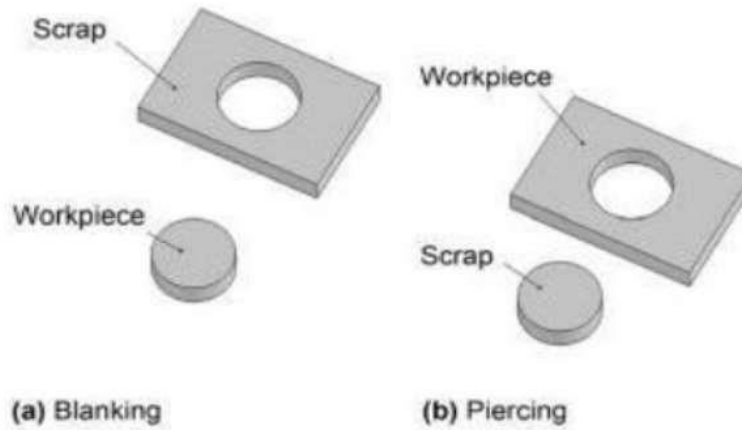
Figure 3.3. Blanking and piercing components [142].

3.2.1. Clearance Between Punch and Die

According to numerous tests, shear strength is not considerably impacted by the value Clear. However, it impacts 1 to 3 mm since it impacts the product's quality. A 0.07 mm wide gap provides the best quality for the sheet. Various procedures are necessary in the metal industry [30].

3.2.2. Clearance Calculation

Several experimental studies [143, 144] suggest that various parameters during a blanking operation for a specific material, such as blanking gap, tool wear status, sheet thickness, etc., impact the mechanical and geometrical characteristics of sheared edges. The gap is expressed in Equation 1 as a proportion of the plate thickness during the blanking process.

$$C = \frac{d_{d-d_p}}{2t} \times 100\%$$
(3.1)

where t is the material thickness (mm), and d_d is the die diameter (mm).

and d_p punch diameter (mm).

When blanking methods are used, one aims to create fractures at the punch and die's sharp edges so The fracture is spread as rapidly as feasible to achieve the total rupture by choosing cutting parameters. For this inquiry, it is presumable that clearance is best when the direction of the crack's propagation corresponds with the line between the punch and die (A and B of Fig. 3.5), leading to cleanly blanked surfaces without subsequent crack formation (Fig. 3.4). In this situation, complete sheet separation is nevertheless achieved despite a smaller punch penetration amount. To get the best clearance value, the angle of the direction of crack propagation (DCP) and the angle of the line linking the locations where cracks first appeared in the punch and die must be equal (Fig. 4).
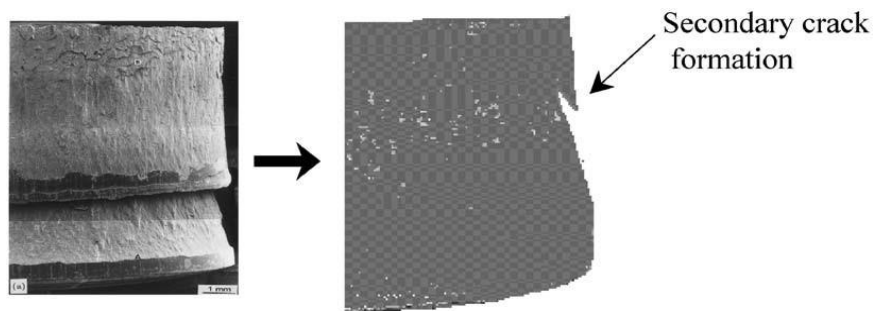

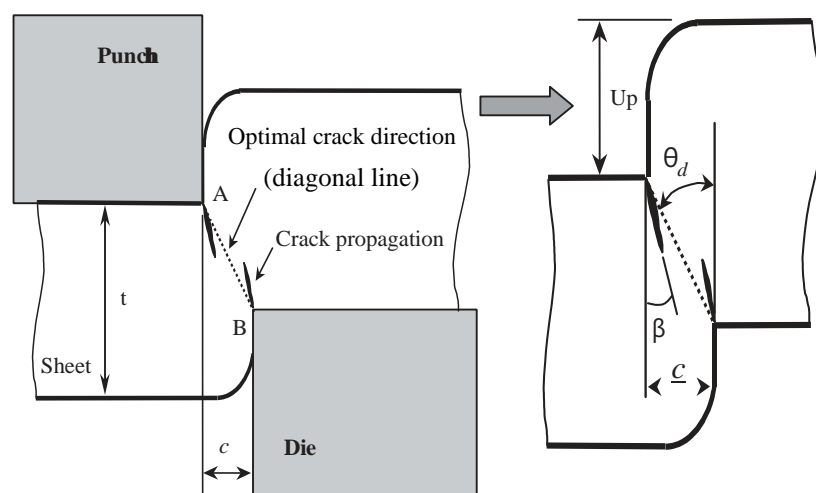Figure 3.4. Secondary fracture development during blanking.

Figure 3.5. Graph showing the diagonal angle and crack propagation angle [145].

Equation (2) can be used to express the diagonal angle.

$$\theta_d = \text{Arc} \tan \beta \left(\frac{C}{t - Up} \right) \qquad\qquad (3.2)$$

The punch penetration initiated the first crack within the sheet [145].

3.3. PUNCH DIE DESIGN

The most often utilized processes in sheet metal manufacturing are punching and blanking.

In this procedure, shear stresses are used to cut a metal sheet. The technique frequently produces sheet metal components in high-productivity industries such as automotive, electrical, electronic, chemical, tool production, etc. The competition in the global market for sheet metal blanking and piercing is increasing. In order to compete in this market, obtaining longer punch life, higher stroke rates, and better quality parts has become important.

To evaluate the quality and accuracy of the workpiece, one looks at the geometry of the cutting edge of the blanked component surface, which is dependent on several factors such as tool design, punch material properties, punching circumstances, and particularly punch wear [146-148] The features of the metal chips, their heights, and the scrap section shape can be used to assess the punching tool's usable life. The performance of the punching tool during punching is determined by its geometries, and one of the key components of optimization is the cut angle. [149].

In Fig. 3.6, the punching geometry is displayed. In the current analysis, the punch fillet supplied close to the intersection of diameters D and D2 represents the real element geometry [31].
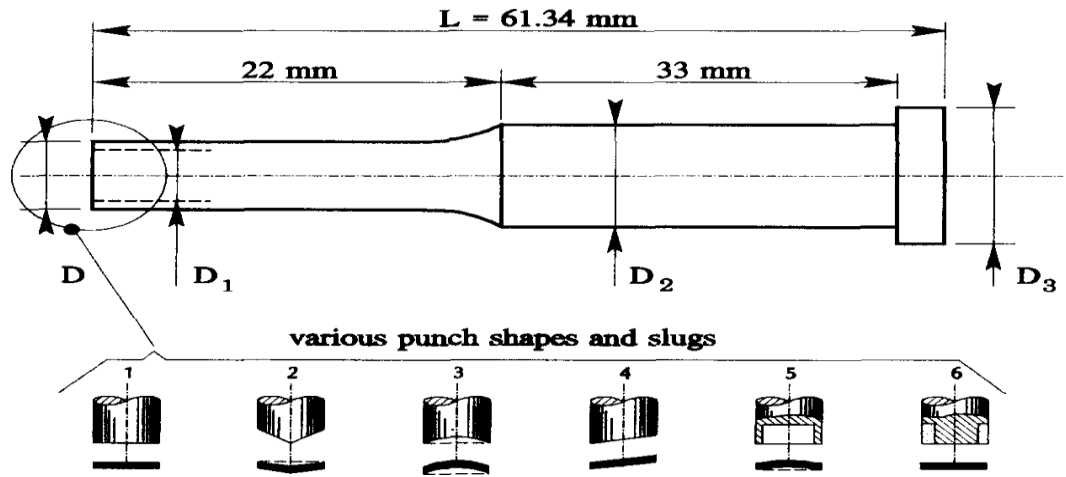
Figure 3.6. Punch set up with various punch and slug configurations [31].

A static load corresponding to the punching load is applied to analyse punch deformation. Poisson's ratio and Young's modulus must be provided for the punch material. When the mechanics of punching are exclusively dependent on shearing, the instantaneous punching force Fp is produced (see Fig. 3.7) [31, 150].
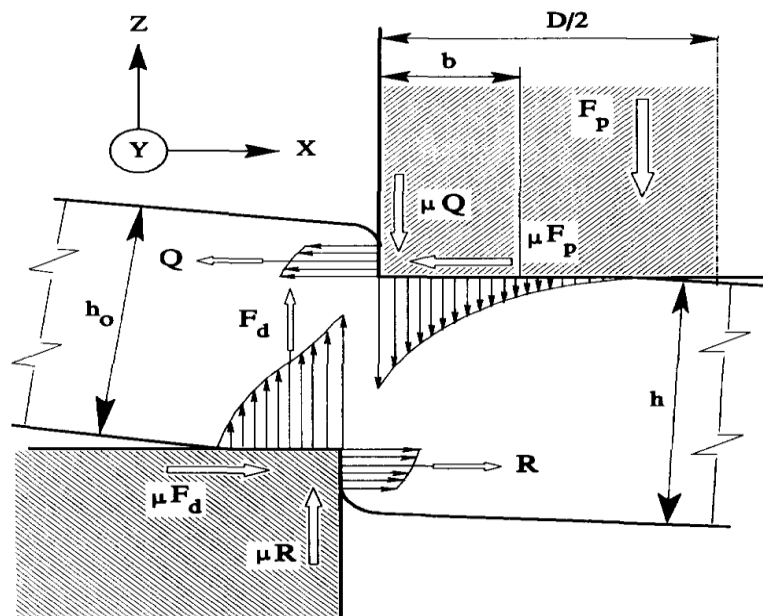
Figure 3.7. Load on the cutting edge of the punch.[31, 150].

$$F_P = 1/3\pi\sqrt{3\,D\,h\,C}\,[k\ln(h_0/h)]^n \qquad (3.3)$$

hence, the strongest force by

$$F_{Pmax} = 1/3\pi\sqrt{3\ D\ h_0\ C}\ [n/e]^n\ k^n \tag{3.4}$$

When ignoring the friction.

It is evident from the idea of plastic instability that a material's tensile strength can be described in terms of:

$$\sigma_B = C\ [n/e]^n \tag{3.5}$$

for $A\sigma_{B_0}$ (eq. (5)) in eq. (4) renders:

$$F_{Pmax} = \pi\ D\ h_0\ k_f\ \sigma_{B_0} \tag{3.6}$$

Where $k_f = \frac{1}{3}\ k^n\ \sqrt{3}$ represents the punching shear factor. The parameter k is a constant characteristic of the process that describes the correlation between the geometrical measure of deformation and the process. h_0/h as well as an average of the actual physical deformation throughout the entire shearing zone. The parameters specify initial and instantaneous blank thicknesses. h_0 and h, respectively. The stress characteristic is specified by parameter C, and the strain-hardening exponent is specified by parameter **n**, σ_{B_0} the blank material's maximum tensile strength is the punch's diameter, and D is the punch [31, 150].

3.4. PUNCH DIE TERMS AND PARAMETERS

3.4.1. Die Materials

A material with properties suitable for the service conditions must be utilized to make a die component. The loads and strains, size, form, and number of the components that must be produced using the die are just as important as the material of the die. The limitations imposed by the available materials typically determine die design. The designer must understand the effects of heat treatment and die component manufacturing processes on the characteristics of the die materials. The materials

employed also depend on the manufacturing procedures used to create the work pieces. A professional metallurgist may occasionally be required for the best possible material selection and heat treatment. This essay concentrates on the steel needed to make sheet metal forming die text. More materials, including nonferrous and nonmetallic ones, are included to complete the picture.

Tool and die steels are specially alloyed for high strength, impact, and wear resistance. They are widely employed to shape and machine metals at low and high temperatures. Most tools and dies require heat-treated steel, frequently hardened and tempered, to provide the properties necessary for the particular application. Tool and die steels must withstand heat treatment with the fewest side effects to deliver favourable changes in material properties consistently.

Applications and characteristics. The machinability and usual uses of popular die steels are listed in Table 13.9.

Table 3.1. Standard uses for common tool and die steels.

AIS1	Machinability Rating	Approximate Hardness (HRc)	Characteristics and Applications
A2	A2	57 to 62	Good size stability during heat treatment, hardenability, and a combination of wear resistance and toughness. Common applications include blanking and shaping rolls, punches, and dies.
A6	65	57 to 60	Blanking and forming rolls, punches, and dies are common applications. Deep hardening, great size stability after heat treatment, and air hardening at low temperatures. Common applications include plastic moulds, punches, coining and bending die, and blanking and shaping dies.
A8	75	56 to 59	The best possible blends of toughness and wear resistance, outstanding size stability, and suitability for highly abrasive hot work conditions. Shear blades, trim dies, forging dies, and plastic moulds are a few examples of applications.
A9	65	35 to 56	Decarburization and wear resistance of medium strength. Die inserts, forming dies, cold heading dies, punches, and solidly constructed rolls.
D2	50	57 to 62	Very strong wear resistance. Excellent size stability and deep hardening in the air. Typical uses include blanking dies, drawing dies, shear blades, forming rolls, and trim dies.
D3	35	57 to 64	high compressive strength, excellent abrasion resistance, and rapid hardening.

			Examples of common applications are blanking dies, drawing dies, shear blades, forming rolls, punches, and cold trimming dies.
D5	50	59 to 63	Extremely high wear resistance, ideal size stability, and outstanding tempering resistance. Applications include cold trimming dies; blanking dies, shear blades, forming rolls, hot and cold punches, and swaging dies.
01	90	59 to 61	Medium wear resistance, safe to harden, and simple to process. Some common applications are shear blades, bending and drawing dies, plastic moulds, and blanking and shaping dies.
02	fairly	57 to 61	Good wear resistance, safe hardening, and machining are all strengths. General-purpose tools that combine moderate hardness and wear resistance.
06	125	45 to 63	Outstanding machinability, galling and wear resistance, and quick hardening. Examples of typical applications are gages, punches, blanking and trimming dies, cold forming dies, bushings, and other machine tool parts.

3.4.2. Upset And Lower Set Configuration and Design

Press's dies can be categorized as high, medium, or low manufacturing quantities of parts, respectively:

Class A- Only high-volume manufacturing uses these dies. The highest-quality materials are used, and fragile or easily damaged places are carefully built for easy replacement. Regardless of the tool's price, the combination of a long die life, continuously needed precision during the life, and ease of maintenance are key factors.

Class B- These dies are solely intended to produce the specified quantity and are suitable for medium production. Die cost becomes a crucial factor when compared to the overall production. Cheaper materials may be utilized if they can produce the required quantity in full, and the issue of ease of maintenance may receive less attention.

Class C- These dies are ideal for low-volume production and are among the most affordable, useable tools that can be constructed dies momentarily. These dies are the most reasonably priced tools to manufacture components and are utilized for low-volume production.

Schematic die classifications for the upper and lower die sets are shown in Fig. 8.1 following the guidance methods:

Die that is plain (Fig. 8.la). These simple dies are used for low-volume, one-off manufacture. They are plain dies with adjustable elastic strippers (Fig. g. kg).-The majority of the time; these dies are employed to punch blank-shaped components out of thinner sheet metal.

Solid stripper and plain dies (Fig. 8.lc). These dies are utilized for punching and blanking simple-shaped components manufactured from thicker materials.
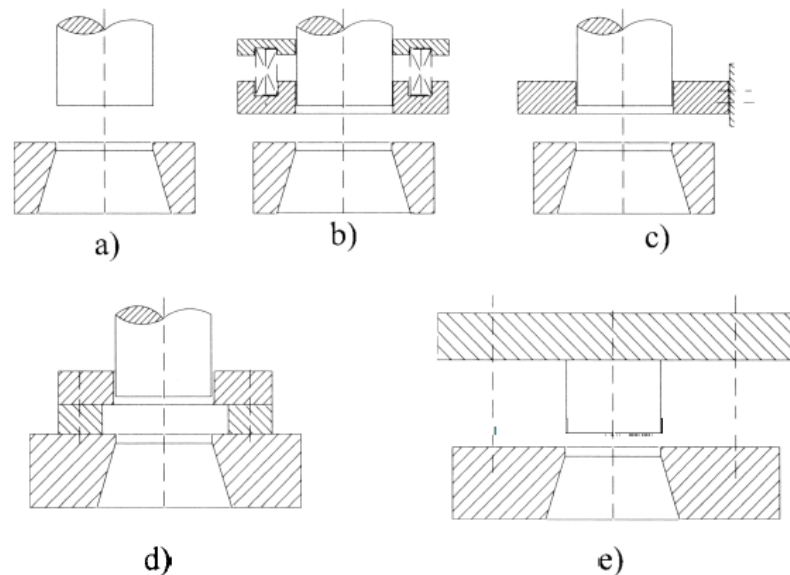

Figure 3.8. Schematic representation of die classifications using the upper and lower die sets' reference techniques: a) plain dies, b) simple dies with a retractable piece of elastic, c) simple dies with a strong stripper, d) mid guide plate for dies, e) with guiding posts dies [28].

3.4.3. The Process of Metal Cutting: the Forces at Work

In addition to the pressing force operating upon the ram and applying vertical pressure to the die and subsequently to the steel-metal material, other forces are also present throughout the metal-cutting process. As the punch engages the material, it is forced downward through the die hole. However, as shown in Fig. 3.9, a small amount of metal is pushed sideways.

The tensile and compressive forces that arise within the cut metal, which are grain dependent, drive this flow away from the cutting tool: In comparison to flowing against the grain, the flow pattern is distinct.

The structure of the sheet is impacted by such material mobility, particularly close to the cutting station. By being pushed aside, the material becomes overcrowded from expanding its content and resorts to bulging through the sheet's surface, which it deforms. When piercing is more crowded, the deformation spreads throughout the entire sheet, causing it to become warped and exhibit excessive camber, waviness, or any other deviation from straightness. The expanding substance exerts a side-directed or thrust force against the body of a punch. The squeeze of expanding material, combined with variations in friction and an increase in heat, suddenly limits the punch's motion. The punch's stability is frequently in jeopardy, and thin, fragile tools frequently break under such a strain. Due to its often smaller size, the cutoff metal portion's distortion is frequently not as severe[151].
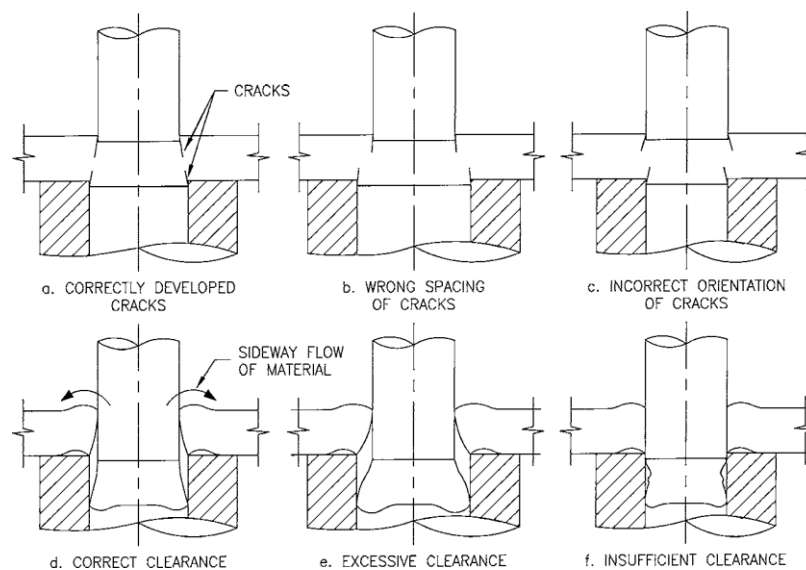

Figure 3.9. Shearing of metal [151].

As demonstrated in Fig. 3.9, the appearance of wear on the working surfaces is also significantly influenced by the development of side-oriented and expanding shifts inside the material due to the flow of tensile and compressive stresses. Some estimate that the side-oriented force produced by the cut material can range from 2 to 20% of the overall blanking force, depending on the material's thickness, composition, and

distance between the cutting surfaces. The size of a sheared aperture is additionally influenced by forces within the cut material. The swelling material slightly flattens out after the punch has been fully retrieved, with its motion directed toward the empty area, which then shrinks in size.

Openings smaller than the size of the cutting punch have been observed to be produced with cutting clearances of up to 0.05t. As previously indicated, frictional forces originating from the structurally changed material constrain the punch's ability to travel as it exits the cut material. A significant force is required to counteract this impact for the punch to continue. By considering the material's composition, strength, thickness, size, and clearance, one can calculate this force, also known as the stripping force. Naturally, the stripping force decreases as the distance between the punch and die arrangement increases. However, as a result, the cut's quality also declines [151].
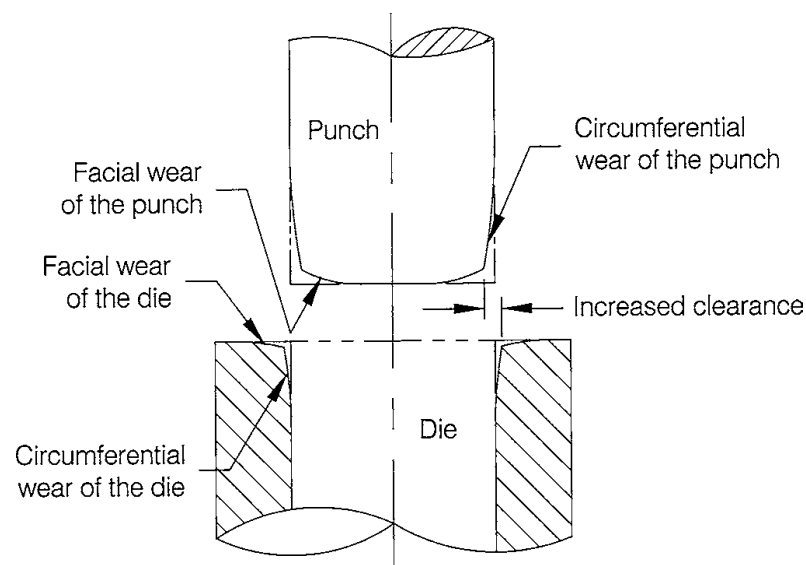

Figure 3.10. Wear of tooling[151].

3.4.4. Punch Face Geometry

By beveling (creating an angle) the punch and die surface, as shown in Fig. 3.11, many kinds of punch face geometries are displayed, allowing the region being sheared to be controlled at any time:

41

a) The face is flat.,

b) The face is concave

c) The face is bevel

d) The face is a double bevel.

If the punch and die surface is flat during cutting, the entire cross-sectional area is being cut at once, which causes the punch force to increase quickly. With a proper shear angle on the die, the punch face geometry in Fig. 3.11 is especially. Since it reduces the effort required at the beginning of the stroke, it is ideal for shearing thick blanks. In addition, noise level 1 is reduced by the angle. Examples of common combinations:

a) punching flatly using a twin bevel die

b) flat die and concave punch

c) Punching a bevel with a flat die

d) Concave die with a flat punch
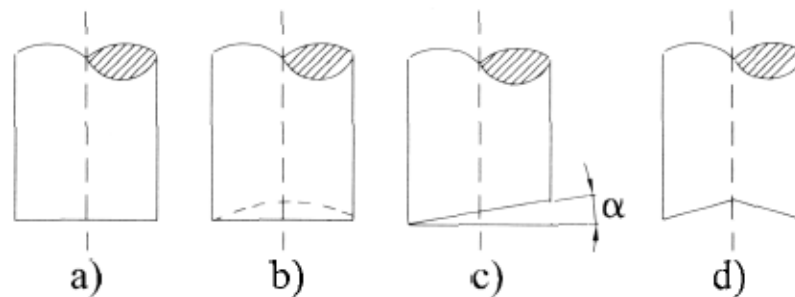
Figure 3.11. Punch face geometry types: a) flat, b) concave, c) bevel, and d) two bevels [28].

Depending on the function of the dice, other combinations may be used. To blank fragile and thin materials, a tubular punch without a die block can be utilized [28].

3.5. METAL SHEARING PROCESSES OF DUAL-PHASE STEEL

3.5.1. Sharing Teory (Detail)

For dual-phase steel plates, forming activities and shearing operations could become difficult. High-strength steel sheets' poor ductility causes the majority of the surface to Shear edges to be low-quality, imprecise fracture surfaces even with polish [152]. While the surface of the sheared edge is fine and clean, the fracture surface caused by crack propagation is rough and somewhat sloped. When high-strength steel plates are sheared, the significant contact pressure can lead to tool failures such as wear, chipping, and breakage [153]. The shear load is lessened. Tool slanted plates and cut corners [154].

3.5.2. Punch Force

3.5.2.1. With Parallel Cut Edges, Punch and Die

From the following equation, the force F for a punch and die with parallel cut edges is computed:

$$F = 0.7LT(UTS) \qquad\qquad (3.1)$$

where:

L = the whole length sheared (hole's circumference)
T = material's thickness
UTS = the material's maximum tensile strength

The punch force and penetration curves can assume various shapes since the shared zone is susceptible to friction, plastic deformation, and fractures. Figure 3.11 depicts a typical curve for a ductile material. The area under this curve represents the overall work done during the punching or blanking procedure [28].
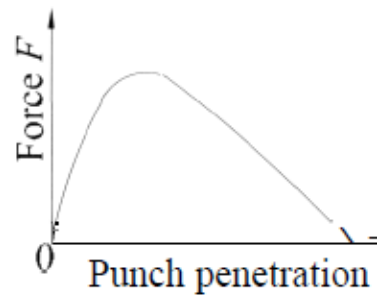
Figure 3.12. common punch force and penetration curve in shearing [28]

3.5.2.2. Bevel-Cut Edges on Punch and Die

If the punch or die's edges are bevel-cut, the punch force can be decreased (Fig. 3.12). Convex or concave chamfer shear angles should be employed in blanking processes to maintain the flatness of the slug workpiece (Fig. 3.12a). During punching operations, bevel-shear or double-bevel-shear angles should be used on the punch (Fig. 3.12.b).
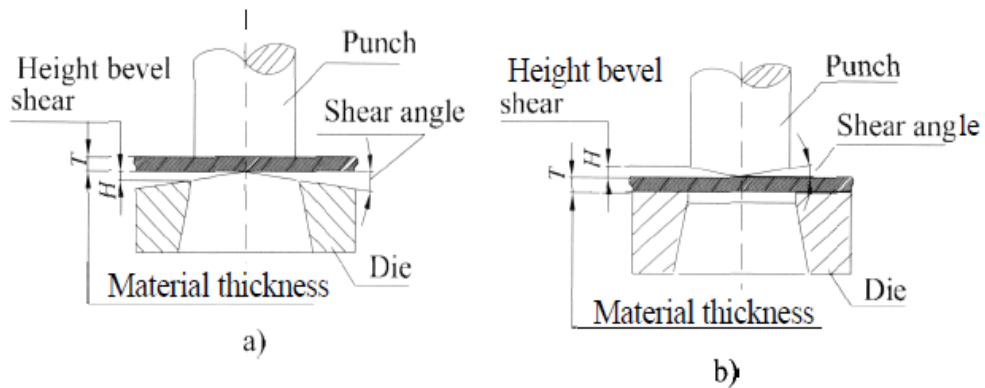

Figure 3.13. Angles of shear a) on a die. b) on punch.[28].

Deformations rise along with shear angle increases, which may cause workpiece warping. The following equation estimates the punch force F during shearing operations when a shear angle is applied to a punch and die: [28]

$$F = 0.7KLT(UTS) \tag{3.2}$$

where:

K = 0.2 to 0.6

3.5.3. Enhancement of Sheared Edge Quality

Applying fine blanking to ultra-high-strength steel sheets is challenging, even though it helps improve the sheared edge's quality. An ultra-high-strength steel sheet's hole edge was smoothed after being punched by shaving the punched edge [155, 156]. Shaving also increases the hole limiting expansion by three times, but die life is short and chip removal is also necessary. A double-beveling punch that punches high-strength steel sheets causes the limiting hole expansion ratio to rise [157]. The rough fracture surface can be smoothed to improve the sheared edge. The taper punch's angle was adjusted to be roughly parallel to the fracture surface's tilt.

The taper punch successfully ironed the 980 MPa ultra-high-strength steel sheet's short edge. The fracture surface changed from rough to smooth, increasing the limiting hole expansion ratio. To increase formability, stretch flanging was ironed using a taper punch [158]. The pierced edge undergoes severe shear deformation while subjected to strong compressive pressures during ironing. The quality of the sheared edge is improved by smearing the rough fracture surface. The angle of the tapered punch was set so that it was almost parallel to the tilt of the fracture surface. The taper punch successfully ironed the 980 MPa ultra-high-strength steel sheet's shorn edge. The fracture surface changed from rough to smooth, increasing the limiting hole expansion ratio. To increase formability, stretch flanging was ironed using a taper punch [158].
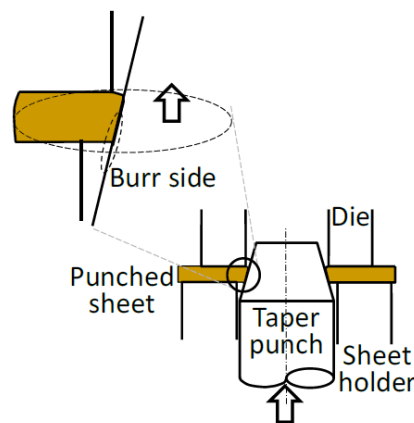

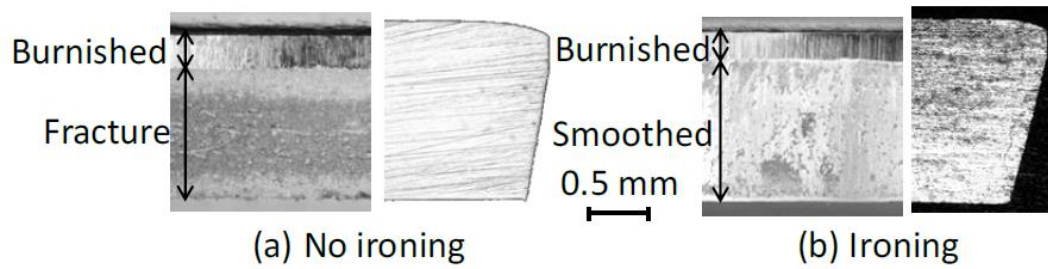Figure 3.14. The punched edge using a taper punch is ironed [158].

Figure 3.15. edges' surfaces and cross-sections (a) without and (b) Perforated 980 ultra-high-strength steel sheet with ironing for a 20% clearance ratio [158].

3.6.1. Edge Ductility Measurements

Edge fracture is considered high danger, specifically those made of modern high-strength steel (AHSS) for automotive parts. They are more vulnerable to edge damage because AHSS have less ductility. Using standard techniques, such as those that rely on ductility testing or the creation of limit diagrams, it is impossible to predict this type of fracture. As a result, stretch-flangeability has become an important formability measure in addition to tensile and formability properties. Damage from sheared edges in AHSS parts affects stretch-flangeability because the resulting microcracks propagate from the edge. By the fracture mechanics, the crack propagation resistance can be described. This study investigates fracture toughness as a tool to understand crack-related problems in various AHSS grades, including edge cracking and stretch-flangeability. Hole expansion tests were used to determine stretch-flangeability, and the foundations of fracture methodology were used to determine fracture toughness. The results show a high correlation between stretch flangeability and fracture toughness. It is conceivable to postulate fracture toughness, determined using the foundational work of fracture technique, to explain the crack propagation mechanisms in AHSS [159].

One of the biggest issues with high-strength sheet metal forming is edge cracking. In advanced high-strength steels (AHSS), there are greater differences in local and global ductility, and the examination of edge formability has gained important importance. Edge fracture prediction is difficult because it deviates from conventional ductility.

Measurements are based on creating limit diagrams and uniaxial tensile testing. Additionally, in addition to material characteristics, it also depends on the edge quality. Numerous factors related to the blanking process (such as cutting/punching clearance, cutting tool condition, etc.) impact it. Due to these ambiguities, many characterization methodologies have been developed to characterise edge cracking resistance. The hole expansion test (HET) is in the scope of ISO 16630 [160]. Further edge cracking resistance studies based on optical strain measurements have thus been recommended to improve edge formability prediction [161-164].

The use of EWF to forecast edge formability in contemporary, high-strength steel sheets Shows that steels with higher fracture toughness give superior edge cracking resistance based on the hole expansion or fracture strain measured in hole tension test specimens. Additionally, research is conducted to determine how cutting clearance influences edge fracture. The investigated DP steel grades significantly affected the cutting clearance for clearances greater than 14%. The CP grades' similar fracture stresses across all cutting settings are consistent, with the punch-to-die clearance having less effect on them.

The optimal punch-to-die clearance within the explored range of punch-to-die clearances (10–20%) is discovered to be about 13–14% based on the fracture strains determined using DIC for the studied steels. CP steel grades generally have higher fracture toughness and edge cracking resistance than DP steels. According to the experimental data, fracture toughness is crucial to understanding edge fracture in high-strength steels because it provides useful information on edge cracking resistance [165].

3.6.2. Cut Edge Quality

The sheared edge comprises the rollover, burnished surface, fracture surface, and burr. Because total elongation reduces as sheet strength rises, increasing the low-quality fracture surface, the onset of cracks in shearing happens earlier. These steel sheets are mild, high-strength, low-alloy, and dual-phase steel.

Figure 3.16 shows punched edges for steel sheets with tensile strengths of 390 MPa for high-strength low-alloy and 980 MPa for dual-phase steel on their surfaces and in cross-section. The clearance ratio, or c, is the product of the distance between the punch and die and the sheet thickness. The quality of the sheared edge is very good, given the low clearance ratio, and around half of it is burnished on the 390 MPa sheets. On the other hand, the 980 MPa ultra-high-strength steel sheet with limited ductility has a small burnished surface and a big fracture surface.

The sheared edge's quality suffers due to the small step separating the secondary burnished and fracture surfaces. Due to the short clearance ratio, the punch and die corners generated cracks that were not properly connected, resulting in the step. The quality of the sheared edge is impacted by clearance [38, 55].
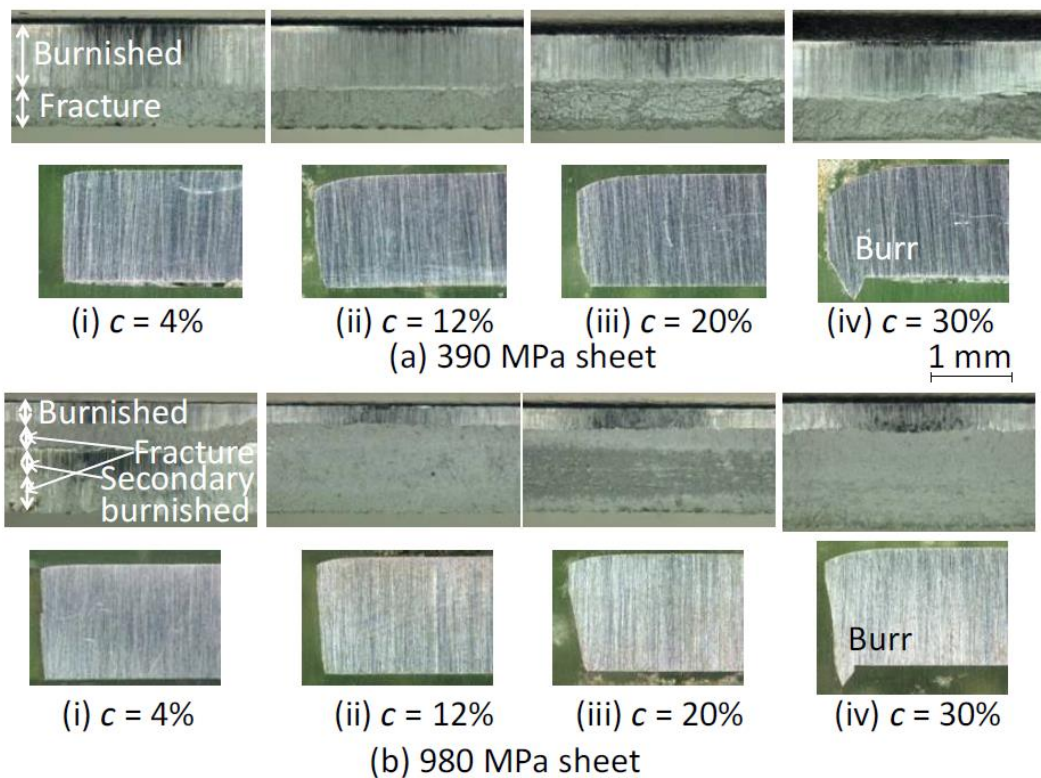
Figure 3.16. Cross-sections and surfaces of punched edges for (a) 390 MPa (b) 980 MPa sheets of high-strength steel [166].

The punching press's distortion is limited to a tiny area distant from the punched edge. Due to the limitation on the deformation area, it is difficult for us to study the microstructure and mechanical characteristics. In their earlier study, the authors

tried to conduct an investigation using nano-indentation testing. The hardness of punched DP steel was found to be unexpectedly close to that of cold-rolled steel, despite the edge having undergone significant strain hardening from the punching press [167]. It suggests that cold rolling would be a suitable substitute for the punching press's severe pre-deformation process for researching the changes in the microstructure and mechanical properties of DP steel brought on by severe pre-deformations because cold rolling uniformly deforms the entire specimen. To clearly define and compare the deformation area in punched DP steel with cold-rolled DP steel utilizing strain measurement and nano-hardness testing, it is more logical to conclude that [168].

3.6.3. Cutting Clearances: Burr Height and Tool Wear

Blanking is one of the most commonly used methods for producing sheet metal. The sheet metal continues to deform plastically as the punch moves forward until a fracture appears on both sides of the component, which subsequently expands and results in the final rupture. It has been shown in numerous experimental experiments that the blanking clearance affects the blanking force and the typical depth of the blanked profile for a particular material [169].

Some research on the blanking process has been proposed to gauge the effects of the process parameters. Mucha's experiments revealed that while punch-die clearance increases as a percentage, punch edge wear increases [169, 170].

They demonstrated the circumstances under which the punch-cutting edges wore out while drilling holes into a thicker AISI 52100 steel plate using punches with different convex shear angles. The main factor causing punch wear while using a punch with a convex double-shear angle of 12.5 is edge wear, according to experimental results. The interaction of abrasive, fatigue and adhesive wear causes it [171].

Examine the effects of different clearances on the height of the burr, the depth of the smooth shearing, and the blanking force. The trials employed aluminium sheet metals with thicknesses of 0.8, 1 and 1.5 mm. These tests used circular blanking dies with 6, 8, 10, and 12 diameters. Six alternative clearances (0.009, 0.064, 0.12, 0.175, 0.231, and 0.287 mm) were employed for every material and diameter. The results demonstrate that the clearance value significantly impacts punch force, burr depth, and smooth-sheared depth.

When the clearance value fell, it was found that the smooth-sheared depth, punch force, and rollover depth all increased while the rollover depth was reduced [172-174].

Figure 3.17 depicts the relative burr height variation for various clearances using experimental observations and finite element models. According to this graph, the smaller clearances between 2% and 21% show the greatest differences between projected and experimental findings. Additionally, Figure 3.18 displays the experimentally cut part's ultimate cutting gap (g) compared to the nominal [174].
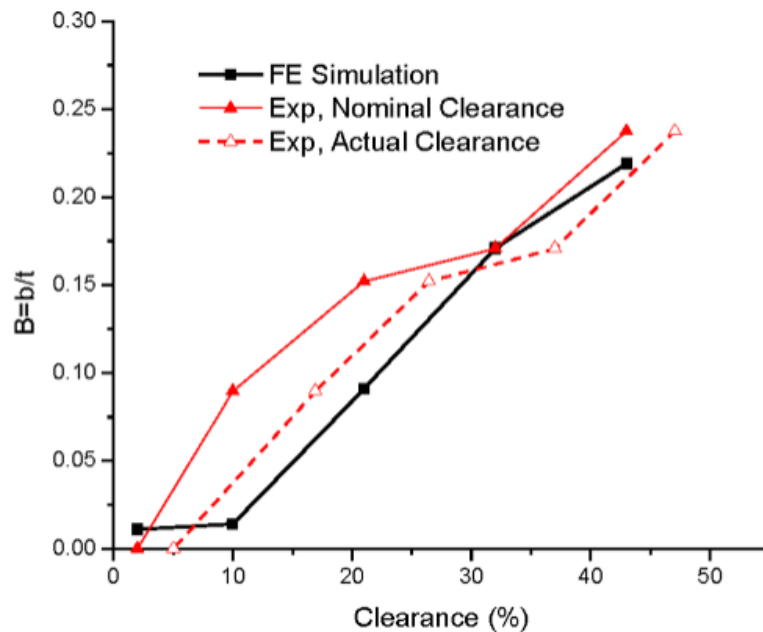
Figure 3.17. The fluctuation of experimental and finite element relative burr heights (b) for various clearances
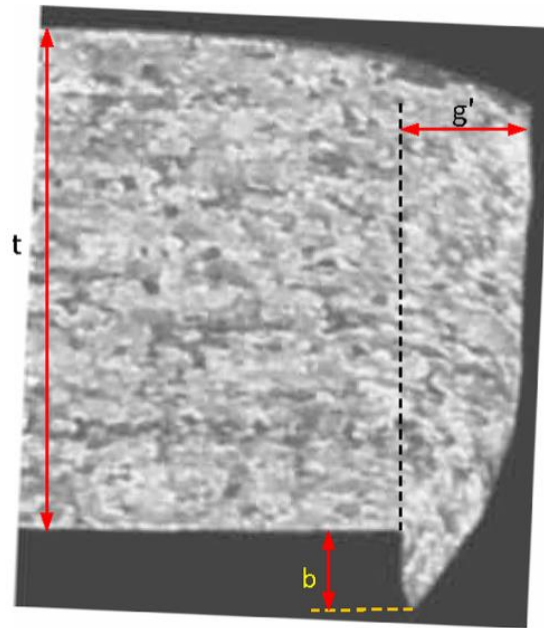
Figure 3.18. Blank thickness (t), The burr height (b), final cutting clearance (g), and cutting with a 21% clearance measure [174].

Experimental research determined the ideal tool hardness and die clearance values. Edge wear diminishes almost proportionally as clearance rises. The test findings also demonstrate that the amount of wear on the punch increases directly as the number of presses increases. Conversely, punch and die wear decreased as tool hardness rose. The cutting edge of the 60 HRC punch exhibits the creation of cracks, making the 3 and 5% die clearances inappropriate for 60 HRC punches when each of the factors that emerged throughout the blanking procedure is treated individually [175].

3.6.4. Cutting Clearances: General Recommendations

The distance between the punch and the die for cutting is essential in all sheet metal production.

The cutting clearance is always included in the die bushing for the particular cutting station. In addition to having the precise size of the hole to be cut, the punch also has a tolerance of. Although it is advised that the proper cutting clearance is between 0.08t and 0.10t per side, some manufacturers employ substantially wider clearances, up to

0.16t per side. Such a gap is typically too large, and the cuts it creates are frequently ragged and uneven. However, with bigger punches and thicker material, higher cutting clearances can be selected without negatively affecting the result.

On the other hand, tool makers for automatic NC machines (also known as turret presses) occasionally employ incredibly small clearances with impressive results. The secret of the process lies in the complete alignment of the punch with the die, which is held firmly in place within the thick ring of a turret and prevented from deviating by its precision-made sleeve. Small spring-loaded strippers are integrated into each assembly of this kind of tooling as independent miniature dies [151].

3.6.5. Punch Face Design

When using round-cutting tools, the face surfaces may occasionally be tapered (sheared), lessening the cutting force required otherwise. The argument behind this claim is as follows: The lesser quantities of press force are applied over a longer period since the punch slices the metal in stages.

In dies where the total cutting force will either exceed or be too near to the whole available press force, this technique for reducing the requirement for press force may be helpful. The required press force surge wave may be too much for the machinery when all punches penetrate the material. A delay in the demand is made possible by offsetting some significant cuts.

Punch or Die Surface using an Incline. Applying shear to the tool's face is one technique to lessen the required cutting pressure. The punch is machined at an angle such that its longest portion might start cutting before the rest of the tool (Fig. 3.19).

Unfortunately, such a configuration is relatively rudimentary since the shearing action is side-shifted rather than centered on the tool axis. As exhibited in Fig. 3. 20. a-e. a superior strategy is to shear the punch (or die) toward the center from

both sides. Due to the surface's center-oriented inclination, cutting forces are distributed more uniformly across the punch during a centered-cutting procedure.
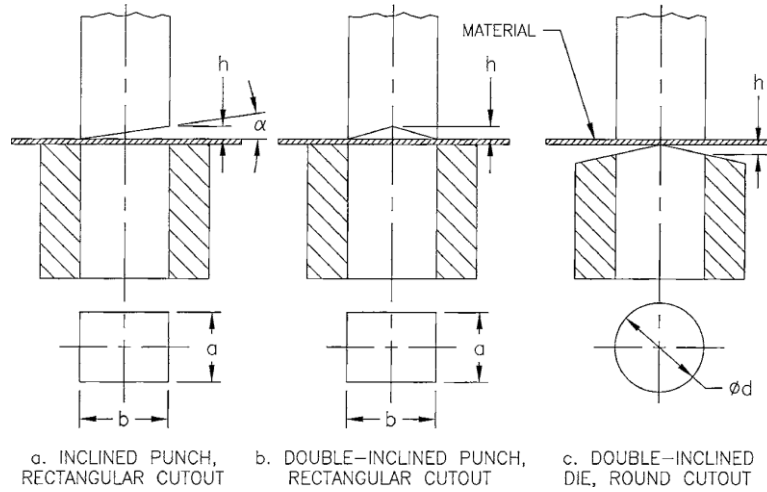
Figure 3.19. Sheared punches[151].
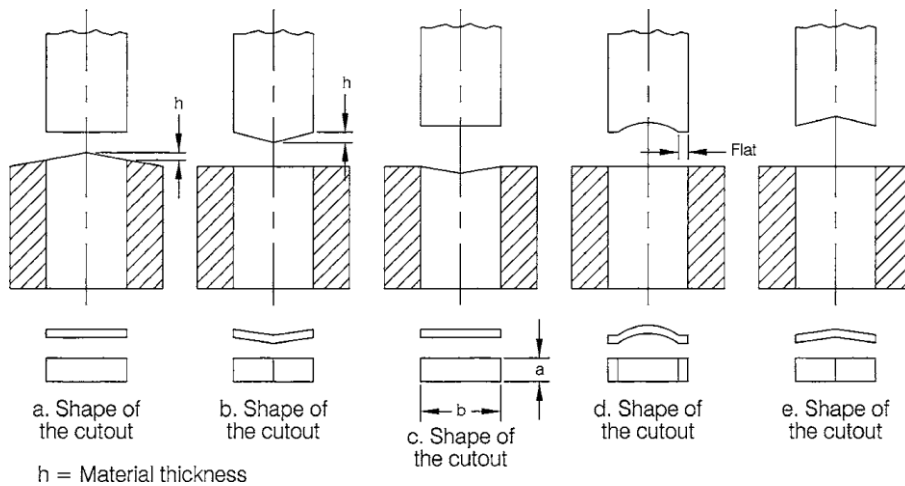
Figure 3.20. Punch and die shear[151].

Cutting surfaces on either the punch or the die can be sloped, with certain thin materials requiring 1.5t of shear, with the amount of shear being equal to the material thickness.

Since the cut-out piece or slug always resembles the shape of the punch, it is better to apply the shear to the part of the tooling that is become the scrap. The punch and die are sheared in this fashion, whether used for piercing or blanking. Here, the punch simultaneously enters the material at both ends of the cut, centered within

the die opening, making the C method of tool face adjustment, shown in Fig. 3.20,c, preferred. A minor inclination is formed on the die button [151].

PART 4

FEM ANALYSES

4.1. SIMULATION OF FORMING OPERATION BY FEM

Since the flow stress and strain distribution are influenced by the deformation temperature, strain rate, and strain [176], industrial metalworking processes have been anticipated and modelled using physical simulation approaches, such as the Gleeble® thermal and mechanical simulators [176-179]. However, these laboratory techniques encounter optimization issues caused by the deformation process, such as the growth of heat caused by the frictional forces between the anvil and workpiece [180]; this alters the behaviour of the flow. The complexity and unevenness of the production process brought on by heat generation affect the final product's attributes [181].

Historically, the industrial production process has been expensive since it relies on the designer's expertise and the "trial and error" method [182, 183]. Process improvement is required to lower manufacturing costs through a more effective design strategy [178] in metal-forming processes [183]. Reduced manufacturing costs necessitate process improvement. Finite element modelling (FEM) computer software applications like Deform® 3D, Abaqus, Marc, ANSYS, etc. have recently been used to assess and optimize the most common metal forming procedures [184, 185], which has reduced the manufacturing cost and time [186]. To foresee metal flow behaviour and deformation loads, researchers have studied several elements of metal forming processes using FEM simulation codes [181, 183, 184].

4.2. PUNCHING PROCESS OF SHEET METALS

Uncertainties exist regarding the impact of several punch sites on sheet deformation, the relationship between load and tool clearance, and other difficulties. The sheet gradually stretches during the forward punch stroke of a blanking or punching

operation. Occasionally, a very localized plastic deformation happens close to the punch and die's edges. At some point in the punching path, cracks start to form due to this localized distortion. With additional forward punch travel, these tool edge fractures eventually separate through the thickness of the sheet [187].

In the process of blanking, the blank quality is of utmost importance. It heavily depends on the blank edges' quality and the sheet plastic's distortion. How a crack spreads along the entire sheet width affects the blank edge's quality [188].

They investigated the spread of cracks using the rigid plastic theory, using the Holloman equation to simulate the material's behaviour and assuming McClintock's strain-based criterion governs fracture [189].

PART 5

EXPLOSIVE WELDING

A high-velocity oblique collision between the components to be linked is created by explosive welding, which is essentially a solid-phase welding technique. Although they were unaware that it was a welding procedure, ordnance professionals initially accidentally discovered the technology. Armament specialists in World War I was reasonably aware that bullets or shell pieces would frequently attach to the metal target plates against which they had been struck [190].

Carl wrote the first paper on explosion welding ever published [191]. In 1944, Carl saw two thin brass discs connecting used in standard, traditional explosive evaluation tests to orient the explosive charge. A part of the aluminium U-channel soldered to the steel die during the explosive formation of the channel, and it was later reported [191]. The explosive welding process has evolved from these odd origins to the point where it is now acknowledged as a valuable joining technology for various applications. Over 260 different and equivalent metal combinations have been successfully combined using explosion welding [192].

5.1. EXPLOSION WELDING PROCESS THEORY

Most scientists believe that the jetting action, which occurs in high-velocity oblique impacts, is crucial to the explosion welding process, despite different researchers having proposed diverse welding mechanisms. When two objects collide obliquely, it is known as a jetting collision[22]. A metal jet or spray is generated at the moment of impact and then accelerated to an extremely high speed before being ejected between the colliding objects. The main components and dimensions of an oblique collision are shown schematically in Figure 5.1.

The jet disperses and removes the surface films during the explosion welding process. The development of the jet during the oblique collision causes the metal surfaces to be scarfed or cleaned as they move toward the contact location[193]. A metallurgical bonding occurs across the interface when the dean or virgin metal surfaces are intimately brought into contact at the impact location by the tremendous pressure from the explosion. Two processes comprise the explosion welding process: first, the jet removes any obstruction-causing surface layers, and second, the high pressure drives the clean metal surfaces together so closely that interatomic forces can be created across the bond interface. Many decades ago, the relationship between jetting and shaped explosive charges was first thoroughly investigated [194]
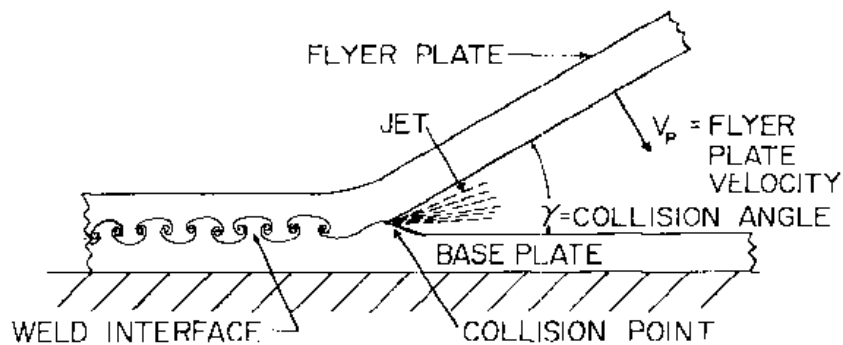
Figure 5.1. Schematic of an oblique collision achieved during explosive welding [191]

It was discovered that using a thin metallic liner in a shaped charge created a metallic jet with sufficient kinetic energy to pierce and cut through several inches of steel plate. Metallic liners are a modern innovation used in shaped charges for piercing and cutting [195]. The circumstances must be met for jet formation to occur in an oblique collision have also been thoroughly examined [196].

Early research in this field, mostly focused on shaped charge applications, has proven extremely helpful in creating useful cutting procedures and techniques. Recent studies [197]. have explored the criteria for jet generation in a standard welding setup. The results of this inquiry indicate the following important conditions for jet development:

1 The pressure generated just before the collision point must always be high enough to exceed the medium's dynamic elastic limit, regardless of whether the collision point

travels at a subsonic, sonic, or supersonic speed. Materials ensure that the metal surfaces are bent into the jet.

2. Theoretically, jetting happens at any oblique angle if the velocity of the collision site is kept at a subsonic velocity. However, a minimum angle is needed to meet the pressure requirements mentioned above.

3. Jetting happens at a particular critical angle if the impact point velocity is maintained at a supersonic velocity. The metal systems and the collision point's velocity significantly impact the critical angle for jetting. As was previously established, the requirement of having a pressure distribution larger than a critical angle is related to the collision point.

When the external variables—such as the type and quantity of explosive, the geometry of the weld, etc.—are controlled to yield the proper collision angle and collision point velocity for a jetting collision, good-quality explosion welding results. The ability to choose the appropriate values for the external elements, which is covered in more detail later in this review, is a requirement for the explosive welding process.

A weld contact resembling that in Figure 5.2 is produced when every element of the explosive welding process is correctly managed. The interface's look, which resembles ripples or waves, makes explosion welding unique. Explosive welding, as a whole, has garnered much interest due to the distinctive appearance of the weld contact. Numerous studies have examined the instances and processes of wave production at the explosion-weld interface [192, 198-200].
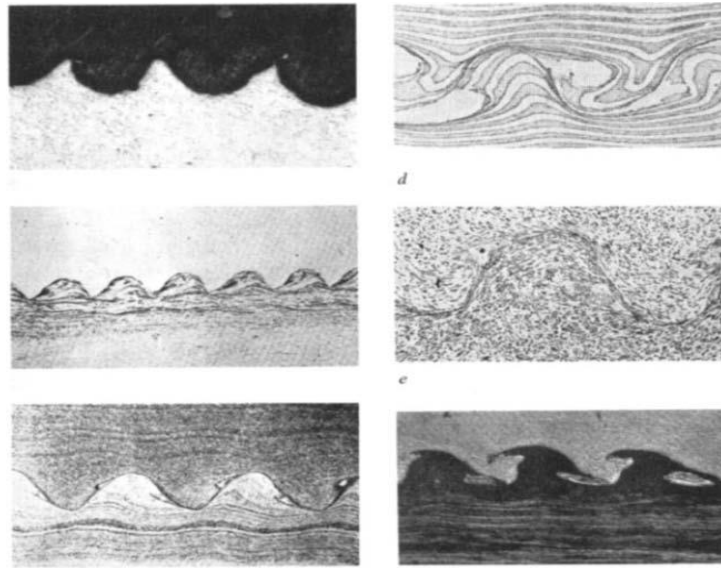
Figure 5.2. Explosion-weld interfaces that are typical (100 x). (a) Mild steel and lead explosive welding (top of photograph); (b) Stainless steel explosion welded to columbium (top of photograph); (e) 4130 steel explosion welded to 4130 steel; (d) explosion welded interface of a sample made of alternate layers of Copper and Nickel Electroplate (each square is 0.0005 in. x 0.0005 in.); (e) explosion welded 1018 steel to 1018 steel; and (f) explosion welded Ni to Cu[191].

Given that the wave structure has been observed in jetting settings rather than welding conditions, it is evident that the development of the wave structure depends on the creation of jets [198].

It is challenging and hard to fully analyze the variables impacting the evolution of the wave structure. Simulations in mathematics [200] have been proposed to explain how the wavy interface formed in great detail. Readers interested in learning more about the mathematical treatment should consult the cited sources.

The graphical representation in Figure 5.3 provides a physical understanding of what transpires throughout the wave pattern's creation.
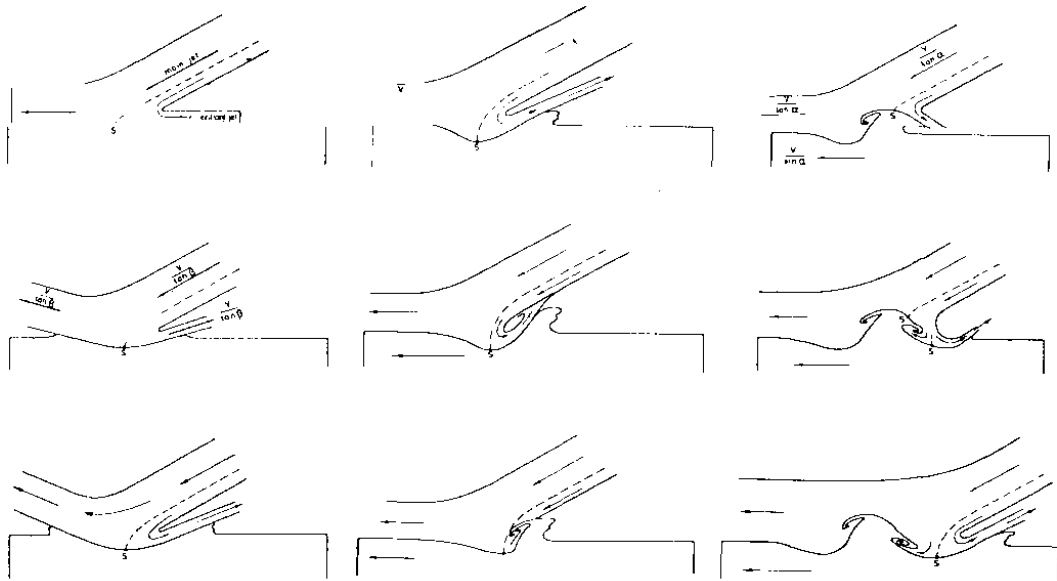
Figure 5.3 Diagram showing the development of the wavy interface during the explosion welding process [191]

This diagram of the wave creation at the weld contact illustrates how it develops gradually, as predicted by Bahrani et al. [191].

Most investigators consider this illustration a fairly accurate depiction of the explosive welding process. The only thing that needs to be adjusted is that the jet should be constructed entirely of base plates rather than just cladding plates. Figure 5.3 shows that while the one on the wave's leading edge should be rich in cladding plate material, the one formed by the jet should be rich in base plate material. Bahrani & Crossland [191] measured the swirls' composition concerning their location using microprobe analysis. The results of the microprobe traces over the swirls have confirmed it. It is clear that during welding, The oblique contact jet's path is incredibly complicated. Not all of the jet is released from between the plates because a considerable part of the jet becomes caught in the swirls or eddies on each side of the wave crest. The portion of the jet that is released and not entangled in eddies or swirls is known as the free jet. The baseplate, the cladder, and the surface films' substance will all be thoroughly mechanically mixed into the swirls and eddies. When the immense kinetic energy of the constrained jet is transferred to heat, these regions frequently melt. The substance in the vicinity quickly cools [197], and the melting pocket solidifies at the swirl when the temperature rises to melt. The weld features are unaffected if the molten pockets

are small and distinct. In the area between the swirls, the two plates are mechanically related to one another directly. A continuous layer of molten material is present at the weld interface if the factors that affect the creation of the jet—such as pressure, collision point velocity, etc.—are not correctly managed, as shown in Figure 5.4.
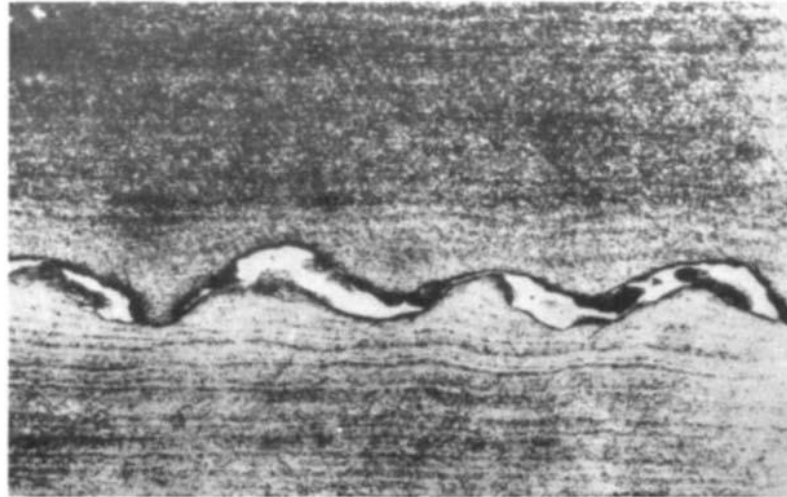
a
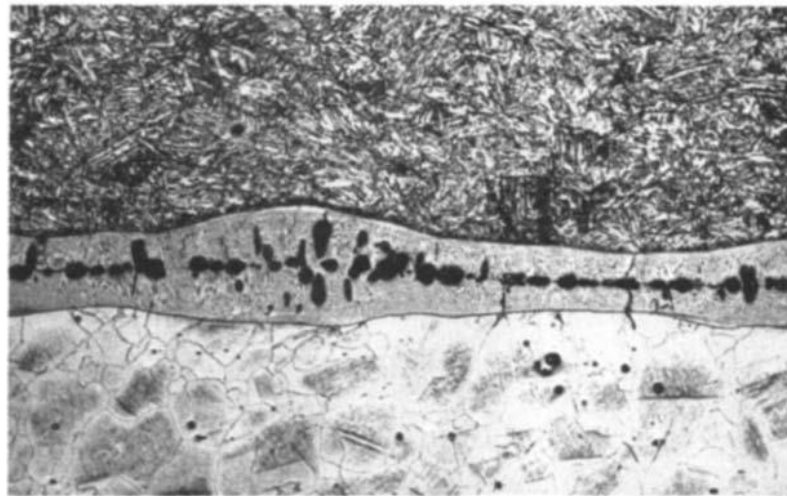
b

Figure 5.4. Interfaces between explosion welds that have too much-melted material (100 times). Too much explosive was used in (a) an explosion weld of 4130 steel to 4130 steel and (b) an explosion weld of Inconel to stainless steel.[191]

Due to the large jet and excessive material trapped at the contact, an interface with a continuous molten layer has been formed. Similar to the previous example, inadequate jet size can result in little to no bonding between the metal surfaces due to poor parameter control. Williams, Dhir, and Crossland researched the swirls or vortices created at the interface of explosive welds [201]. Their findings suggest where the

vortices melting and alloying take place. The nonequilibrium effects could be expected to be similar to those seen in splat cooling based on estimates of the cooling rates. Their analysis of the vortices in various distinct metal-weld interfaces X-ray diffraction demonstrated that the alloy compositions of the explosion-weld vortices significantly deviate from equilibrium conditions. Microprobe investigation and electron microscopy (replica and transmission), when used to examine an explosion-weld interface like that in Figure 5.2, both support the sudden change in metal composition between the swirls. Composition analyses utilizing electron microprobe traces reveal a discontinuous transition between two metal plates, demonstrating the absence of a diffusion layer at the interface. High-magnification electron microscopy-based investigations [202, 203] have dispelled scepticism regarding a diffusion layer's presence. Sections of the explosion-weld contacts are shown at extremely high magnification in Figure 5.5.

The images presented offer convincing proof that explosive bonding is a metallurgical bond. Data and information on the quantity and distribution of defects such as dislocations, micro twins, and stacking faults are other outcomes of the transmission electron microscopy examinations. Describing the fault structure at the weld interface accurately is quite challenging. Numerous microstructural characteristics may be anticipated because of the unequal distribution of loads and local temperature fluctuations along the contact. Although most welding is done at modest pressures (below 100 kbar), the weld interface experiences significant plastic deformation.

Regarding Figure 5.2d, it is clear that 90% of the length or thickness of the 0.001-inch thick layers have changed close to the interface. Despite the extreme cold working close to the interface, the material seems unaltered from a distance of 0.010 inches on each side. One can further quantify the degree of plastic deformation by monitoring the lengthening of the interface by the ripple pattern. The average of several measurements reveals that the interface is frequently enlarged by about 150%. The high plastic deformation is cause considerable changes in the defect structure at the contact.

According to research using transmission electron microscopy[202, 203], About 1011 dislocations per square centimetre are present. The high dislocation density and metal flow at extremely high strain rates result in a significant concentration of vacancies. Even though it only extends a short distance on either side of the weld contact, the defect structure along the interface should be extremely recognizable and contain dense dislocation tangles, a high vacancy concentration, and maybe large numbers of micro twins. The defect structure, caused by the considerable plastic deformation at the interface, is thermally stable to rather high annealing temperatures, according to two recent tests [201, 202], on various metal alloys. In one investigation, the atomic diffusion over the Cu-Ni weld's explosion-weld interface was compared [204], similar to what was seen in a roll-bonded composite created from the same substance. The findings show that the explosion-welded pair has significantly superior diffusion to the roll-bonded composite. The outcomes are contrasted in Table 5.1.

Table 5.1. Cu-Ni diffusion data comparison [191]

Type of Composite	Activation Energy (Q)	Frequency Factor (D_0)
Explosion welded	36,400 kcal/mole	1.09×10^{-4} sec^{-1}
Roll-bonded	53,000 kcal/mole	1.9×10^{-1} sec^{-1}

5.2. BASIC EXPLOSION WELDING CONFIGURATIONS

In the process of explosive welding, there are two basic configurations:

- The first is the ongoing standoff situation.
- The stand-off arrangement with a fixed angle.

Each of these configurations offers a difference between the flyer and base plate. In the initial standoff, there are two variables at work. First and foremost, the stand-off offers a space over which the flyer plate can be propelled to the required impact velocity for jetting and welding. Even though a straightforward method for calculating the velocity-distance profile has not been developed, the flyer plate is driven to its maximum velocity for welding at a distance of between 1/10 and 1 times the flyer plate

thickness. The explosive's detonation parameters and the metal's physical properties determine the velocity-distance profile.

Creating a clear channel for the free jet and the air between the plates is another crucial duty of the standoff. Most of the flyer plate's kinetic energy is converted into jet energy (both free and restricted) during the collision phase [205]. The free jet is thought to collide with the stand-off air, transforming it into a plasma flame that the crashing plates sweep away. Additionally, it is believed to cause swirls and eddies inside the confined jet that frequently result in melt pockets appearing along the interface when it collides obliquely with the flyer and base plate surfaces, where the kinetic energy is transformed into heat on impact. The temperature rise of the flyer and base plate surfaces is minimal, and no melting occurs other than that brought on by swirls and eddies if the heat generated by the free jet is dispersed through a sufficient volume of gas in the stand-off and/or over a sufficient surface area of the plates. The jet's kinetic energy is quickly converted into heat at the surface of the plates if the jet is blocked by a dense object between the flyer and base plate or if the flyer or base plate is in the path of the jet exit due to the stand-off configuration. The consequent heat surge may exceed the melting point if the surface area is tiny, which would cause substantial melting and generally defective welds [205].

5.3. EXPLOSIVE CONDITIONS AND SHOCK RESULTS

Shock rarefaction's adverse effects have led to the employment of various explosives for explosive bonding. A significant discontinuity in pressure on one side of the transmitting medium separates the rapid motion brought on by high pressure from a practically silent situation in the natural material. This circumstance may result in tensile strains that are strong enough to break the explosive connection. Shock waves won't be audible if the shock front's velocity is below the transmission medium's sonic velocity. A definition of sonic velocity is[19]:

$$U_S = \sqrt{\frac{E}{P}} \qquad (5.1)$$

where :

Us = The sonic speed

E = A suitable elastic modulus

P = The substance density

If the shock wave propagation does not exceed the sonic velocity, the shock front expands, and the magnitude of the stress and stress gradients is greatly reduced. Utilizing explosives with detonation velocities in this range is preferred because the sonic velocity of most metals is in the 2000–6000 m/s range. According to Carpenter et al. [206], using explosives with detonation velocities greater than 120% of the metal's sonic velocity is not advised.

It has been shown that the explosive type's characteristic of detonation velocity is inversely proportional to explosive density. Eq. (5.2), calculated empirically for the nitroguanidine explosive, illustrates this proportion.[207].

$$V_d = 1440 + 4020 P_e \qquad (5.2)$$

where :

V_d = corresponding to detonation velocity

P_e = density explosion

Nitroguanidine typically operates between 2000, and explosive densities between 0.14 and 0.9 g/cm3 are equivalent to 5000 m/s.

Additionally, inversely related to explosive density is the explosive pressure, P., P_e, as the Bernoulli equation demonstrates:

$$p \; \alpha \; V_d{}^2 P_e \qquad (5.3)$$

The Gurney models can be used to calculate flyer plate speeds [208], provide the use of specific energy with a unique value for each explosive (the Gurney energy) and assume that the driven metal was propelled perpendicular to the direction of the explosion propagation. Kennedy [209] gave several reconstructions and thoroughly justified the Gurney model. Gurney equation reconstructions account for variations in geometry. The following equation can describe the parallel-gap explosive bonding method:

$$V_P^2 = 2E \frac{3}{\left[1+5\left(\frac{m}{c}\right)+\left(\frac{m^2}{c^2}\right)\right]} \tag{5.4}$$

where :

Vp = The speed of the flyer plate

E = The Gurney force.

m = Mass of the flyer plate

c = The mass of explosive

m/c = The factor for explosive load

If the flyer plate and detonation velocities are known, defining the dynamic nature of the flyer plate bend angle through geometry is simple. The following formula holds for the parallel gap geometry displayed in Fig. 5.5:
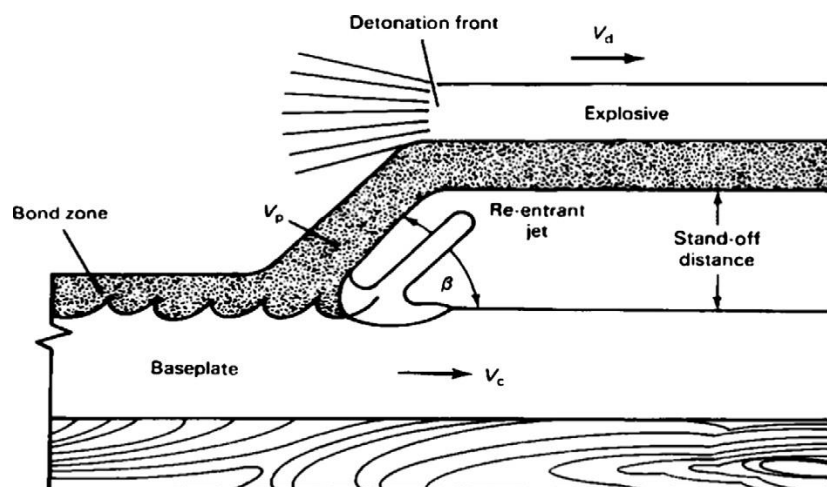
Fig. 5.5. Flyer plate deformation and impact resulting from a moving explosive detonation front, shown schematically [210].

$$V_P = 2V_d \sin \left(\frac{\beta}{2}\right) \qquad\qquad 5.5$$

where :

Vp and Vd are the speeds that are specified in Eqs. (5.4) and (5.5), respectively.

β = The dynamic bend angle of the flyer plate

The majority of models created for explosive bonding are based on Eqs. (5.1)–(5.5) and familiarity with metals' mechanical and physical characteristics. These models are then broadly discussed after briefly discussing bonding and the methods utilized to locate explosive parameter boundaries that produce acceptable bonds.

PART 6

THEORETICAL AND EXPERIMENTAL STUDIES

DP steels have been used as distinctive materials for the past forty years. Due to their effective crashworthiness, these steels are employed in the automobile sector, particularly in producing lightweight car bodies. Due to its capacity to combine metals with various melting temperatures, explosive welding is a special and appropriate method for creating plate composites employing metals and related materials. The advantages of DP-Al metal plate composites in terms of technology and cost make them one of the best combinations. On the other hand, the sheet metal sector relies heavily on the economic and technological advancements of blanking and piercing operations as manufacturing procedures. Generating the appropriate shear force for thick, high-strength material is difficult when cutting or piercing sheet metal and plate composites—higher performance standards for the press machines and cutting force increase as the punch and die wear increases. Applying a shear angle to the punch or die is one method to lessen the necessary force. Utilizing punches that have been machined into different shapes is another method. Therefore, a thorough investigation of the effects of punch shear angle and punch form on the critical forces for blanking/piercing operations was conducted in this work. Figure 6.1 presents an abstract as a flow chart that illustrates the research used in this study.
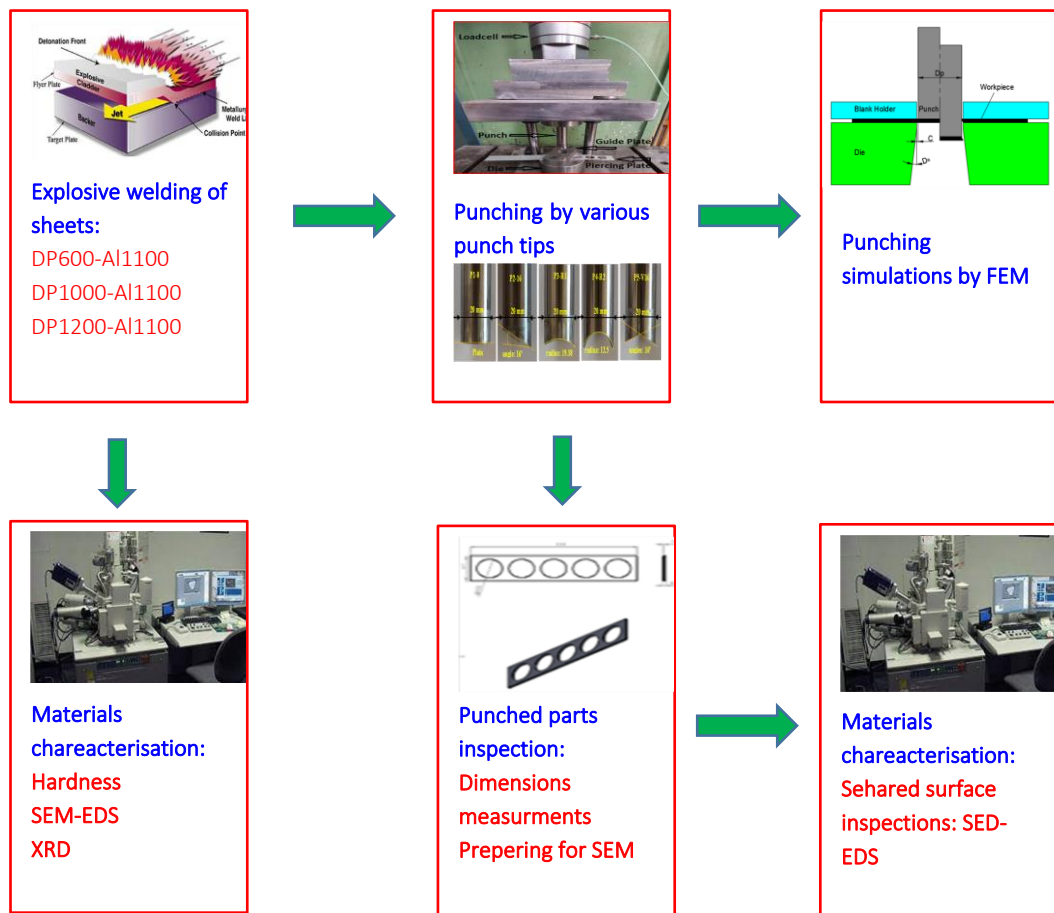
Figure 6.1. The flow chart of the studies applied in this thesis

6.1. MATERIALS AND CHARACTERISATIONS

In this study, steel and Al sheet have welded explosively. Then, Manufactured plate composites, base steels, and Al sheets were performed for punching experiments using different punch tips. Commercial dual-phase steel sheets were available in the DP600, DP1000, and DP1200 grades, and commercial aluminium sheets were available in the Al 1100 grade. In addition, The work samples were finely ground, polished, and etched in a 2% Nital (2% HNO_3 + 98% methanol) solution before being ready for microstructural analysis using the usual metallographic procedure. Utilizing an energy dispersive spectrometer (EDS), digital microscopy, and an optic and scanning electron microscope (SEM, Carl Zeiss Ultra Plus), microstructural characterizations and punching shear surface investigations were carried out.

6.1.1. DP600 and Al 1100

Tables 6.1 and 6.2 provide the chemical compositions of the DP600 and Al1100 materials used in the investigation. Steel sheets are 1mm thick, while Al1100 sheets are 1.4mm thick. Additionally, Fig. 6.2 provides information on the microstructure of the DP600 steel sheet.

Table 6.1. The chemical makeup of the DP600 steel sheet (wt.%).

Material	C	Si	Mn	P	Cr	Ni	Mo	Cu	Ti	V
DP600	0.123	0.265	1.763	0.02	0.22	0.033	0.05	0.015	0.003	0.005

Table 6.2. The chemical makeup of the Al1100 (wt.%).

Material	P	Ca	Si	Ga	Mg	Fe	Al
Aluminium	0,01	0,05	0.6	0,02	0,09	0.55	98.66

Figure 6.2. DP600- steel microstructure.

6.1.2. DP1000

Table 6.3 lists the chemical makeup of the DP1000 substance employed in the investigation. The sheet thickness for DP1000 steel is 1.2mm. For DP1000-AAl 1000 explosive welding, the sheet thickness is 1mm without explosive welding. For Al 1100, the sheet thickness is 1.4mm. Additionally, Fig. 6.3 provides information on the microstructure of the DP0100 steel sheet.

Table 6.3. The chemical makeup of the DP1000 steel sheet (wt.%) .

Material	C	Si	Mn	P	Cr	Ni	Mo	Cu	Ti
DP1000	0,136	0,203	1,57	0,021	0,003	0,022	0,039	0,136	0,203
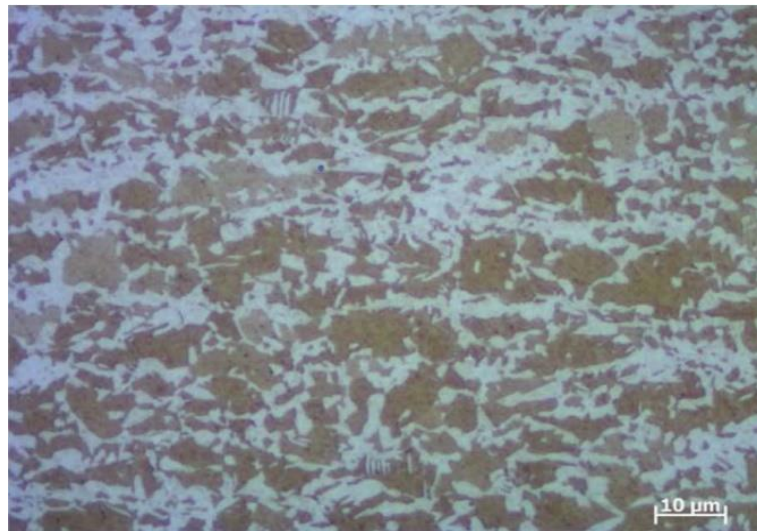
Figure 6.3. Micrographs of DP1000 steel showing the micro constituents ferrite and martensite.

6.1.3. DP1200

Table 6.4 lists the chemical makeup of the DP1200 substance utilized in the investigation. For DP1200 steel, the thickness of the sheet is 1mm. For Al 1100 aluminium, the sheet thickness is 1.4mm. Additionally, Fig. 6.4 provides information on the microstructure of the DP1200 steel sheet.

Table 6.4. The chemical makeup of the DP1200 steel sheet (wt.%).

Materials	C	Si	Mn	P	Cr	Ni	Mo	Cu	Ti	Fe
DP1200 Dual-phase steel	0.125	0.182	1.513	0.018	0.023	0.023	0.05	0.012	0.04	Rest of wt

Figure 6.4. Base materials OF DP1200.

6.2. EXPLOSIVE WELDING

To create the laminated bimetal composite, three pairs of sheets—DP600-Al 1100, DP1000-Al 1100, and DP1200-Al 1100—were fused explosively. The flyer plate comprised Al 1100 sheets, while the base plate was constructed from dual-phase steel. The explosion rate (R) was kept constant at 1.4 using the mass of the flyer plate and rubber. There was 1.0 mm between the base plate and the flyer plate. To decrease the distortion of the sheets during detonation, rubber layers were employed as a buffer zone between the DP1200 and the explosive and the Al 1100 and the anvil. ANFO (ammonium nitride plus 4-5% fuel) has a detonation velocity between 2500 and 3000 m/sn [211]. However, in response to our inquiries, 3.0% TNT was added to ANFO, and MKE Barutsan Company said that, based on their test results, the explosive's detonation velocity was 3200 m/sn when it contained 90% ammonium nitride, 4.5 fuel, and at least 3% TNT.

V'p (flying plate-Al 1100-velocity) was calculated using Equation 6.1, and according

to the explosion rate utilized in this experiment, it was found to be 1145 m/sn. Gurney's constant, the flyer plate's weight, and the explosive charge's mass are represented here by 2E, M, and C.

$$V^{\wedge'} p = \sqrt{2E} \ ((\sqrt{3})/(1+2M/C)) \tag{6.1}$$

Fig. 6.5 depicts a schematic picture of the explosive welding.
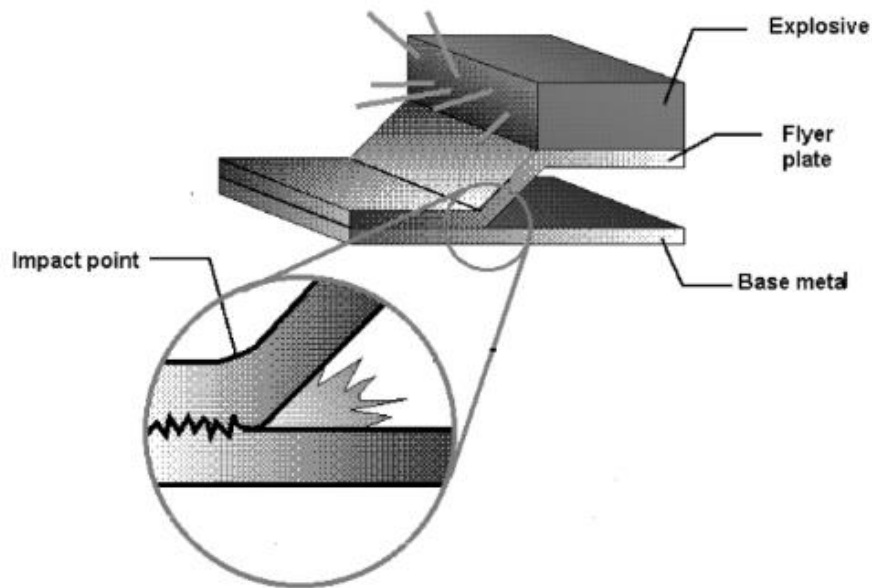
Figure 6.5. Schematic viewing of the explosive welding[212].

The best-known feature of explosive welding is its ability to directly combine a wide range of metal combinations, both comparable and dissimilar, that cannot be united by fusion welding or bonding methods. Explosive welding is particularly useful for joining materials with high melting points to materials with lower melting points, such as aluminium and steel, because it is essentially a solid-state process with no active large-scale heating or diffusion mechanisms [213].

High-strength, low-alloy (HSLA) steels classified as dual-phase steels have a microstructure comprising a dispersion of around 15–25% hard martensite particles in a soft, ductile ferrite matrix. These steels have several special characteristics, which are typically referred to as dual-phase characteristics. These characteristics include continuous yielding behaviour (no yield point), a low 0.2% offset yield strength, a high

tensile strength, a high work hardening rate, a typically high uniform and total elongation, and a high impact strength. After only 3-5% deformation, the high work hardening rate increases yield strength by roughly 150–200 MPa [214-216].

Flyer plates were made of aluminium, and parent plates were made of HSLA and dual-phase steels. The dimensions of the aluminium and steel plates were 1001502 and 10015010 mm, respectively[217]. The explosive substance chosen was ELBAR 5, which M.K.E. Barut Company, TR, provided. It contains 90% ammonium nitrate, a minimum of 4.5% fuel oil, and a minimum of 3.0% TNT.

The explosive material's detonation velocity is 3000–3200 ms−1[22].

6.3. TENSILE TEST

The foundation materials and the composite plate specimens made by explosive welding underwent a tensile test. On a Zwick/Roell 600 kN machine, tensile tests were performed using the ISO 6892-1 standard and a 2 mm/min tensile velocity. The real stress-strain curves were calculated using the engineering stress-strain curves derived from the testing. Fig. 6.6 provides a technical drawing of the tensile test sample.
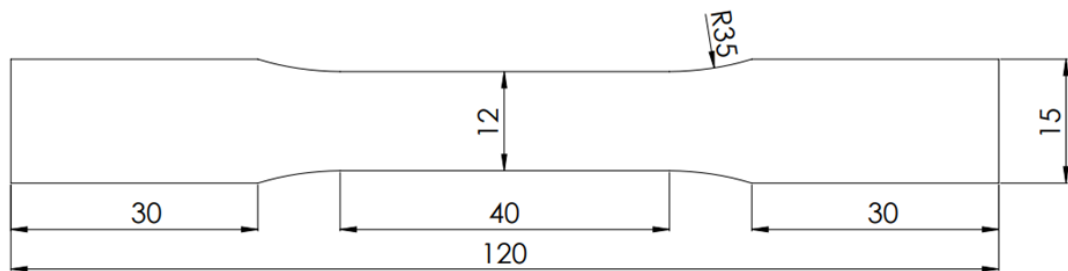
Figure 6.6. Tensile test sample.

6.4. PUNCHING OPERATION

The experiment used 20mm-diameter punches (DIN 1.3343, HSS). Fig. 6.7 displays five manufactured and utilized shearing punch tip forms. Wire EDM was used to shear punches from the HSS bulk. The ends of these punches were flat (P0°), concave (P R1 and P R2), and angled (P 16° and P V16). Numerical modelling in the Simufact software was employed in addition to the real investigation to simulate the punching operations to ensure these materials' shearing characterizations and strain-stress distributions.
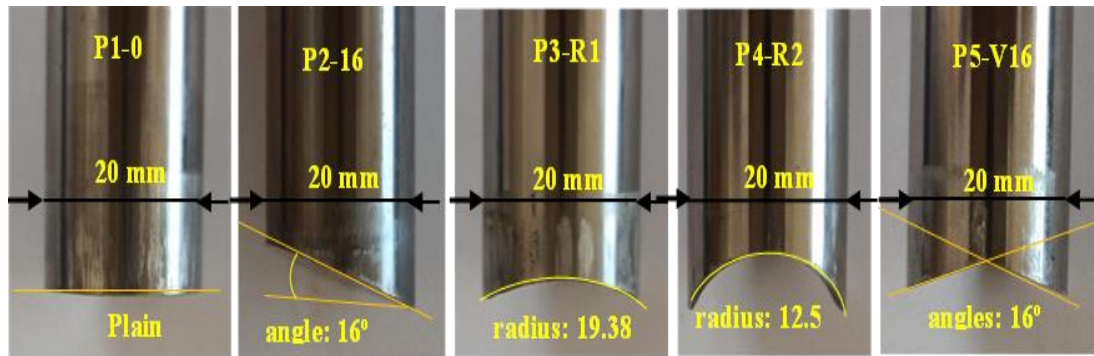
Figure 6.7. Types of punches employed in the experiments

The system of the Punching experiment and data (shearing force-time, F-s) received is schematically shown in Fig. 6.8. As seen in this figure, a modular mould was used to experiment. A load cell was attached to the upper portion of the mould during the trials to measure the loads instantly. The capacitance of the load cell was 240 kN. The data for this study is set at 2000 data points per second, despite the load cell's ability to read 10,000 data points per second. A load cell, data card, amplifier, and computer software were used to send the data from the die to the computer.
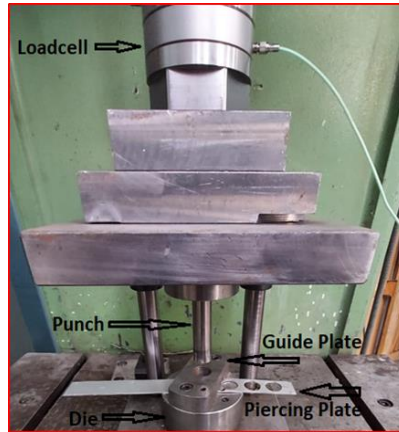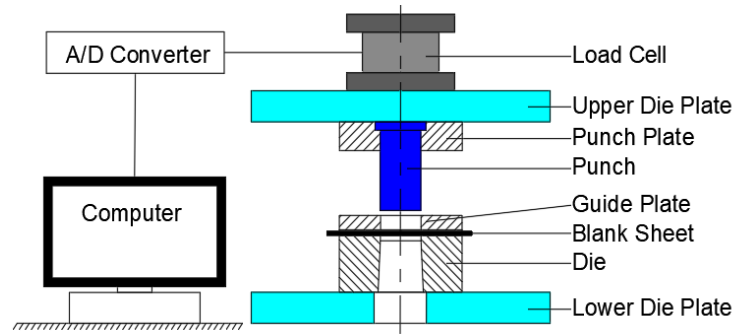
Figure 6.8. The experimental punch-die and load cell setup with samples as photos and technical drawings.

The punch, die, and blanking processes apply shear and stripping forces to the sheet material. When the punch action is at a straight angle to the die, the force required for a blanking operation is calculated using equation 6.2.

Derived from $F_{MAX} = \gamma \times L \times t \times \sigma_{UTS}$ (for flat punch) $\qquad$ (6.2)

Where;

L is the shear perimeter's length. σ_{UTS} is the substance's shear strength, γ is a factor, and t is the sheet's thickness. Dependent on various difficult-to-measure criteria, including the shape of the component, the lubrication, the sharpness of the die, and the sheet material's elastic limit/tensile strength ratio, is frequently between 0.6 and 0.9. Equation (6.1) can then be normalized to isolate the effects of material strength for various sheet thicknesses, and the part sizes are as follows:

In this research, According to (Eq.6.3), the maximum shear force was computed [218, 219].

Originating from Sp = F / Ap, $S_{max} = \frac{F_{max}}{L \cdot T} = \gamma \cdot \sigma_{UTS}$ (6.3)

The normalization of F is comparable. The shearing stress serves as a symbol for the normalized F and normalized F_{max}, S and the maximum shearing stress, S_{max} respectively.
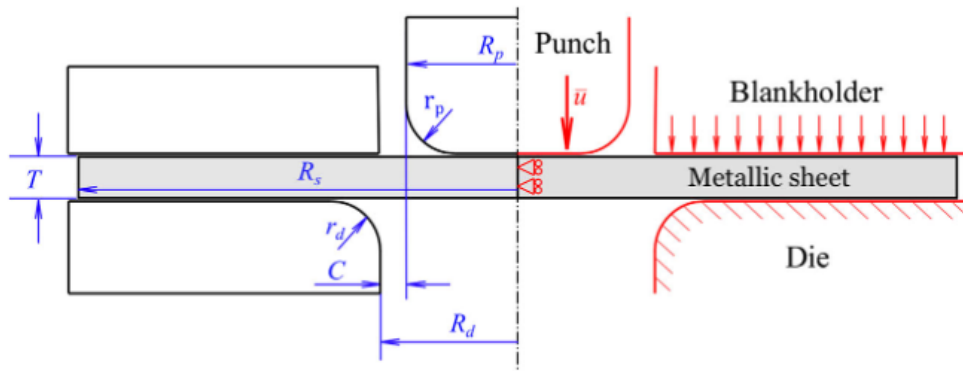
Figure 6.9. Important parameters in punching processes[220].

Table 6.5. Boundary conditions used in punching.

Sheet metal material thickness, T DP1200 and DP600	1 mm
Sheet metal material thickness, T DP1000	1.2 mm
Aluminium sheet thickness. T Al 1100	1.4 mm
Space between punch and die C	%4×T
Punch radius, Rp	10 mm
Die corner radius, rd	0,01 mm
Punch corner radius, rp	0.01mm
coefficient of friction	0.1
Press speed, Vp	1.5m/s

6.4.1. Fem Analyses

The tensile test results were used to determine the material properties of the materials (DP600, DP1000, DP1200, and Al 1100) and the bimetal-composite plates (DP600-Al 1100, DP1000-Al 1100, and DP1200-Al 1100). The SolidWorks design program created the geometric model, which was then loaded into the Simufact simulation

application. The correlations between tangential and normal surfaces' chances of making contact were developed using a friction factor typical of the materials used. Only the sheet material was used to define the mesh structure. The blank holder, punch, and die plates were considered solid beings. The mesh of the sheet material consists of 3000 tetragonal units. The numerical model was evaluated using nonlinear static analysis since no inertia forces existed. The die was entirely fixed when the boundary conditions were defined. In contrast, the sheet material's symmetric blanking resulted from the punch displacement in the vertical axis. The analysis could be done again after changing the punches. The punch velocity was set at 50 mm/s for all analyses. Fig. 6.10 depicts the simulation configuration utilized in the FEM analyses.
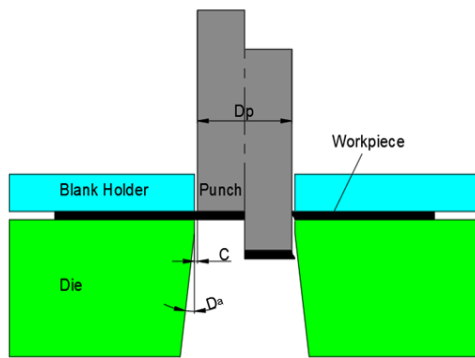
PARAMETERS	VALUE
Punch tip shape	Varied
Punch diameter (Dp)	20mm
Die cutting angle (Da)	2°
Clearance (C)	0.05 mm
Punch velocity (V)	50 mm/s
Mesh density	3000 tetragonal
Coefficient of friction	0.1

Figure 6.10. Cutting/punching FEM Simulation Setup.

6.5. DIMENSIONS AND SHEARED SURFACE ANALYSIS

After punching, product diameter dimension measurements and cutting surface analyzes were performed using a stereo microscope. Size measurements were made vertically under a stereo microscope. The samples were split half along the axis using a saw for the cutting surface analysis. The cutting profile was used to assess the cutting surfaces. In the cutting surface examination, the images of the cutting regions considered in the literature were obtained. The stages of the damage analysis investigations in the flowchart display the study's elements. For example, samples are cut at their center and inspected in two directions, as shown in Figure 6.11. Sheared surface quality was inspected by SEM electron microscopy.

X

A

B

y

- SEM inspection direction, and
- Inspection points

Strip moving direction in punching
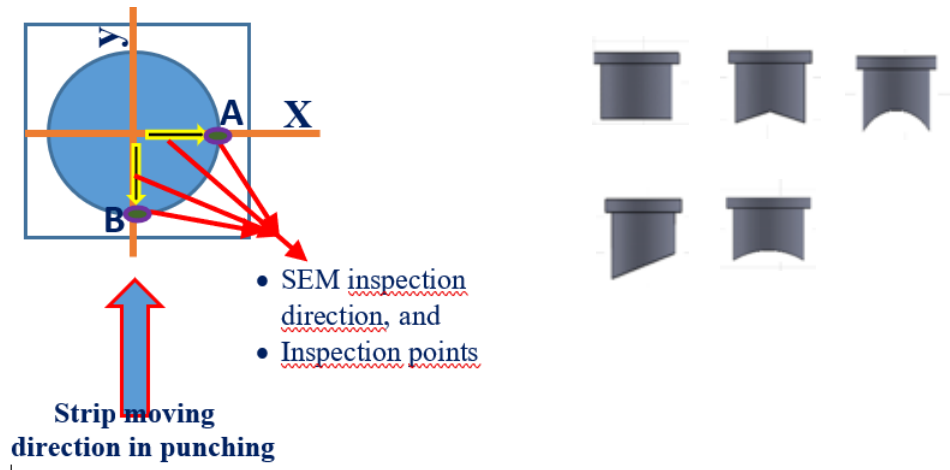
Figure 6.11. SEM inspection viewing

PART 7

RESULTS AND DISCUSSION

7.1. MICROSTRUCTURES OF PLATE COMPOSITES FABRICATED VIA EXPLOSIVE WELDING

7.1.1. DP600-Al 1100 Plate Composite

Fig. 7.1 shows the DP600-Al1100 steel microstructure after explosive welding, with SEM images and EDS analysis as interface and base materials.
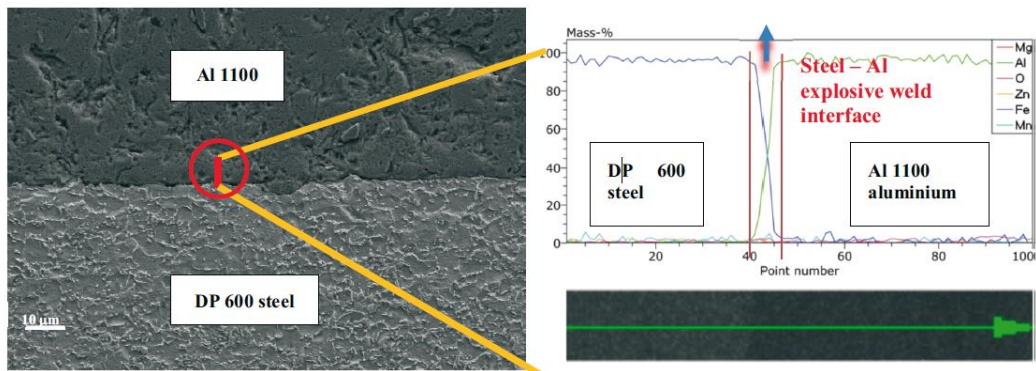
Figure 7.1. The SEM photos of DP 600-Al 1100 sheet samples that were explosively welded were analyzed using an EDS map.

Etching with 2% Nital revealed the composite's steel and Steel-Al interface character. DP600 steel contains soft-phase ferrite and highly durable second-phase martensite. This structure is the classical DP steel microstructure. Due to this structure, even though it has a high strength value, there is some martensite-ferrite orientation The biphasic steel piece at the interface deformed in that direction due to the explosive welding collision's high energy output.

Except for the interface, the basic material's microstructure remains unchanged, as shown in Fig. 7.1. Conversely, the interface of the composite structure created by DP steel-Al explosive welding jointing is partially flat and wavy. This wavy interface: The high collision surface is due to the energy burst density. Researchers[22, 221-226] reported that explosive welded joints could exhibit a flat, partially wavy, and often wavy interface between two metals. Intermetallic formation occurs at these interfaces depending on the properties, compositional abilities, and explosive weld parameters of two similar or dissimilar metals joined by an explosion[22, 221-226]. In this study, as demonstrated by the SEM-EDS studies and photos in Figure 7.1, it has been observed that an interface with a Fe-Al mixture at the interface and a region of about 2.9 mm thickness, up to the wavelength level occurs in areas where protrusions indent the steel part. Due to the high melting rate on the Al side, it gives a more flat appearance.

7.1.2. DP1000 - AL1100 Plate Composite

Commercial sheet materials in the DP1000 and Al1000 grades were employed in this study. Their relative chemical compositions are listed in Tables 6.3 and 6.2. Additionally, DP1000 and Al100 had thicknesses of 1 mm and 1.4 mm, respectively. The interface of the composite DP1000 and Al1000 plates created by an explosion is depicted in Fig. 7.2 using an SEM image and an EDS analysis.
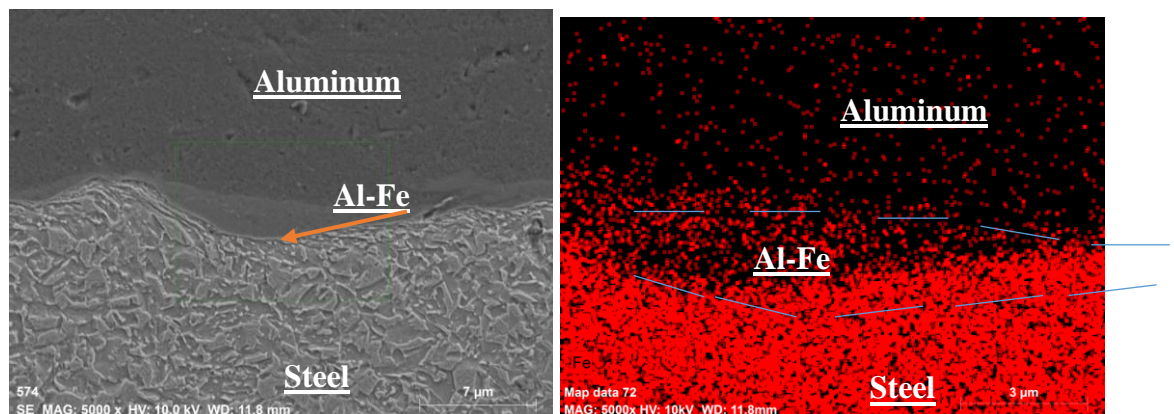
Figure 7.2. SEM photos of the explosive weld contact of the DP 1000-Al 1100 sheets with EDS analysis.

Fig.7.2. The DP1000-Al1100 explosive source microstructure as interface and base materials with SEM images and EDS analysis. Etching with Nital deduced the steel part of the composite and the Steel-Al interfacial character. This figure demonstrates that the soft phase ferrite in DP1000 steel has a rather large volume proportion of strong phase martensite. The single-phase features of this traditional dual-phase steel structure include good formability, low yield, high tensile strength, and high hardening. Due to the enormous energy produced by the explosive weld collision, this structure shows martensite-ferrite orientation in the deformation direction of the dual-phase steel portion at the interface while having a high strength value.

In this study, the interface of the composite structure produced by DP steel -Al explosion-weld joint was formed as wavy, as seen in Fig. 7.2. This is the wavy interface; It occurs due to the high collision surface energy due to explosion intensity. Researchers[193, 227, 228] reported that explosive-welded junctions could exhibit a smooth, partially wavy, and generally wavy interface between two metals. They also said intermetallic formation occurs at these interfaces depending on the properties of two similar or different metals joined by an explosion, their compounding abilities, and explosive welding parameters. In this study, as understood from the SEM-EDS analysis and images given in Fig. 7.2, it is understood that Fe-Al intermetallic is formed from the chemical Fe-Al mixture. It is observed that these interfaces occur in a region of about 3 micrometres thick, up to the wavelength level, in the areas where the protrusions indent the steel part.

On the other hand, a minimal intermetallic formation is observed in the Al part, where the steel material enters Al. Also, a severe deformation in the DP part is kept in the wave cape adjacent to the interface in this region. However, it is observed that melting is more effective than deformation in part formed towards the steel part, in which Fe-Al intermetallic is formed, and the deformation is minimalized. Basariya and Mukhopadhyay[229]. reported intermetallics formed in this molten/solidified region, Fe-Al intermetallic and mainly Al_3Fe, Al_5Fe_2, and Al_2Fe compounds. Like most intermetallics, these intermetallics are hard and brittle. Interfacial separations seen in some areas of punching processes can probably be considered a disadvantage of these strong and brittle intermetallics[229].

7.1.3. DP1200-AL1100 Plate Composite

The interface of explosively welded specimens of DP 1200-Al 1100 sheets with hardness values (HV 0.3) in a line perpendicular to the interface is depicted in Fig. 7.3 using SEM pictures and EDS analyses. As shown in Fig. 7.3, a difficult phase, martensite, makes up a very high volume percentage of the ultra-high-strength DP1200 steel (VFM). About 75% of this value is martensite, while 25% is soft-phase ferrite. An explosive joint with an uneven, wavy interface is also supplied, as seen in this figure. The employed Al sheet has not been further classified as microstructural because it has a well-known, unalloyed, single-phase structure.
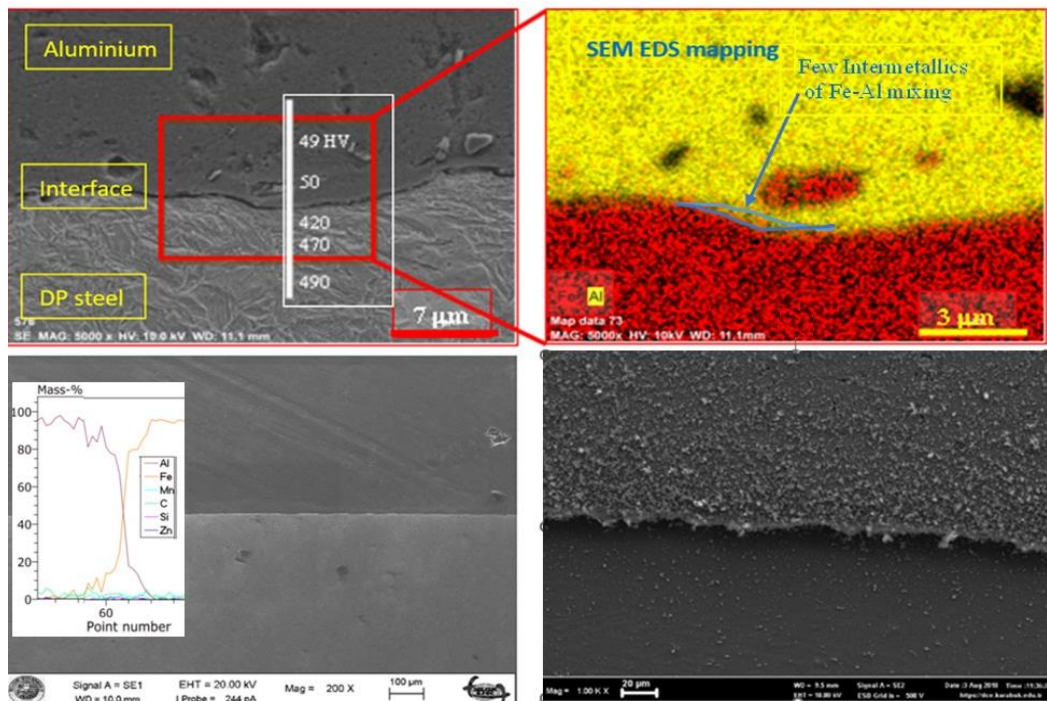
Figure 7.3. Explosively welded metals and interface according to EDS analysis (chemical.

According to the researchers, few intermetallics were generated at the bimetal's explosive welding contacts, as shown in the EDS study in Fig. 7.3. [19, 230, 231]. The steel particles can be seen to split at the interface and move toward the aluminium-rich interfacial regions. According to studies, the settings and conditions of the explosive welding process determine how the interface is created, making the elements of Al between the steel wave particularly susceptible to vortexing and melting [212, 230].

This situation can be assessed due to melting and vortexing due to the enormous energy released by the rapid impact of the aluminium and steel pieces' surfaces during explosive welding. The strong strength, high melting point, and limited steel melting of the DP1200 steel part also allow for assessing the interface's prolonged, uneven, and wavy appearance. In addition, some minute steel particles penetrate the Al side during the collision and produce waves, as shown in the EDS study in Fig. 7.3.

However, as shown in Fig. 7.3, the hardness of the DP1200 dual-phase steel decreased in the vicinity of the weld interface compared to distances from the interface or the original DP steel. These observations might be explained by martensite tempering and ferrite softening at the interface due to the enormous energy released by the collision of explosive weld portions during the explosion. Martensite is significantly more common than ferrite phase in DP1200 or other commercial dual-phase steel grades, such as DP1000, DP800, etc. These findings may also address the limited intermetallic formation. Previous researchers brought attention to the situation. In a welded heat-affected (HAZ) zone, martensite's mechanical characteristics may decrease after being heat-tempered. The first instance of this phenomenon, When DP steels were flash butt welded for rim applications, a process known as HAZ softening occurred [79, 232, 233]. [43] [234]. The maximum practicable HAZ softening is a linear function of the steel martensite composition, and the HAZ softening of a DP steel weld is a sigmoidal function of the weld heat input. A method for attaching solid-state components is explosive welding. As a result, in the metals that are explosively welded, the HAZ zone does not form. However, localized melted-solidified patches depending on the explosion rate, be observed close to the interface. As was said previously, actual melting-solidification took place during explosive joining. Tempering may have resulted from the contact's high temperature from the explosion. The hardness often increases near the contact because explosive welding involves significant plastic deformation. However, a temperature rise can stop the hardening from happening.

7.2. TENSILE TEST

Figure 7.4 shows the engineering and actual stress-strain curves for the three materials used: DP600, Al100, and explosively welded bimetal composite. Al sheet material shows low strength and hardening and, therefore, low yield/tensile strength ratio-yield ratio. DP600 steel, contrasted, offers a strong yield rate compared to its high strength. The composite sheet, joined by the explosion from these two primary materials, shows tensile properties close to the mixing rule of the two materials[235]. True stress- true strain values are used predominantly for force calculations of punch operations.
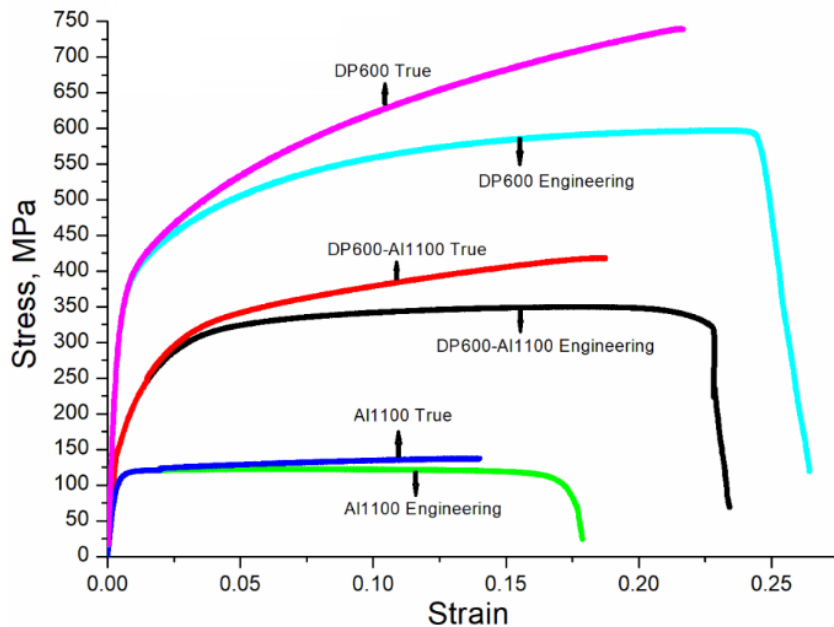
Figure 7.4. Tensile test results for DP600, Al1100, and explosively welded DP600-Al1100

Table 7.1. Tensile test results as engineering and true stress-strain values.

Group number	Materials	%0,2 Proof Yield stress MPa	UTS MPa	True stress MPa	Engineering strain (%)	True strain (%)
1	DP600	420	598	740	20	25
2	Al 1100	117	119	135	17.5	15
3	DP600-Al1100 plate composite	290	350	418	18	22

The materials' actual stress-strain curves and engineering (DP1000, Al100, and explosive welded bimetal composite) are given in Fig.7.5. Table 7.2. shows results of

the tensile test on Al, DP steel, and DP-Al plate samples were typical tension flow curves correctly all samples character. Al sheet material shows low strength and hardening and, therefore, low yield/tensile strength ratio-yield ratio. DP1000 steel, contrasted, offers a strong yield rate compared to its high strength. The composite sheet, joined by the explosion from these two primary materials, shows tensile properties close to the mixing rule of the two materials[235]. True stress- true strain values are used predominantly for force calculations of punch operations.
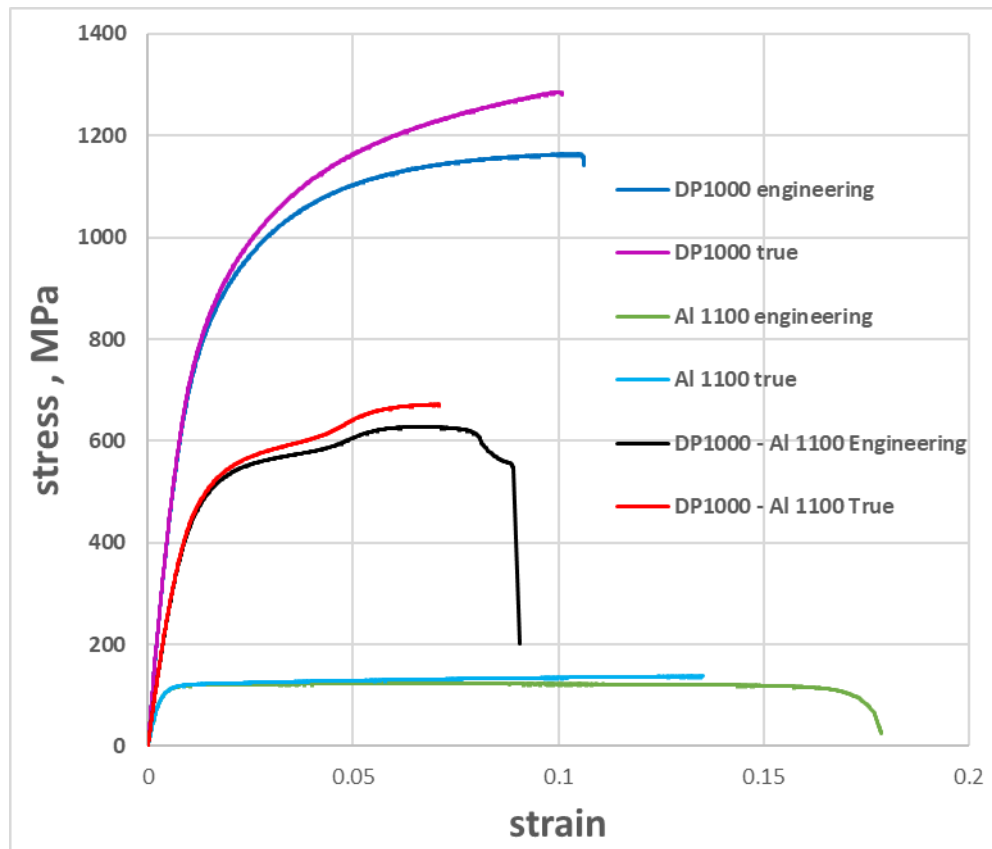
Figure 7.5. Tensile test results for DP1000, Al1100, and explosively welded DP1000-Al1100.

Table 7.2. Tensile test results as engineering and true stress-strain values.

Group number	Materials	Proof (0,2%) Yield Strength σ_{YS} MPa	UTS MPa	True stress MPa	Engineering strain (%)	True strain (%)
1	DP1000	770	1075	1195	10	9
2	Al 1100	117	119	135	17.5	15
3	DP1000-Al1100 plate composite	465	610	668	8	7

Figure 7.6 shows the engineering and actual stress-strain curves for the three materials used: DP1000, Al100, and explosively welded bimetal composite. The findings of the study's tensile test are shown in Table 7.3. These results show that unalloyed has not shown a significant yield strength/tensile strength ratio, whereas the composite DP 1200 sheet steel and DP 1200-Al 1100 plate values were 0.84 and 0.675, respectively. This phenomenon's genesis was explained by calculating the composite's tensile strength using the composite rules [236, 237]. In addition, while the yield strength/tensile strength ratio increased with composite manufacture, the elongation value did not significantly change. Additionally, the composite's strength dropped due to the field effect of aluminium. Composite bimetal structure rules can predict these outcomes [22, 58].

Table 7.3. Tensile test results of all specimens

Group number	Materials	Proof (0,2%) Yield Strength σ_{YS} MPa	True tensile strength MPa, σ_{UTS} (UTS)	Yield ratio $\sigma_{YS}/, \sigma_{UTS}$	True uniform strain, ε_u (%)	True fracture strain, ε_f (%)
1	DP1200	1240	1354	0.96	4	5
2	Al 1100	117	135	0.86	15	17.5
3	DP1200-Al 1100 (Steel-Al composite)	450	643	0.70	4.6	5.7
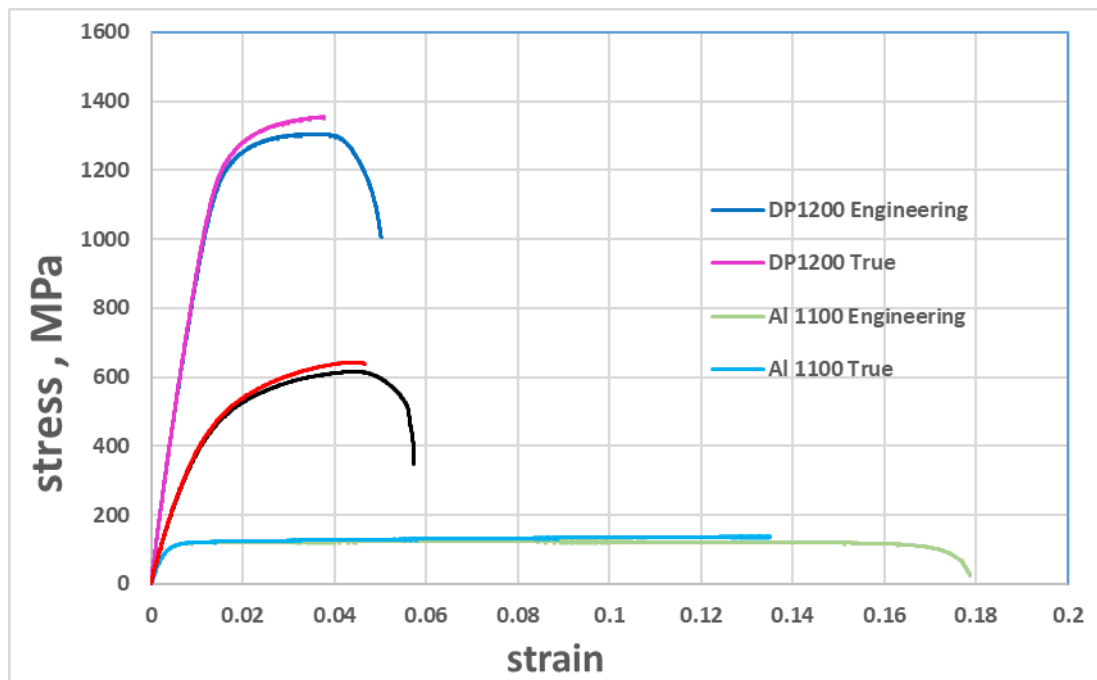
Figure 7.6. Tensile test results for DP1200, Al1100, and explosively welded DP1200-Al1100.

7.3. BASE MATERIALS

Several types of punches were used and applied to the metals used in this study, and the results were as follows:

7.3.1. DP600

As displayed in Fig. 7.7, the experimental findings from the studies utilizing five different punch shapes have demonstrated that the punch shape considerably influences the blanking force. For all of the sheet materials employed, it was observed that a flat-ended punch (punch 0) produced the highest blanking force value. Using V16, R1, and R2, the blanking forces were reduced by approximately 63%, 61%, 69%, and 77%, respectively, compared to the flat-end (0) punch.
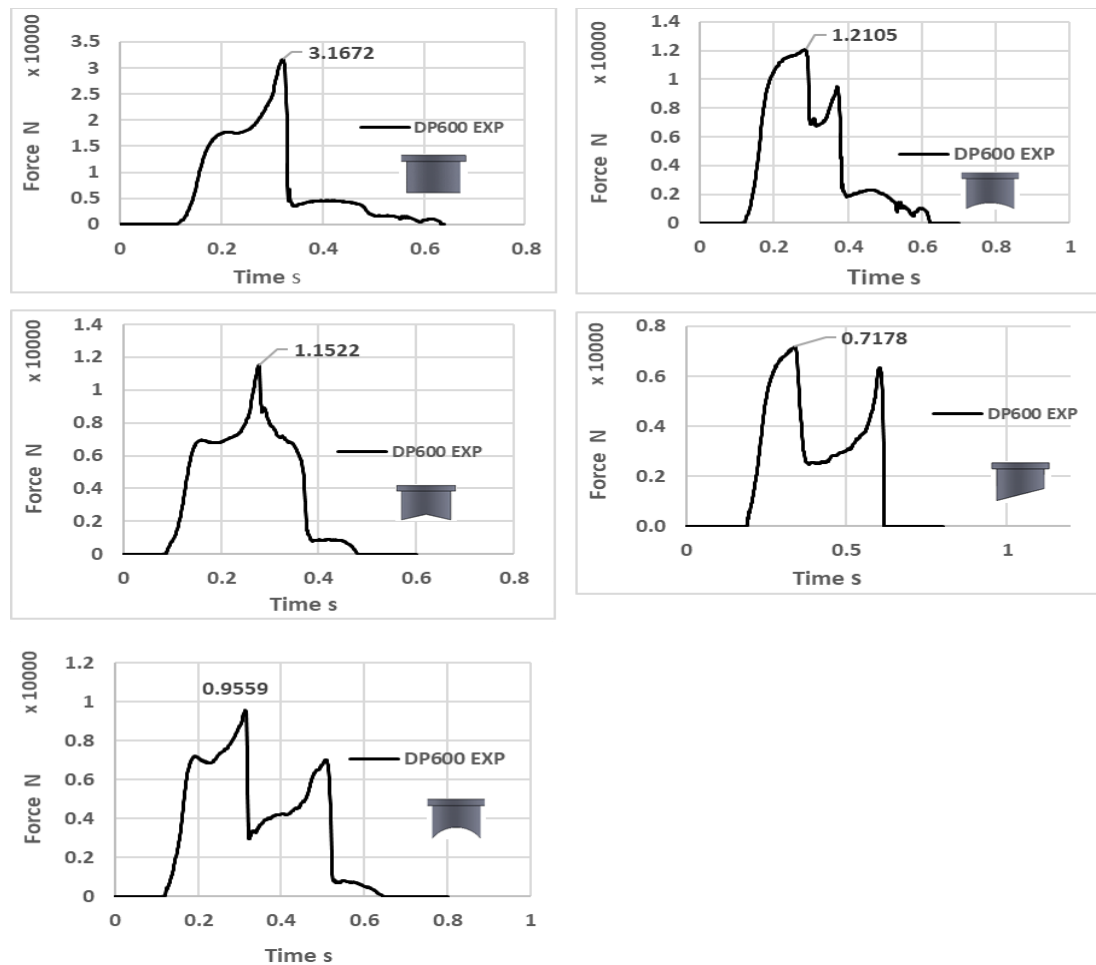
Figure 7.7. Studies were conducted on DP600 steel to compare the shearing forces vs time when employing various punches.

7.3.2. DP1000

As shown in Figure 7.8, the punch type significantly impacted the shear force in all of the studies using five different punch tip types and DP1000 sheet material. The highest value possible while punching "0" is 52658 N. Using the R1, V16, R2, and 16 punches, cutting forces of 19673, 17190, 18238, and 10268 N were measured. It is evident that the cutting force is quite high when punching type "0" and significantly lower when utilizing other punches.
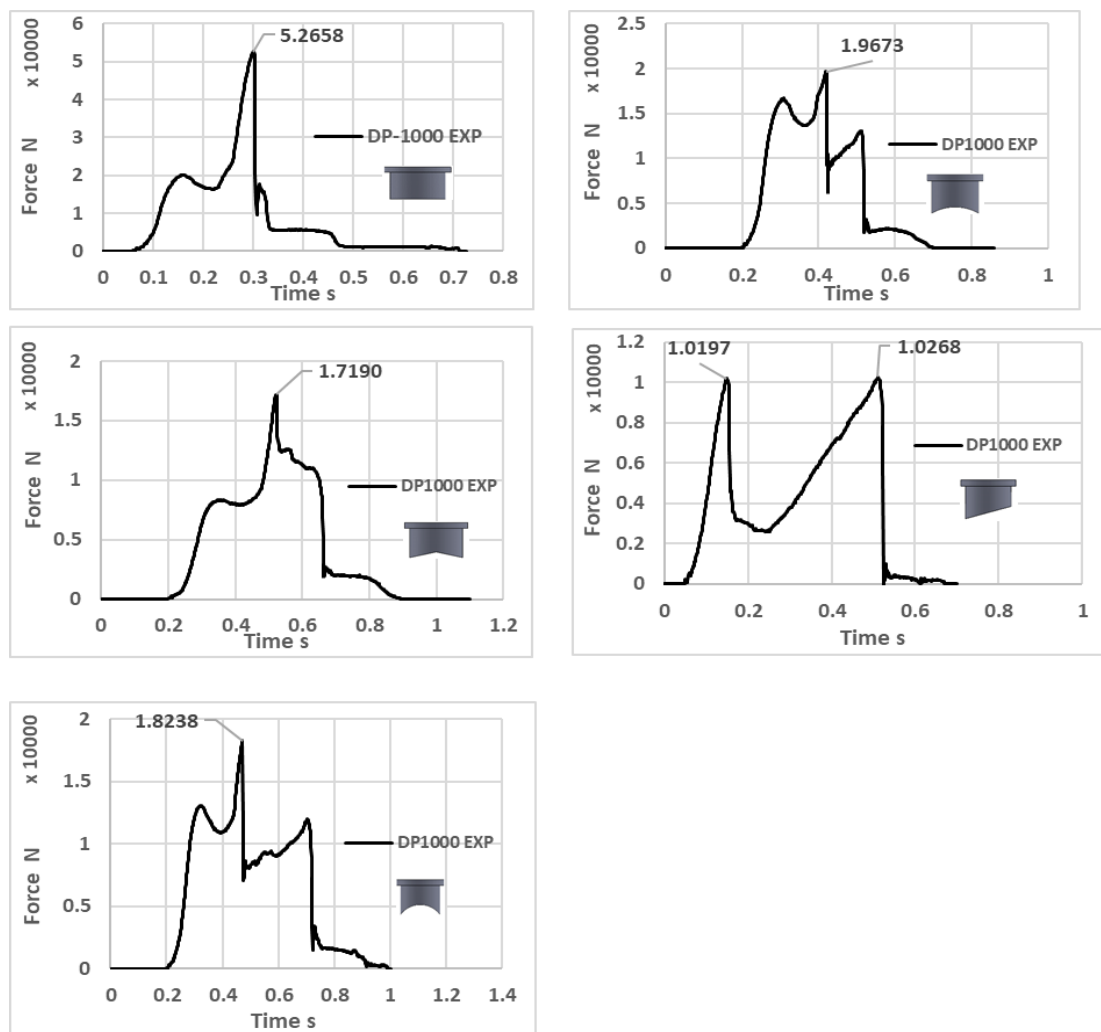
Figure 7.8. Studies were conducted on DP1000 steel to compare the shearing forces over time when employing various punches.

7.3.3. DP1200

F max is compared when striking DP1200 sheet steel with five punch tips under experimental settings. As shown in Fig. 7.9, when punching "0" was used, the shearing force reached its maximum value of 45452.2 N. When the punches R1, V16, R2, and 16 were employed, the shearing forces were measured as 19949, 17118.9, 16535.5, and 11237.8 N, respectively.
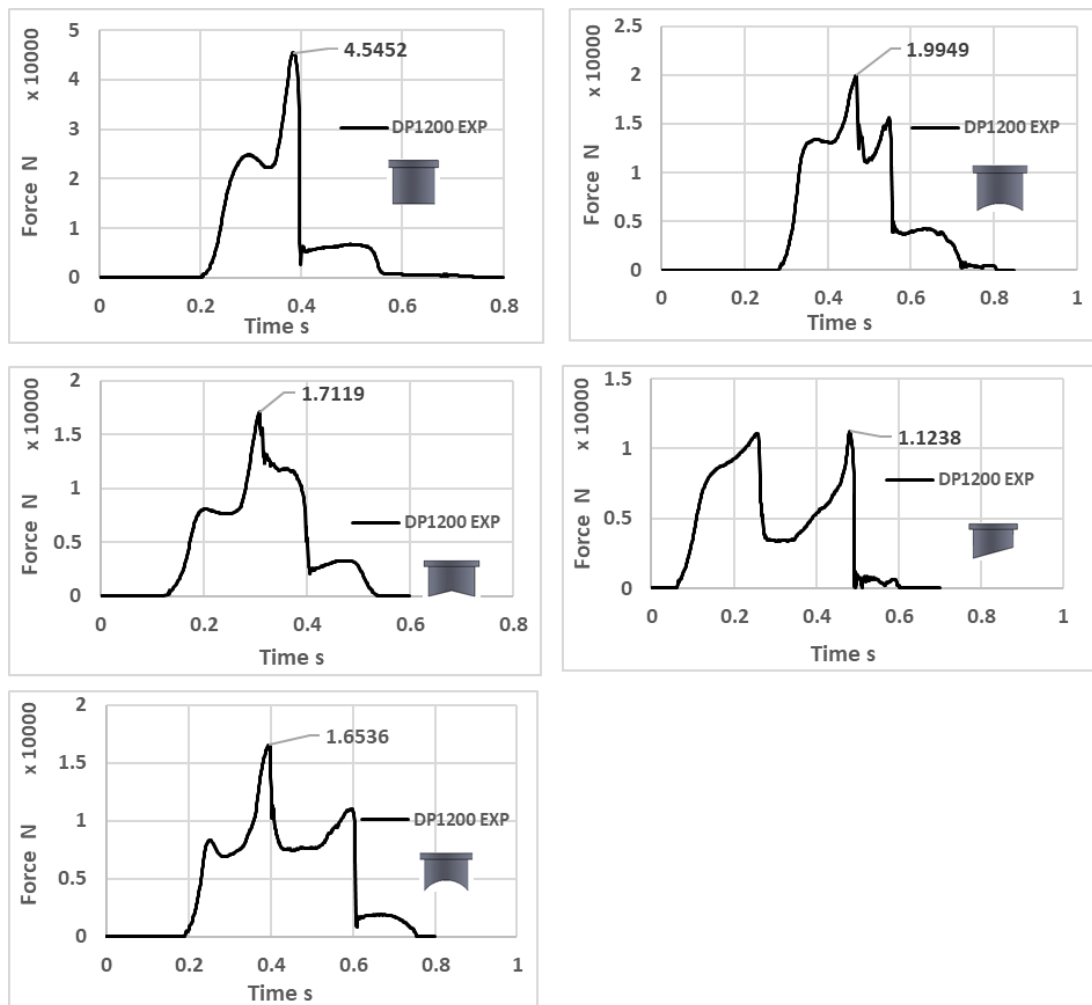
Figure 7.9. When employing various punches, studies were conducted on DP1200 steel to compare the shearing forces over time.

7.3.4. Al 1100

By applying punches of different shapes on Al1100, The "0" punch required a cutting force of 7872 N to operate. When the punches P R1, P V16, P R2, and P 16 were employed, the shearing forces were measured as 3781, 4734, 2955, and 2538 N, respectively. as demonstrated in image 7.10 below:
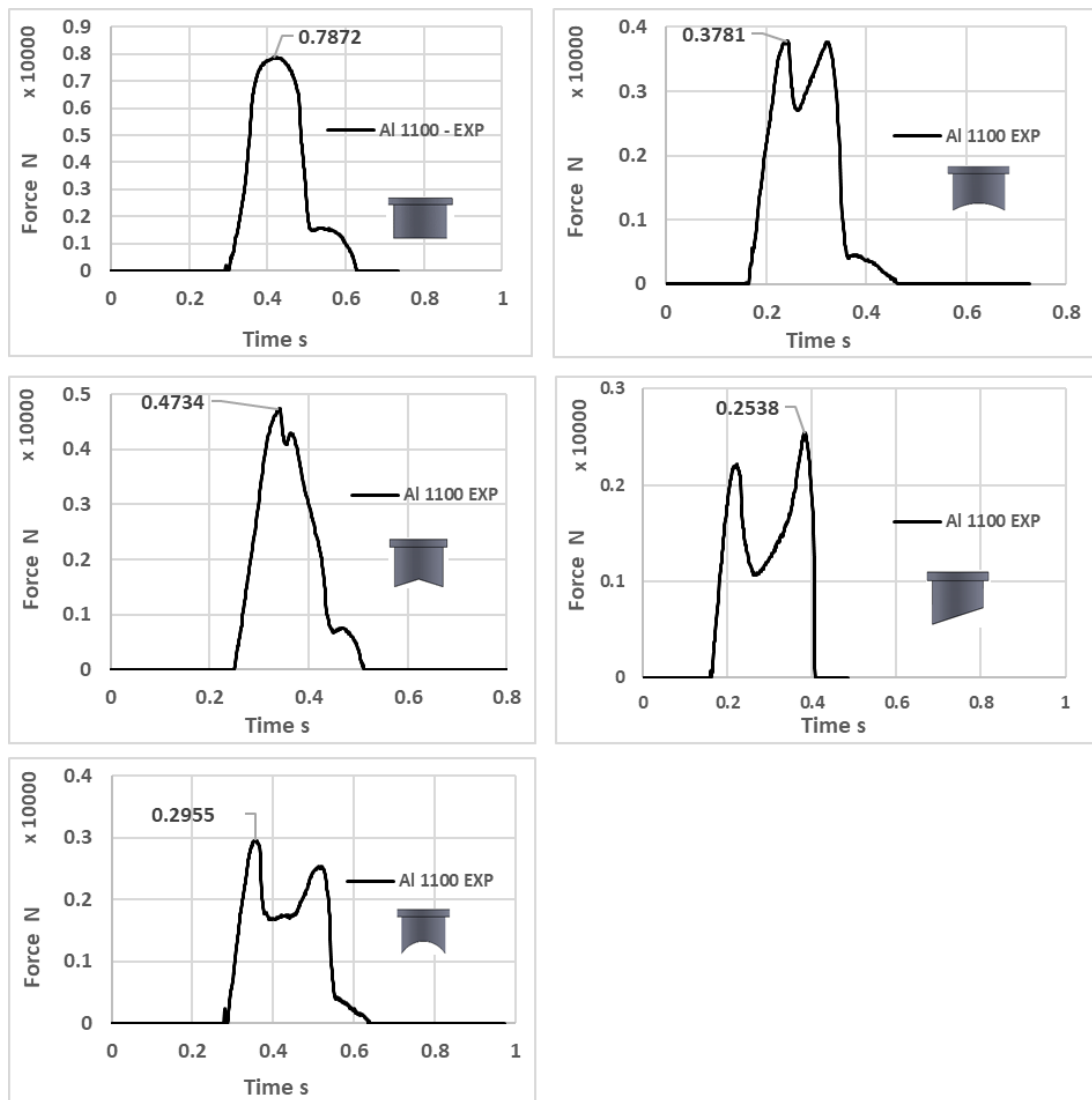
Figure 7.10. Studies were conducted on Al 1100 to compare the shearing forces over time when employing various punches.

7.3.5. Explosive Welded DP600 – Al

In addition, On the explosively welded sheet materials made from DP600-Al 1100, cutting tests and analyses were done. The punch "0" produced a cutting force of up to 34431 N. For the punches designated R1, V16, R2, and 16, respectively, the cutting forces were determined to be 17868, 18152, 13847, and 11963 N (Fig. 7.11).
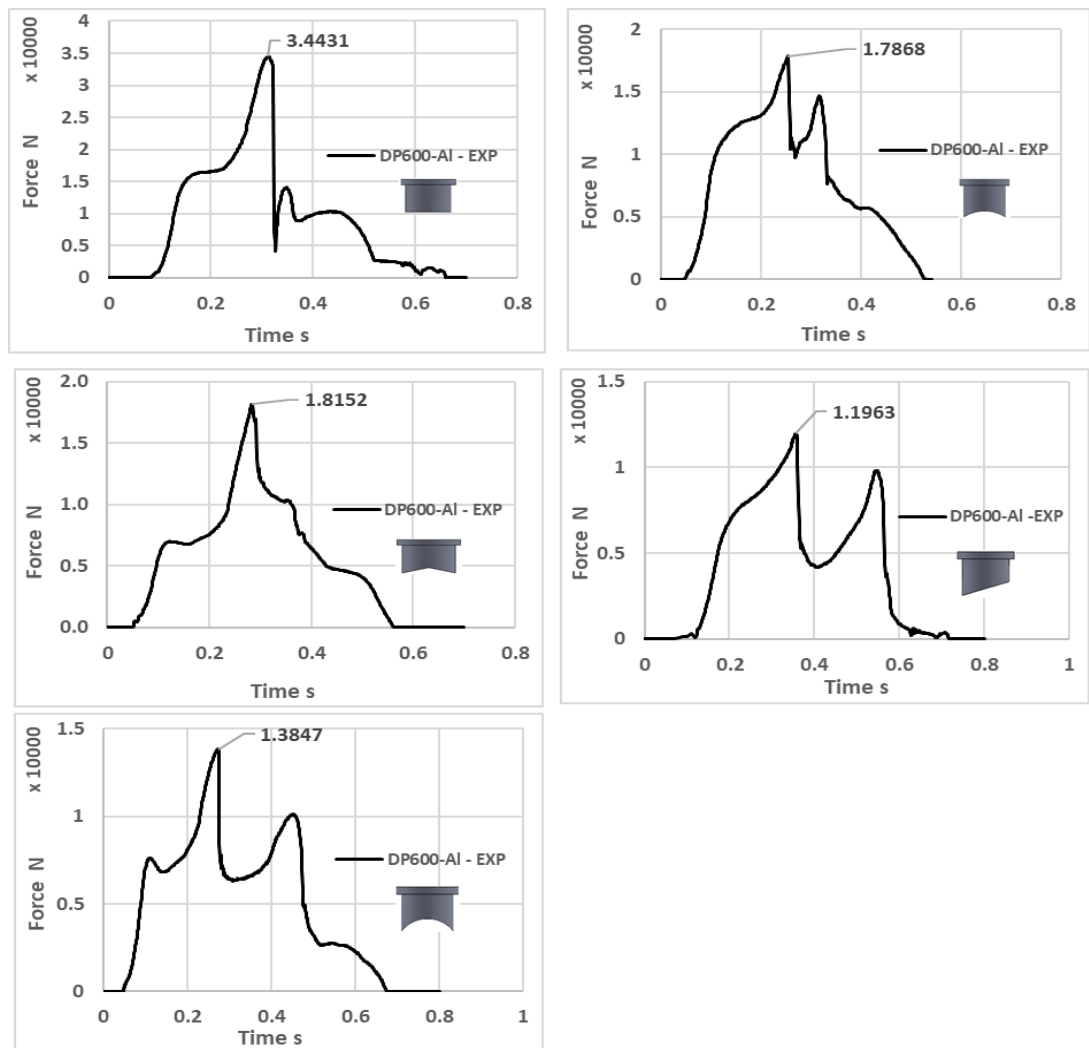
Figure 7.11. Studies were conducted on DP600-Al 1100 plate composite when employing various punches to compare the shearing forces over time.

7.3.6. Explosive Welded DP1000 – Al

Fig. 7.12 shows that Piercing/punching experimentally and theoretically studies results from the DP1000-Al 1100 explosive welding procedure' punching sheet materials— the max. Cutting force was obtained as 47242 N with the punch "0". At the same time, Punches R1, V16, R2, and 16 produced cutting forces of 20667 N, 21502 N, 18806 N, and 11569 N, respectively.
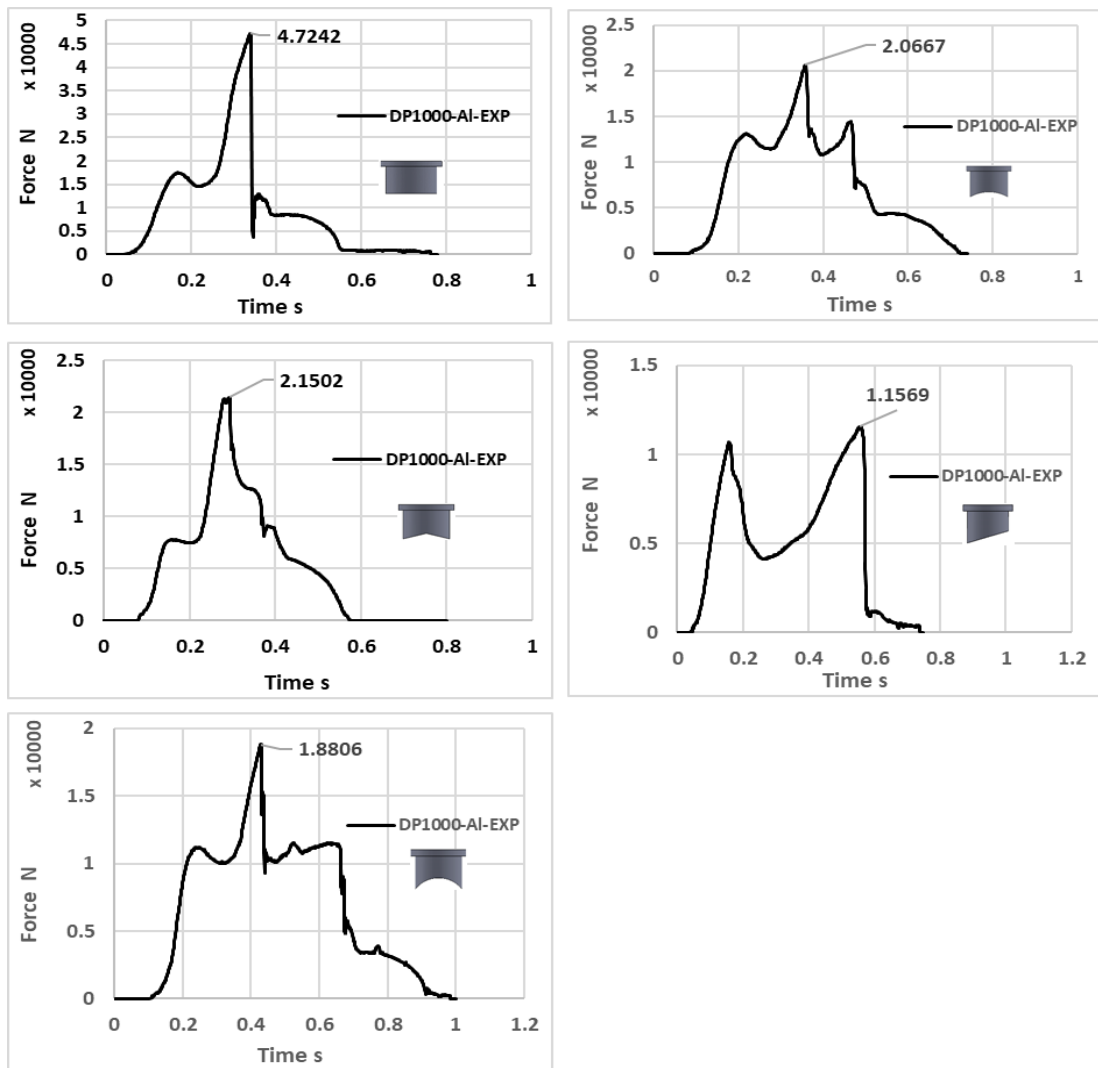
Figure 7.12. Studies were conducted on DP1000-Al 1100 plate composite when employing various punches to compare the shearing forces over time.

7.3.7. Explosive Welded DP1200 – Al

On DP1200 and Al 1100, explosive welded sheet materials, punching and shearing tests and analyses were performed experimentally and numerically. As shown in Fig. 7.13, the shearing forces for punches P R1, P V16, P R2, and P 16 were 20485 N, 21644 N, 18089 N, and 13374 N, respectively, while the shearing force for punch "P 0" was 47541 N at its highest.
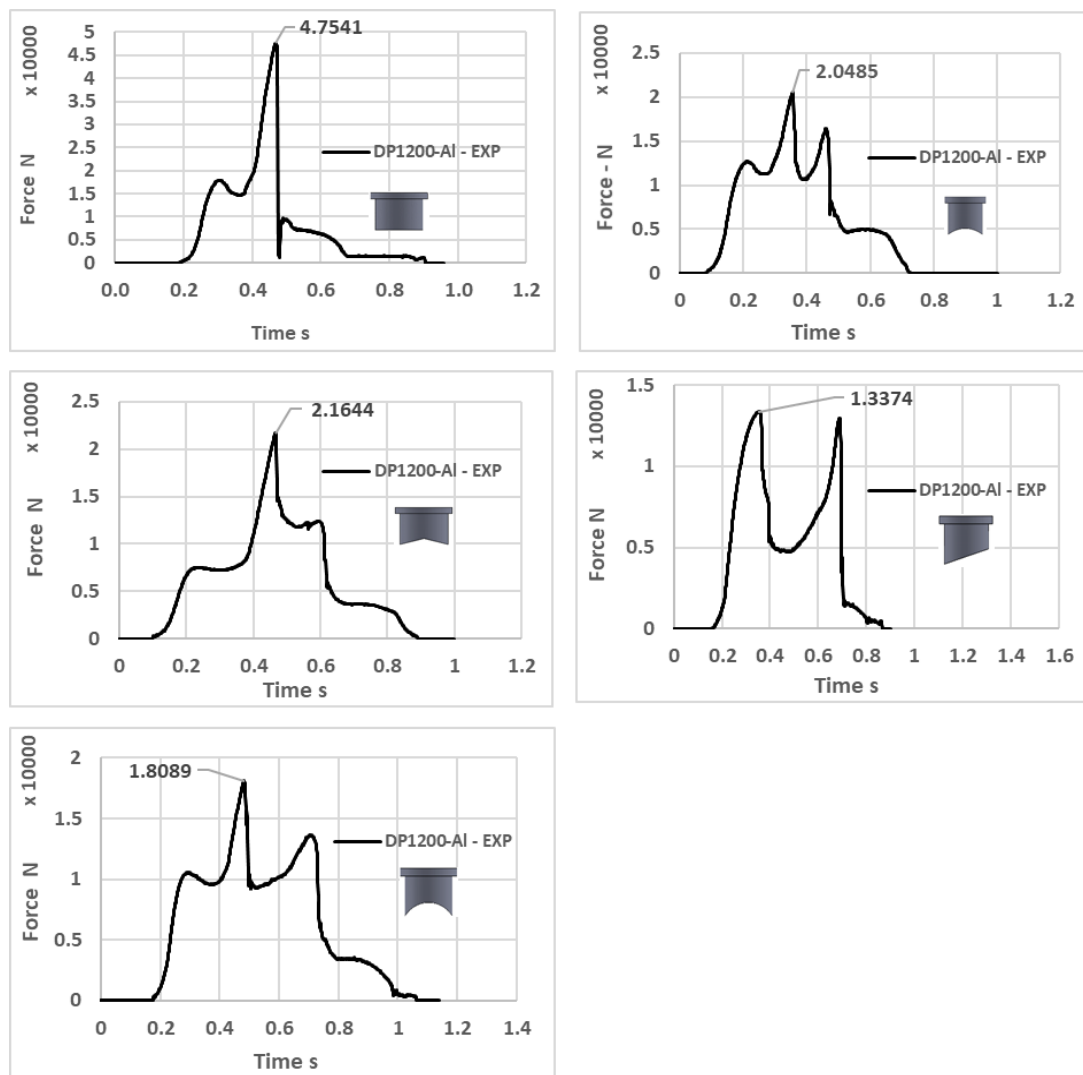
Figure 7.13. Studies were conducted on DP1200-Al 1100 plate composite when employing various punches to compare the shearing forces over time.

Therefore, it is evident that the blanking force is significantly greater when using punch number 0, and it dramatically reduces while using the subsequent punches. Furthermore, results were compared to the punch "0" to understand the forces that

arise while forming. When the punches R1, V16, and R2 were employed, it was seen that the cutting force significantly decreased when compared to when the punch "0" was used. According to the force changes during the punching operations, the blanking and piercing operations employing the punch "0" happen simultaneously in one shot along the cutting line. Using the additional punches (R1, V16, R2, and 16) results in a longer and slower process. This shifting of the cutting area also affects the cutting surface quality and thickness fluctuations. These findings are important because it is easy to understand how cutting and deformation relate.

7.4. EXPERIMENTAL AND SIMULATION PUNCHING/PIERCING PROCESS

Sheet steels of DP600 and DP1200 had a thickness of 1mm. However, DP1000's thickness was 1.2mm, and the thickness of Aluminum 1100 was 1.4mm with specific dimensions of 130x27mm. as shown in Figure 7.14, and prepared the materials by cutting, cleaning and finishing from scratch.
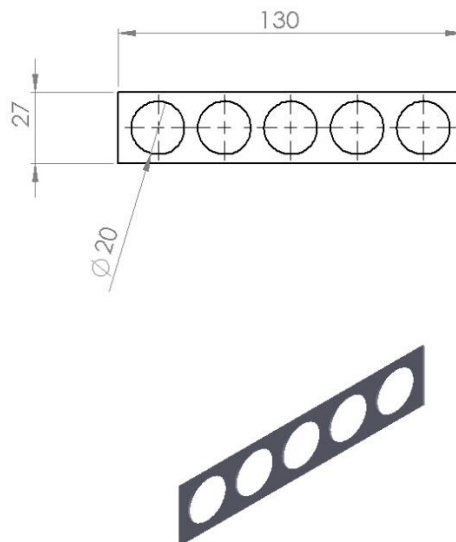
Figure 7.14. DP steel and AL with specific dimensions.

Sheet steels of DP explosive welding with specific dimensions of 130x27mm with thickness 1mm steel and 1.4mm Aluminum 1100 as shown in figure 7.15 and prepared the materials by cutting, cleaning and finishing from scratch.
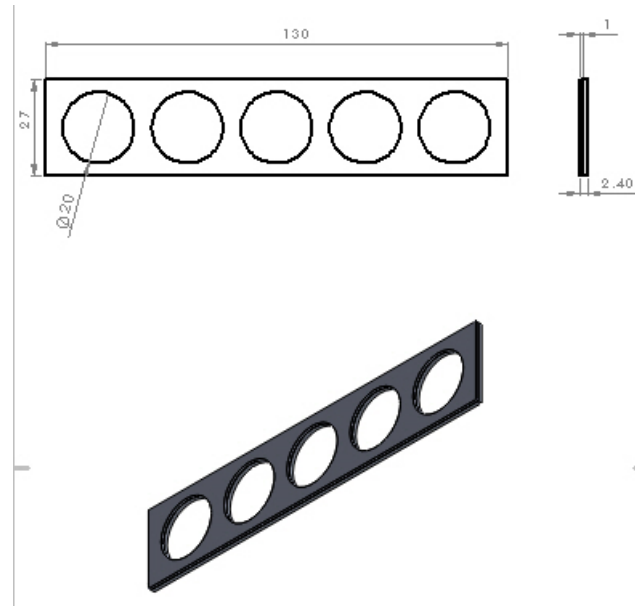
Figure 7.15. DP Explosive welding steel with specific dimensions.

7.4.1. DP600 Analysis

It was discovered that the theoretical investigations carried out using the FEM Program produced results that were very similar to the practical ones. The punch "0" has a maximum cutting force of 31412 N, as determined by FEM analyses, and the experimental outcome for the same punch is 31672 N. The maximum cutting forces for the punches R1, R2, 16, and V16 were also determined to be 11976 N and 12105 N, 9834 N and 9559 N, and 7169 N and 7178 N, respectively. The first numbers listed are the outcomes of the FEM analyses, while the second values are the experiment outcomes. Fig. 7.14 displays the outcomes of the experiments and the deform program. Based on the strikes made. Fig. 7.15 compares the maximum cutting forces for all the punches used to cut DP600 sheet material. FEM studies and testing determined these values.
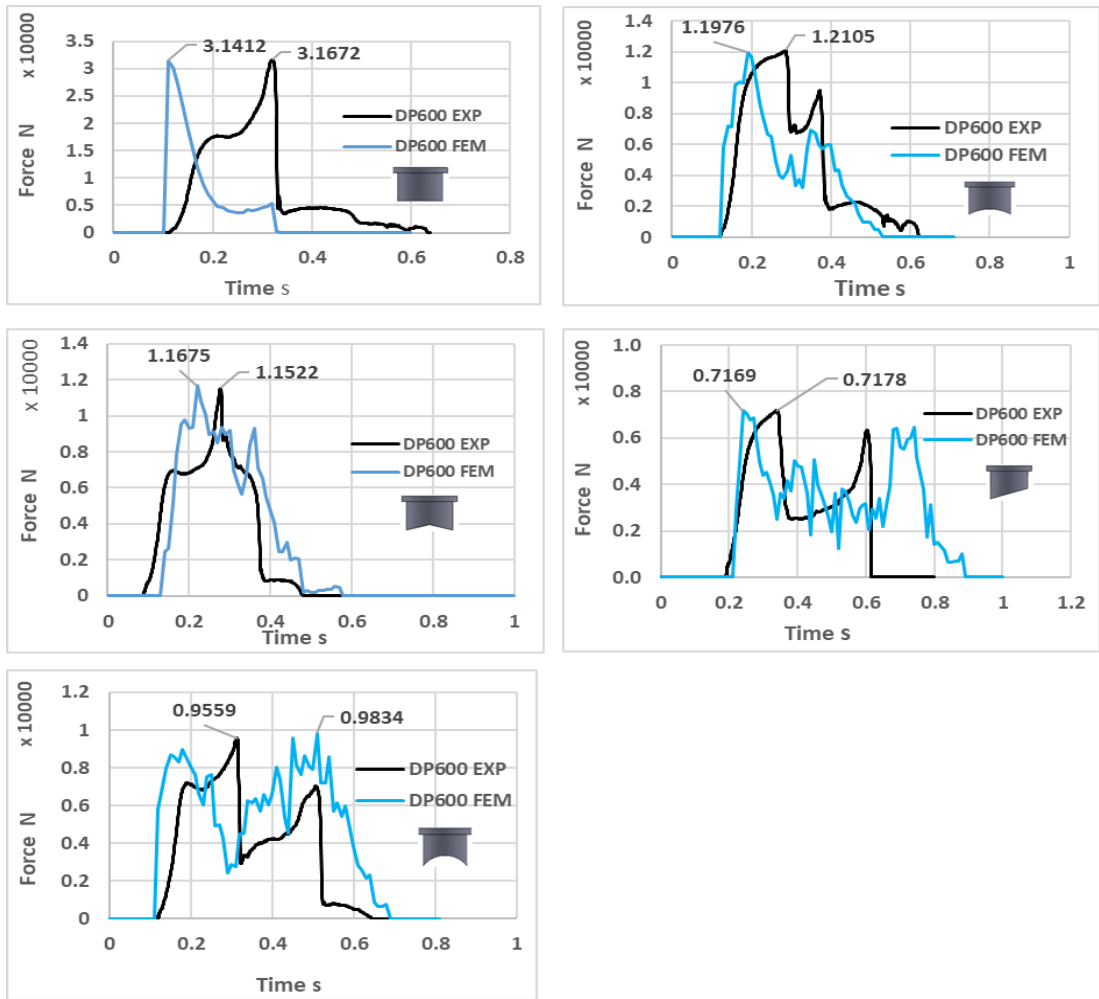
Figure 7.16. Comparative force-time graphs were created using different punch shapes
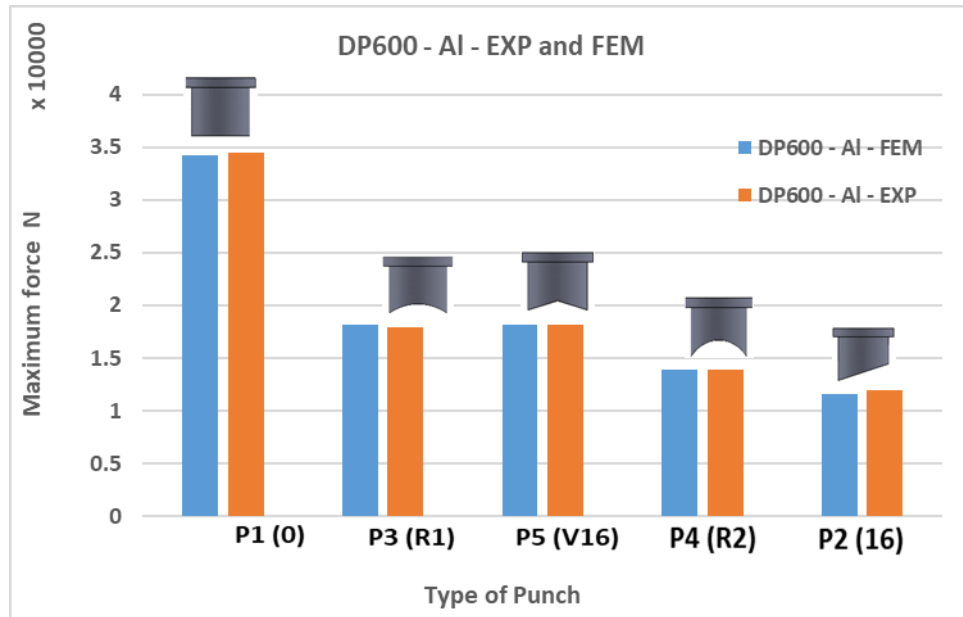in analysis and experiments on the DP600.
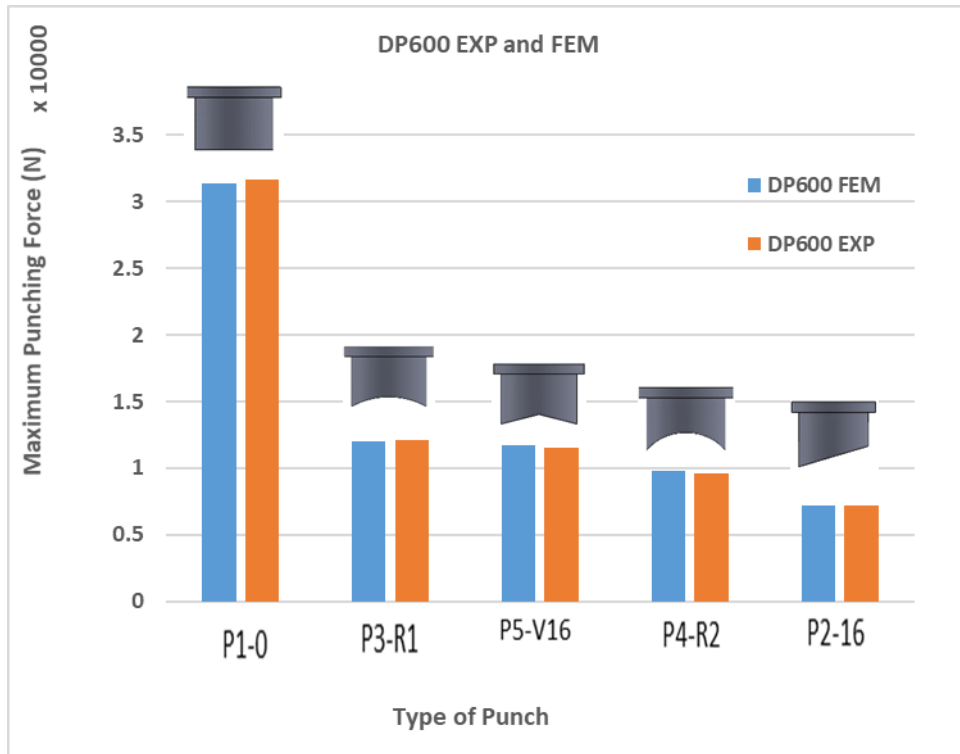
Figure 7.17. The maximum shearing forces for various punch forms on DP600 sheet
material, as determined by experiments and FEM analysis, are compared.

FEM analyses were used to conduct the studies and simulations. The investigations
employed 3D models to test the software's performance in simulating punching
operations and guarantee experimental results' consistency. The assessments produced
using 3D models for punching all holes in DP600 sheet material are shown in Fig.
7.16.
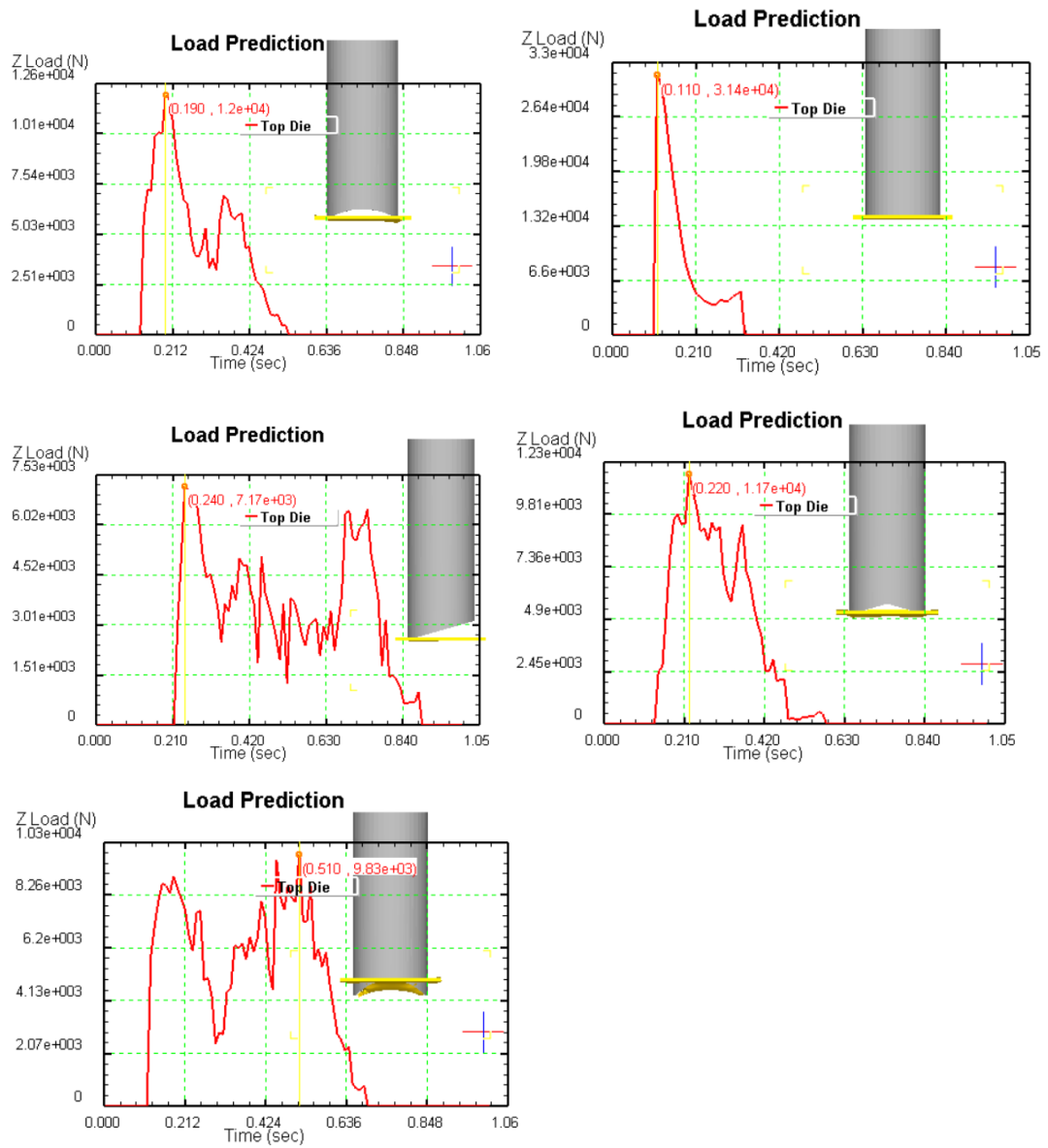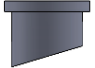
Figure 7.18. Analyses were produced by cutting DP600 sheets using 3D models.

Table 7.4 compares the highest cutting forces between FEM and the real-world experimental DP600.

Table 7.4. The difference between FEM and practical experimental DP600.

Punch shape	maximum cutting forces FEM	maximum cutting forces experimental	the difference %
	31412 N	31672 N	0.83%
	11976 N	12105 N	1.08%
	11675 N	11522 N	1.33%
	9834 N	9559 N	2.88%
	7169 N	7178 N	0.13%

7.4.2. DP.1000 Analysis

As shown in Figures 7.17 and 7.18, all the trials and FEM analysis findings employing five different punch tip types and DP1000 sheet material demonstrated that the punch type greatly influenced the shear force. The highest value possible while punching "0" is 52658 N. Using the R1, V16, R2, and 16 punches, cutting forces of 19673, 17190, 18238, and 10268 N were measured. Thus, it is evident that the cutting force is extremely high when punch type "0" is used and significantly lower when punch type "0" is used. On the other hand, when theoretical experiments utilizing FEM analysis were conducted, the outcomes were remarkably comparable to those in practice. The test result for a straight "0" punch is 52658N, higher than the cutting force calculated by the FEA program, which is 52270N. Similar outcomes were found for R1, 19005N, 18238N for R2, 10691N–10268N for punch 16, and 16365N–17190N for V16 punch, respectively.
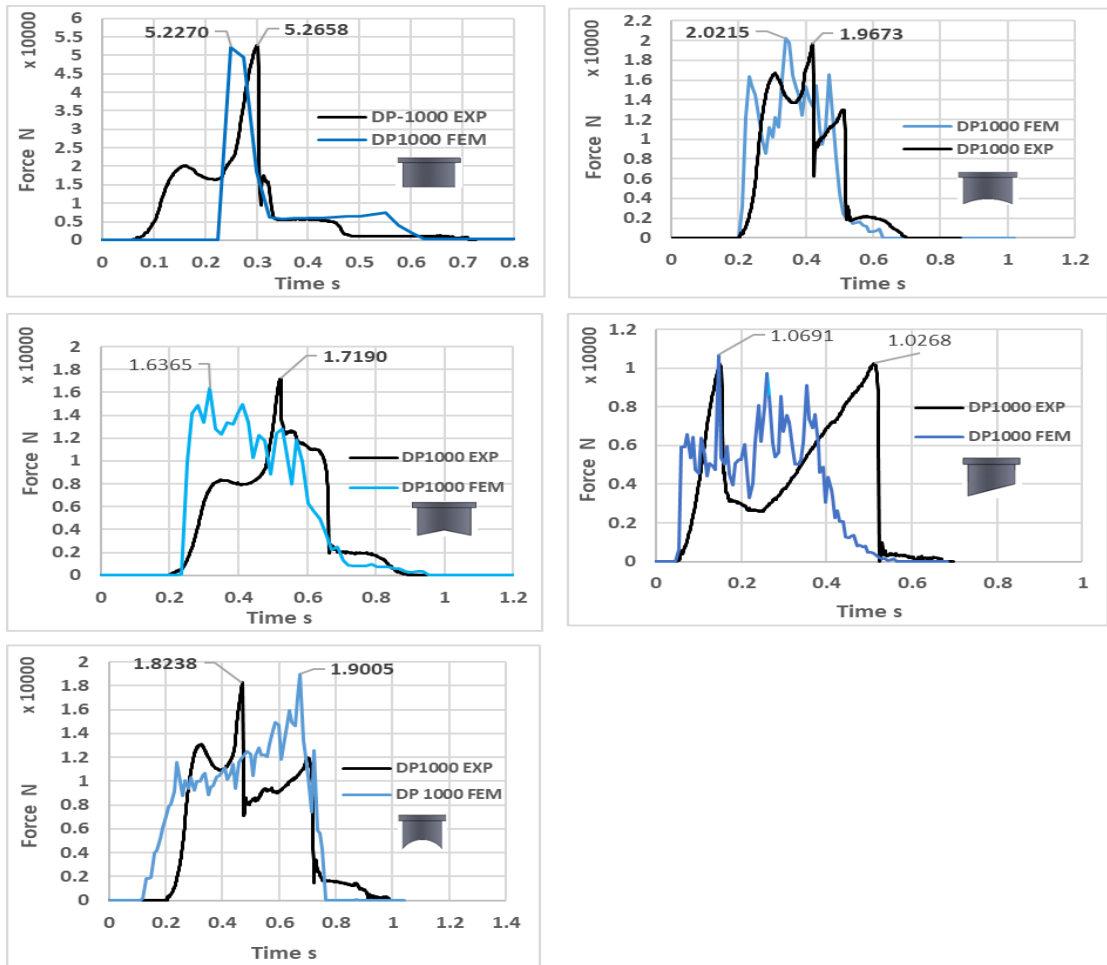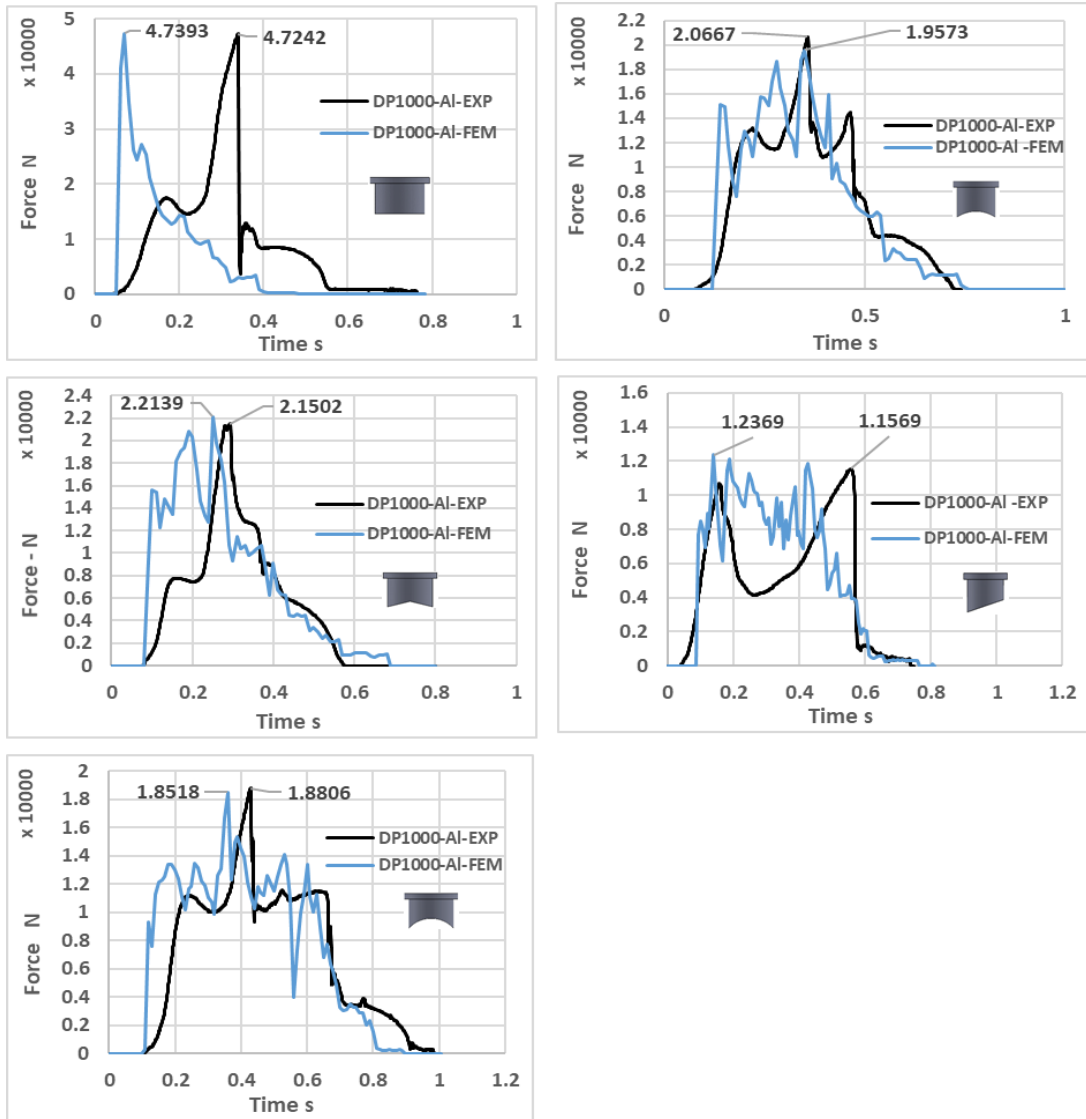
Figure 7.19. Comparative force-time graphs were created using different punch shapes in analysis and experiments on the DP1000.
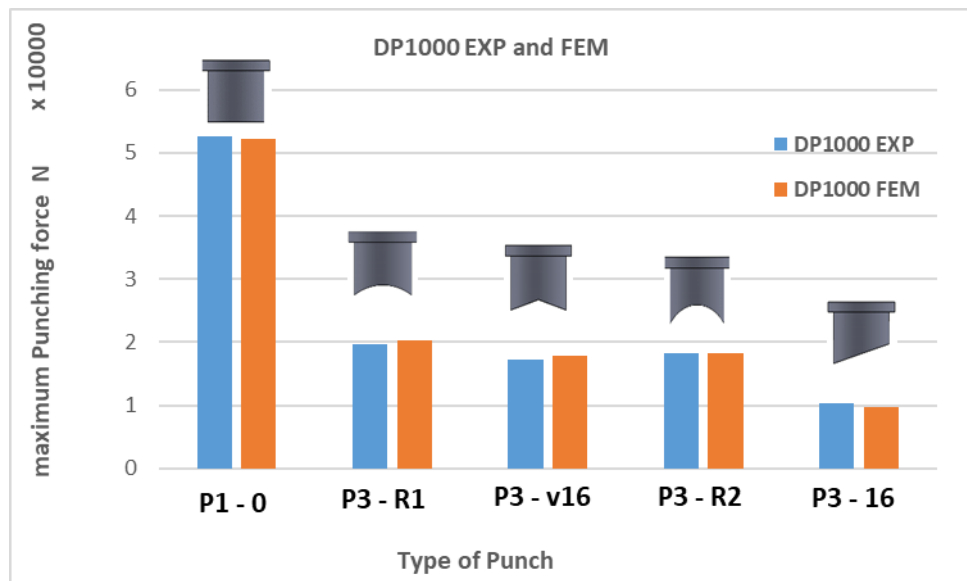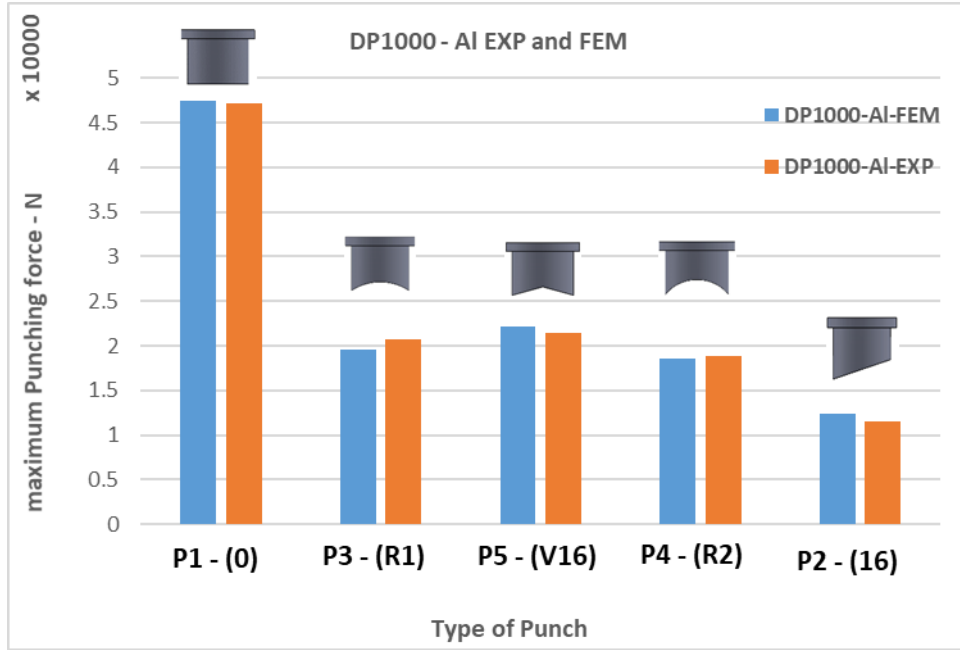

Figure 7.20. The maximum shearing forces for various punch forms on DP1000 sheet material, as determined by experiments and FEM analysis, are compared.

FEM analyses were used to conduct the studies and simulations. The investigations employed 3D models to test the software's performance in simulating punching operations and guarantee experimental results' consistency. The analyses produced by cutting DP1000 sheet material with all punches using 3D models are shown in Fig. 7.19.
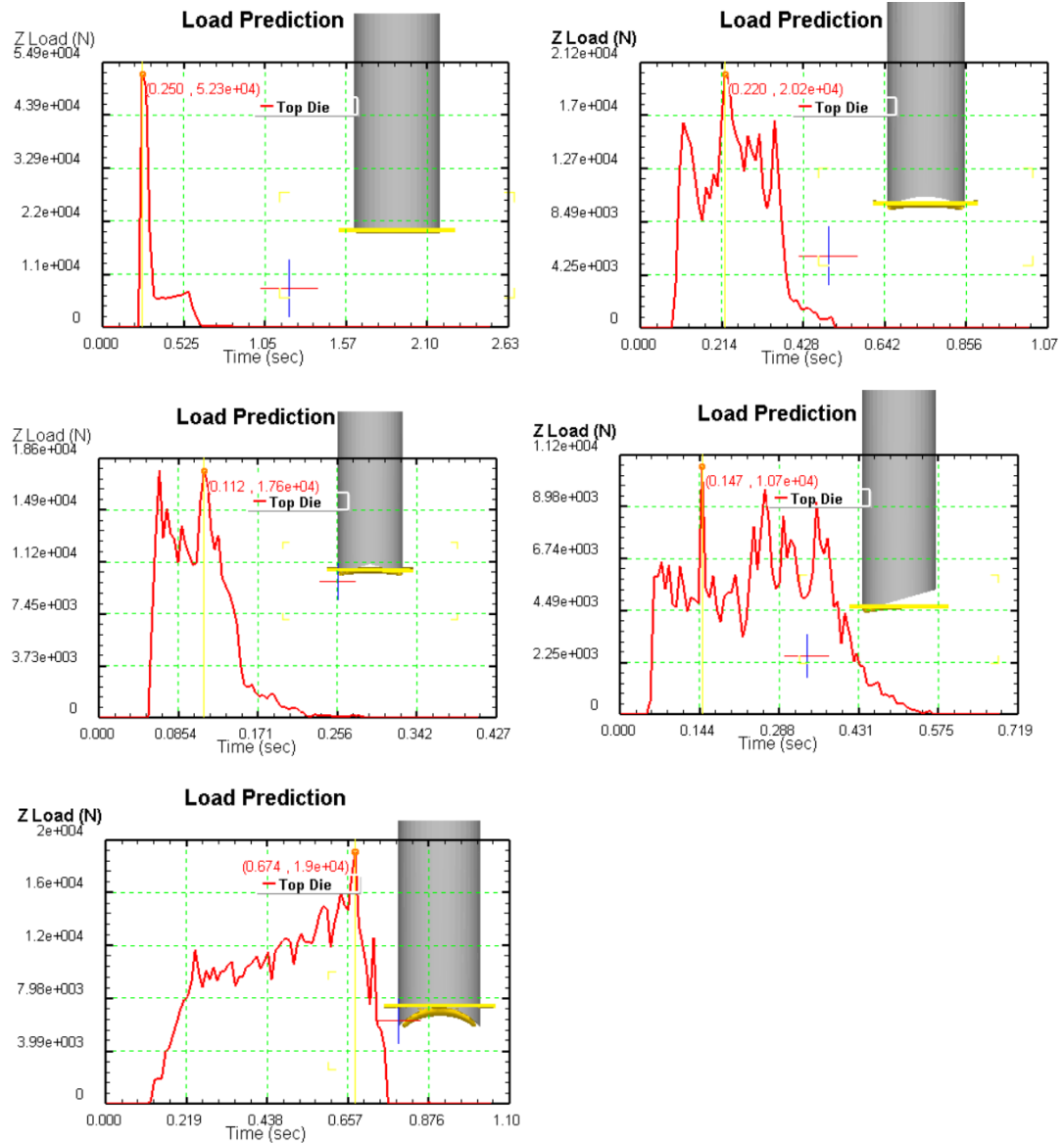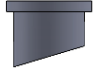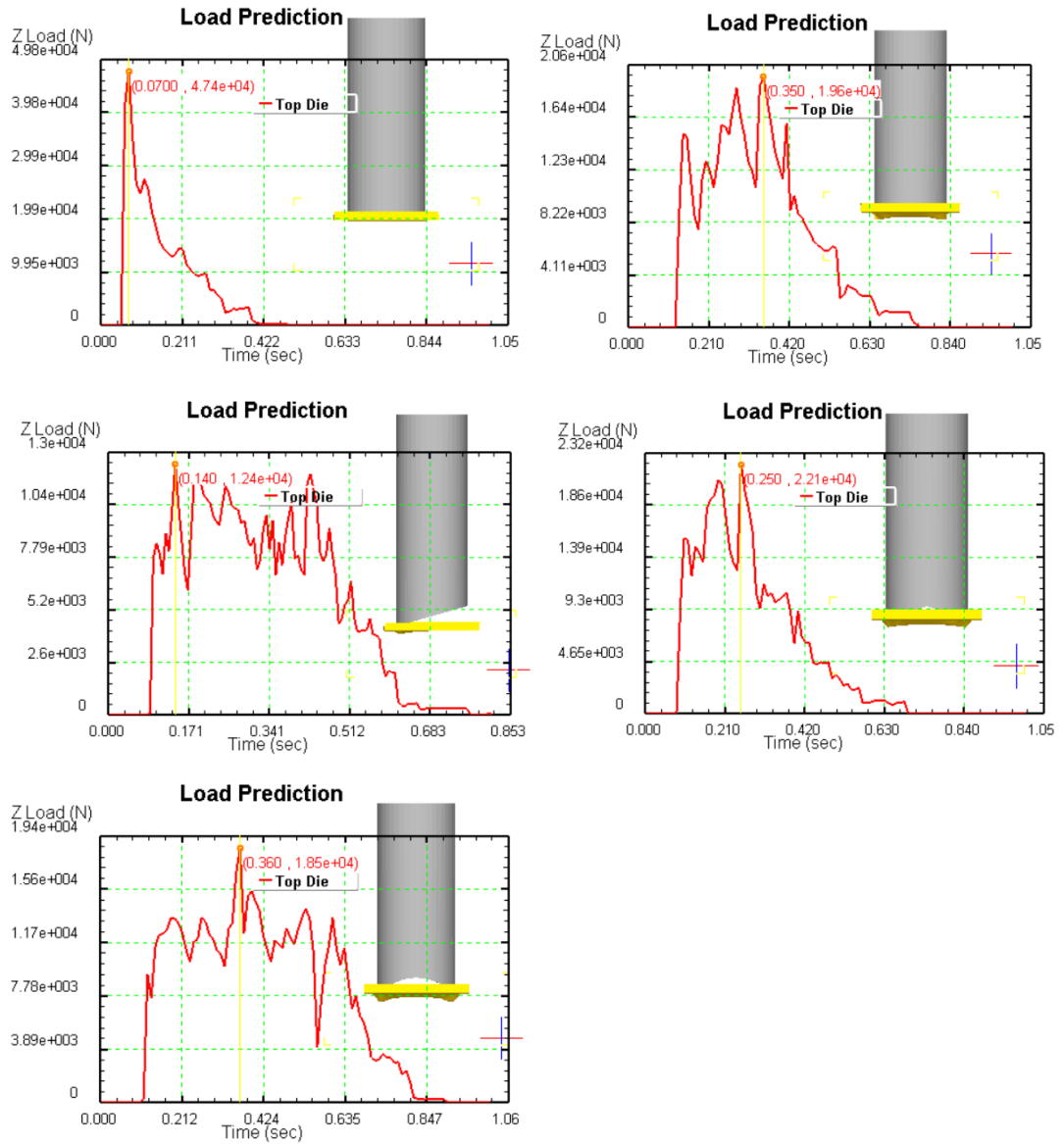

Figure 7.21. Analyses were produced by cutting DP1000 sheets using 3D models.

Table 7.5 compares the highest cutting forces between FEM and the real-world experimental DP1000.

Table 7.5. The difference between FEM and practical experimental DP1000

Punch shape	maximum cutting forces FEM	maximum cutting forces experimental	the difference %
	52270 N	52658 N	0.74%
	20215 N	19673 N	2.76%
	16365 N	17190 N	5.04%
	19005 N	18238 N	4.21%
	10691 N	10268 N	4.12%

7.4.3. DP1200 Analysis

As seen in Figures 7.20 and 7.21, it was discovered that the outcomes were compatible when numerical analyses employing FEM analysis were undertaken alongside experiments. 45725N is the shearing force determined by the FEM program, and 45452N is the experiment's finding for the punch "0". Similar to that, the results for R1 were 20090N and 19949N, 16535N and 15959N for R2, Punch 16: 11002N, and 11237N, 17118N and 17245N for punch V16, respectively.
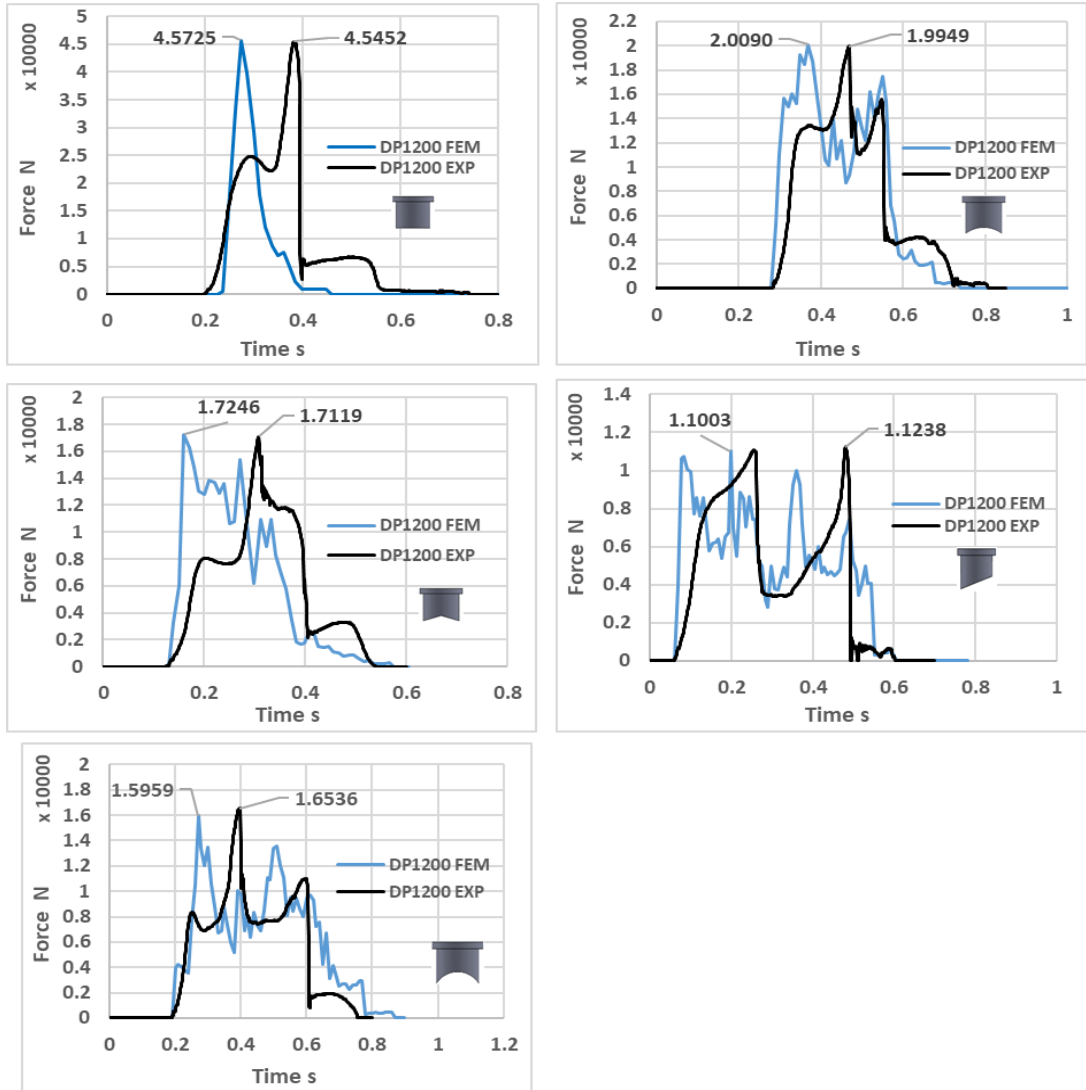
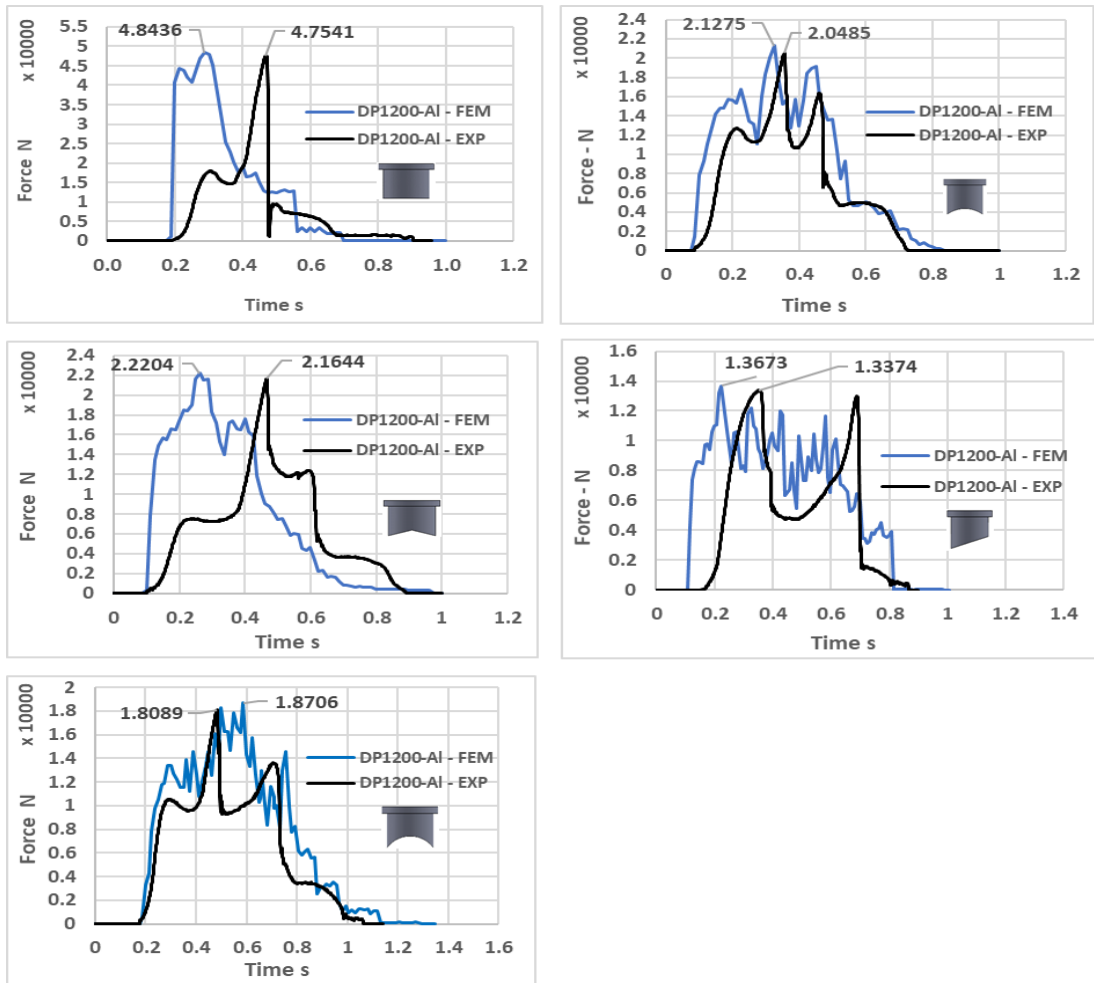Figure 7.22. Comparative force-time graphs were created using different punch shapes in analysis and experiments on the DP1200.
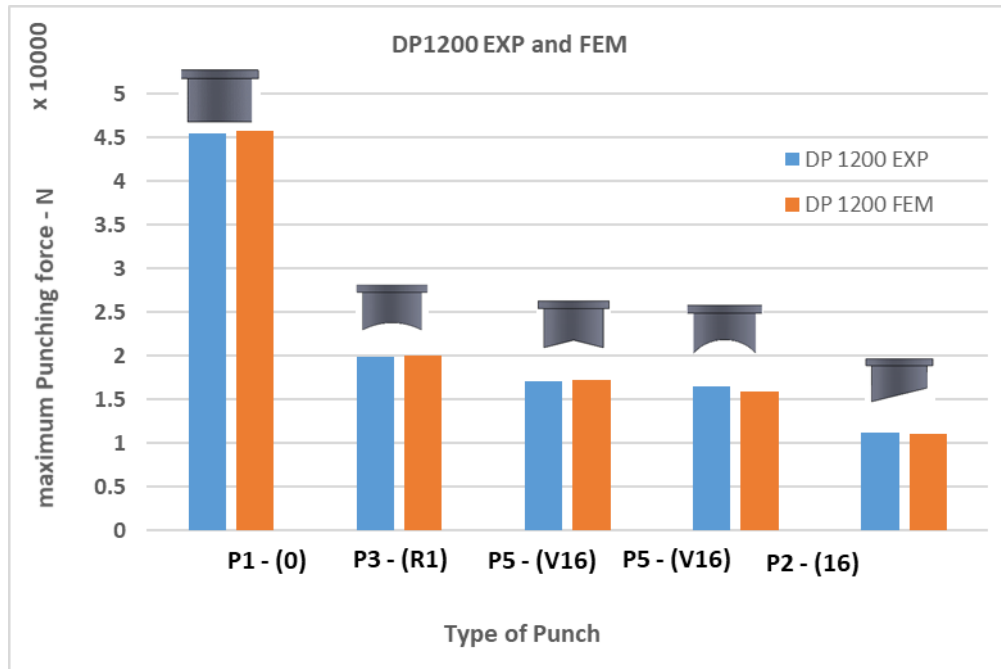
Figure 7.23. The maximum shearing forces for various punch forms on DP1200 sheet material, as determined by experiments and FEM analysis, are compared.

FEM analyses were used to conduct the studies and simulations. To check for compatibility with experimental tests and to assess how well the program performed when simulating punching procedures, 3D models were employed in the assessments. The analyses produced by cutting DP1200 sheet material with all punches using 3D models are shown in Fig. 7.22.
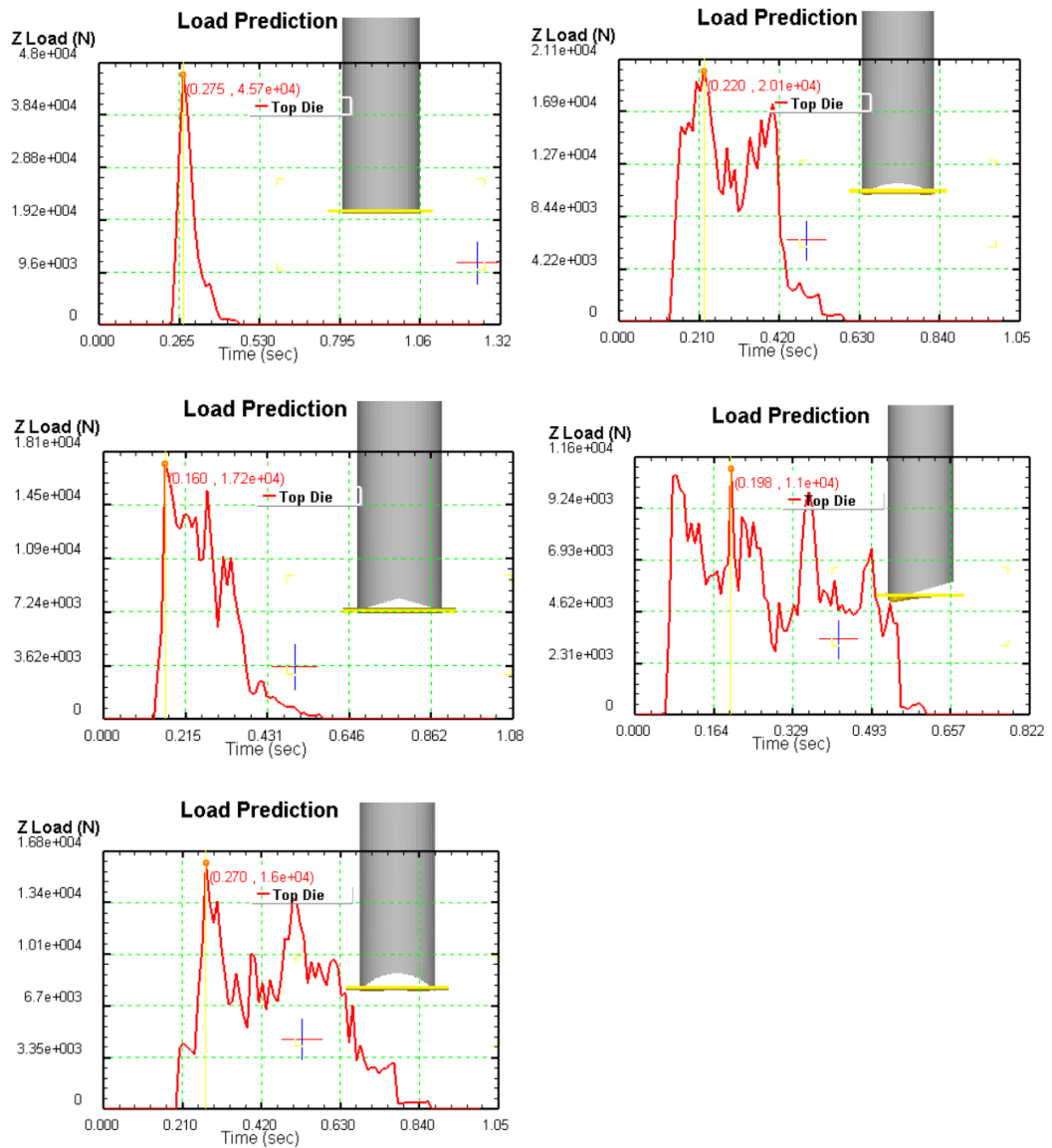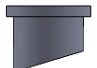
Figure 7.24. Analyses were produced by cutting DP1200 sheets using 3D models.

Table 7.6 compares the highest cutting forces between FEM and the real-world experimental DP1000.

Table 7.6. The difference between FEM and practical experimental DP1200.

Punch shape	maximum cutting forces FEM	maximum cutting forces experimental	the difference %
	45725 N	45452 N	0.60%
	20090 N	19949 N	0.71%
	17245 N	17118 N	0.74%
	15959 N	16535 N	3.61%
	11002 N	11237 N	2.14%

7.4.4. Al 1100 Analysis

The findings show that the needed cutting forces for cutting Al-1100 sheet material are quite close to each other due to experimental tests and analysis. The punch "0" has a maximum cutting force determined by FEM calculations of 7491 N. In comparison, the corresponding experimental value is 7872 N the punch R1 results are 3730 N and 3781 N. 2788 N and 2955 N for punch R2 were the other outcomes; for punch 16, 2685 N and 2538 N, for punch V16, 4671 N and 4734 N The first numbers listed are the findings of the FEM analyses, while the second values listed are the experiment's outcomes. Figures 7.23 and 7.24 compare the cutting forces discovered through FEM analysis and experiments when cutting Al-1100 sheet material with all the punches employed.
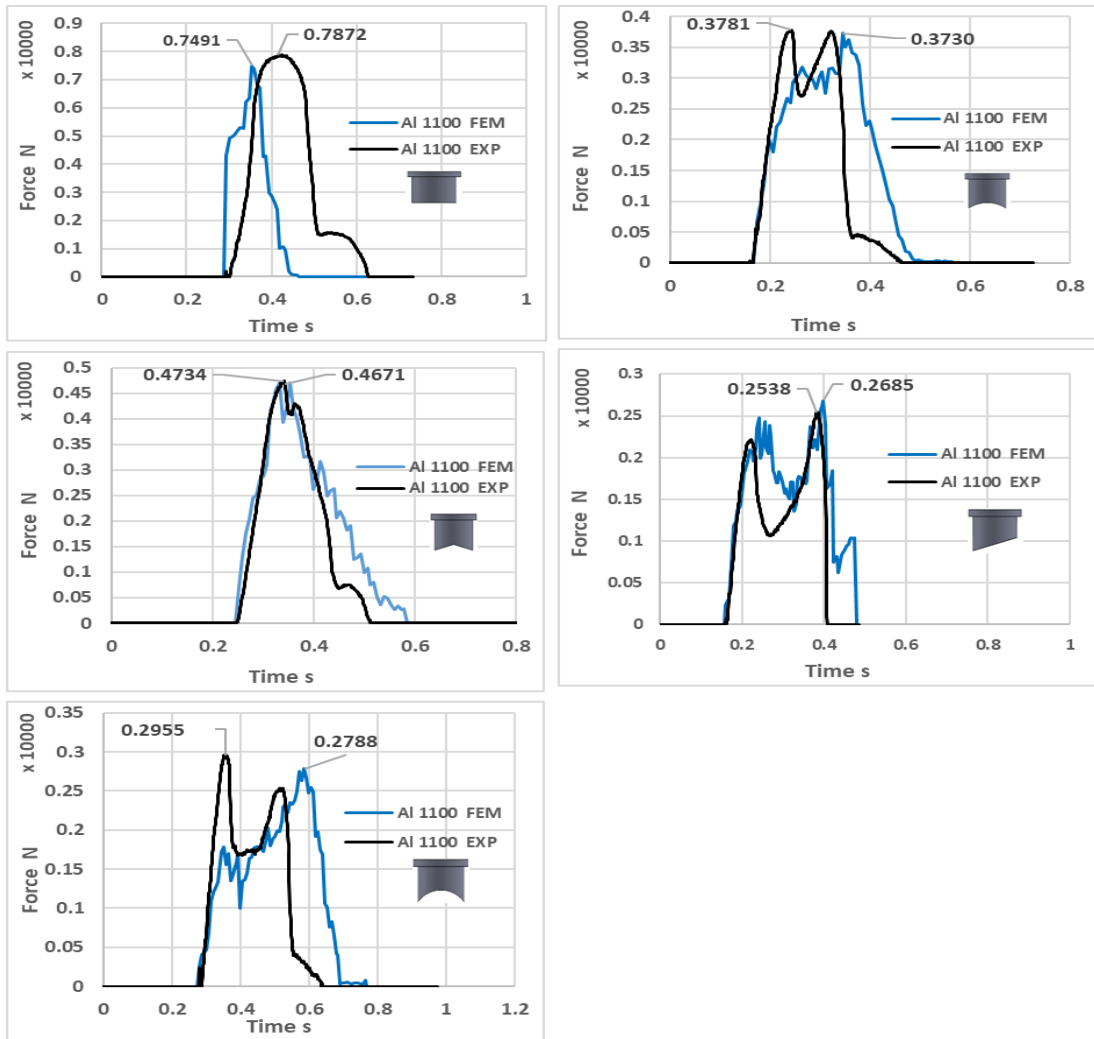
Figure 7.25. Comparative force-time graphs were created using different punch shapes in analysis and experiments on the Al 1100.
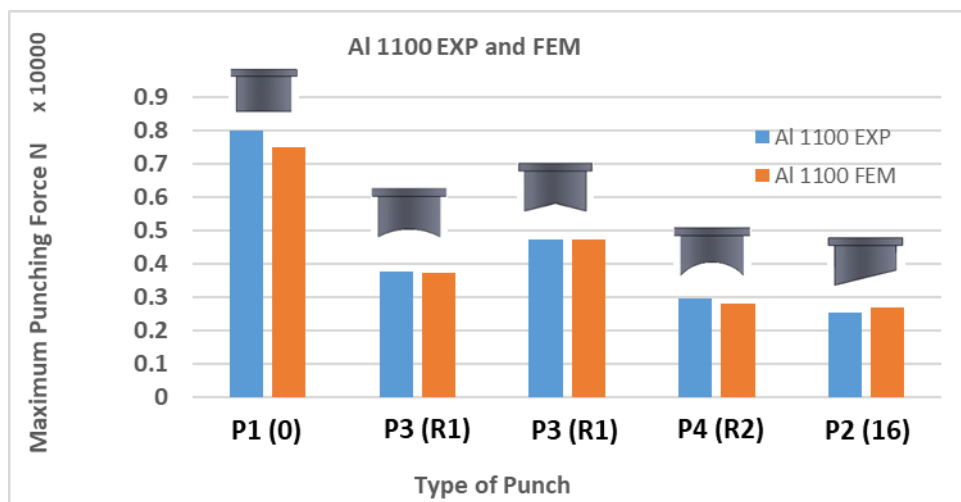
Figure 7.26. The maximum shearing forces for various punch forms on Al 1100 sheet material, as determined by experiments and FEM analysis, are compared.

FEM analyses were used to conduct the studies and simulations. The investigations employed 3D models to test the software's performance in simulating punching operations and guarantee experimental results' consistency. The analyses from cutting Al 1100 sheet material with all punches using 3D models are shown in Fig. 7.25.
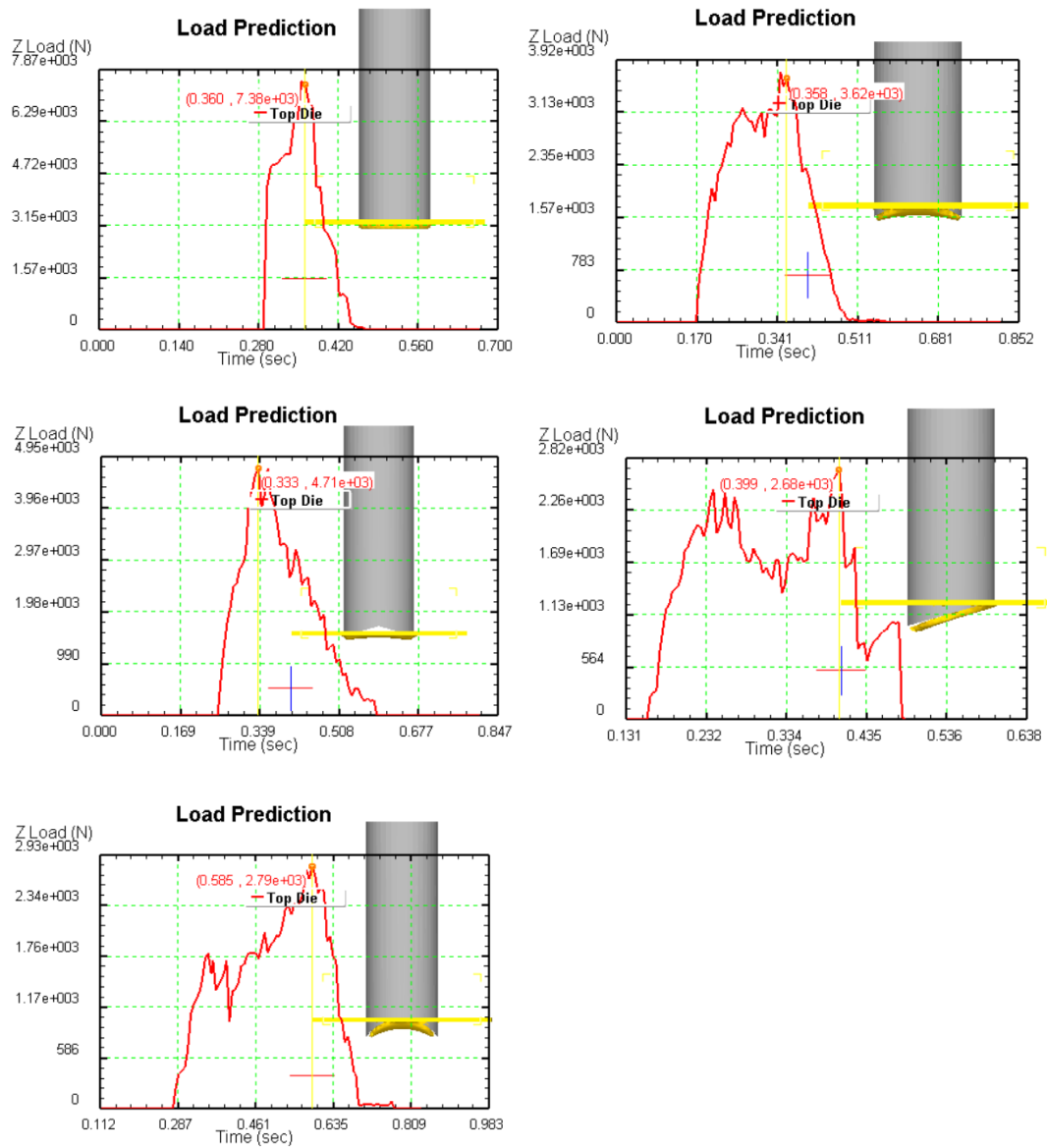
Figure 7.27. Analyses were produced by cutting Al 1100 sheets using 3D models.

Table 7.7 compares the highest cutting forces between FEM and the real-world experimental Al 1100.

Table 7.7. The difference between FEM and practical experimental Al 1100.

Punch shape	maximum cutting forces FEM	maximum cutting forces experimental	the difference %
	7491 N	7872 N	5.09%
	3730 N	3781 N	1.37%
	4671 N	4734 N	1.35%
	2788 N	2955 N	5.99%
	2685 N	2538 N	5.79%

7.4.5. Explosive Welded DP600 – Al 1100 Analysis

Additionally, it can be seen that the necessary cutting forces for cutting the DP600-Al1100 explosive welded sheet material are extremely similar as a result of experimental tests and analysis. The cutting force for punch "0" determined by FEM studies is 34181 N, while the cutting force determined experimentally is 34431 N. Both outcomes for punch V16 were 18153 N and 18152 N. For punch R1, the additional results were 18154 N and 17868 N for punch R2, 13898 N and 13847 N; and for punch 16, 11562 N and 11963 N. The first numbers listed are the findings of the FEM analyses, while the second values listed are the experiment's outcomes. Figures 7.26 and 7.27 compare the cutting forces discovered through FEM analysis and testing when cutting DP600-Al1100 explosive welded sheet material using all the punches employed.
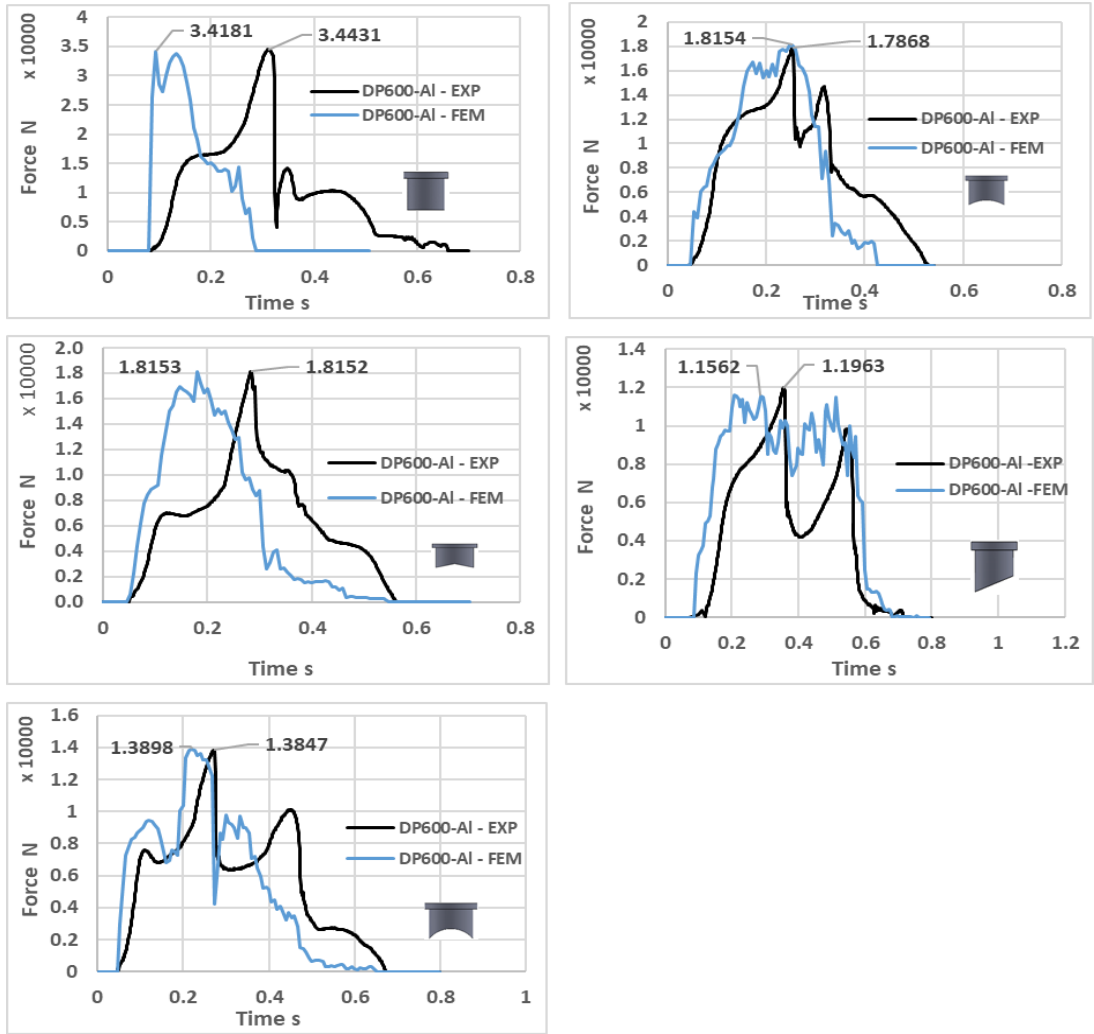
Figure 7.28. Comparative force-time graphs were created using different punch shapes in analysis and experiments on the DP600-Al1100 explosive welded sheet material.

Figure 7.29. The maximum shearing forces for various punch forms on DP600-Al1100 explosive welded sheet material are compared by experiments and FEM analysis.

FEM analyses were used to conduct the studies and simulations. To check for compatibility with experimental tests and to assess how well the program performed when simulating punching procedures, 3D models were employed in the assessments. The analyses from cutting DP600-Al1100 explosive welded sheet material with all punches using 3D models are shown in Fig. 7.25.
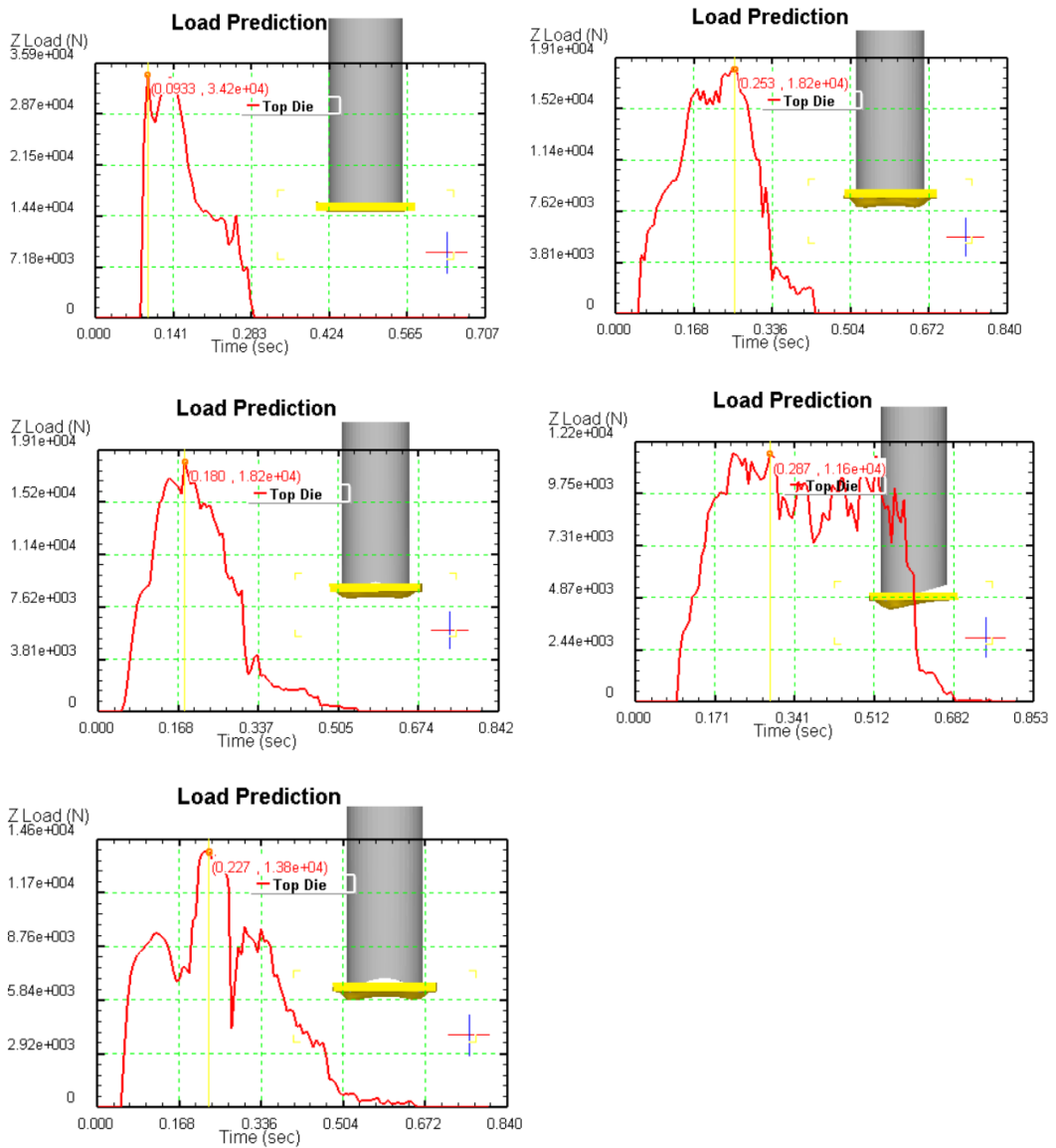
Figure 7.30. Analyses were obtained using 3D models for cutting on DP600-Al1100 explosive welded sheet material.

Table 7.8 Compares the highest cutting forces between FEM and the real-world experimental DP600-Al1100 explosive welded.

Table 7.8. The difference between FEM and practical experimental DP600-Al1100 explosive welded.

Punch shape	maximum cutting forces FEM	maximum cutting forces experimental	the difference %
	34181 N	34431 N	0.73%
	18154 N	17868 N	1.60%
	18153 N	18152 N	0.01%
	13898 N	13847 N	0.37%
	11562 N	11963 N	3.47%

7.4.6. Explosive Welded DP1000 – Al 1100 Analysis

Experimental investigations and analysis show that the needed shearing forces for cutting off the DP1000-Al1100 explosive welded sheet material are near. The practical outcome for punch 0 is 47242N, while the shearing force determined by the FEM is 47393N. The additional findings were obtained as 19573N and 20667N for the punch R1, for punch R2 they were 18518N and 18806N, for punch V16 they, were 22139N and 21502N; and for punch 16, were 12369 N and 11569N. Figures 7.31 and 7.32 compare the cutting forces discovered through FEM analysis and testing when cutting DP1000- Al1100 explosive welded using all the punches employed.

Figure 7.31. Comparative force-time graphs were created using different punch shapes in analysis and experiments on the DP1000-Al1100 explosive welded sheet material.

Figure 7.32. The maximum shearing forces for various punch forms on DP1000-Al1100 explosive welded sheet material are compared by experiments and FEM analysis.

FEM analyses were used to conduct the studies and simulations. The investigations employed 3D models to test the software's performance in simulating punching operations and guarantee experimental results' consistency. The analyses from cutting DP1000-Al1100 explosive welded sheet material with all punches using 3D models are shown in Fig. 7.31.

Figure 7.33. Analyses were obtained using 3D models for cutting on DP1000-Al1100 explosive welded sheet material.

Table 7.9 Compares the highest cutting forces between FEM and the real-world experimental DP1000-Al1100 explosive welded.

Table 7.9. The difference between FEM and practical experimental DP1000-Al1100 explosive welded.

Punch shape	maximum cutting forces FEM	maximum cutting forces experimental	the difference %
	47393 N	47242 N	0.32%
	19573 N	20667 N	5.59%
	22139 N	21502 N	2.96%
	18518 N	18806 N	1.56%
	12369 N	11569 N	6.92%

7.4.7. Explosive Welded DP1200 – Al 1100 Analysis

Experimental investigations and analysis show that the needed shearing forces for cutting off the DP1200-Al1100 explosive welded sheet material are near. The shearing force determined from FEM analysis is 48436N, while the real result is 47541N for punch "0.". The two outcomes for punch R1 were 21275 N and 20485 N, for the punch R2, they were 18706N and 18089N, for punch V16 they were 22204N and 21644N, for punch 16, they were 13673 N and 13374N.

Figures 7.34 and 7.35 compare the cutting forces discovered through FEM analysis and testing when cutting DP1200-Al1100 explosive welded sheet material using all the punches employed.

Figure 7.34. Comparative force-time graphs were created using different punch shapes in analysis and experiments on the DP1200-Al1100 explosive welded sheet material.
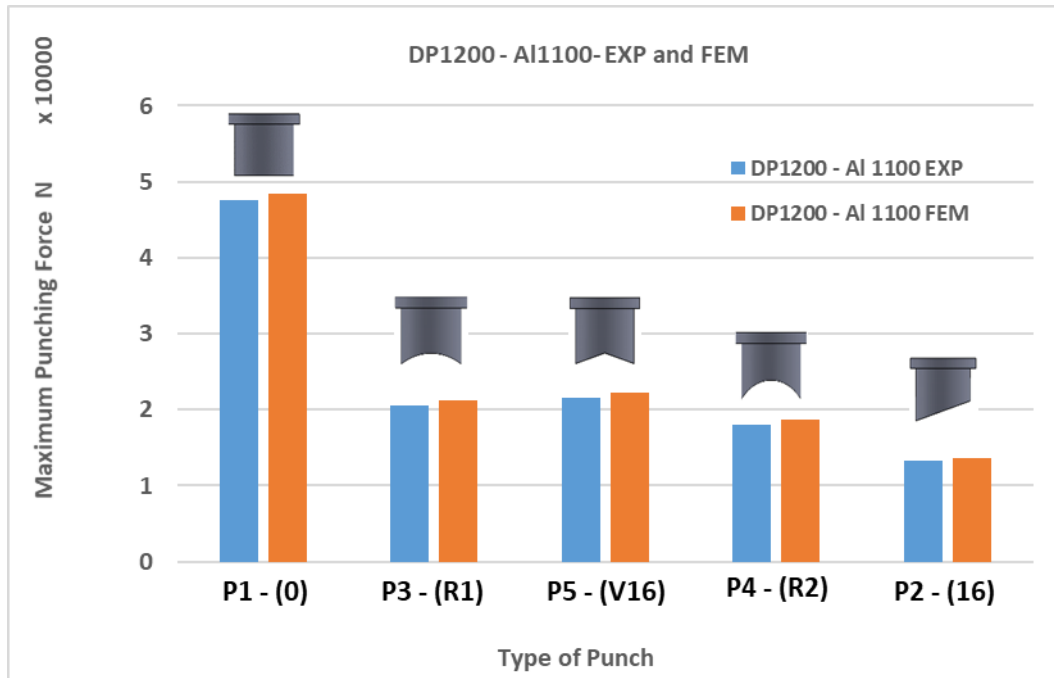
Figure 7.35. The maximum shearing forces for various punch forms on DP1200-Al1100 explosive welded sheet material are compared by experiments and FEM analysis.

FEM analyses were used to conduct the studies and simulations. The investigations employed 3D models to test the software's performance in simulating punching operations and guarantee experimental results' consistency. The analyses from cutting DP1200-Al1100 explosive welded sheet material with all punches using 3D models are shown in Fig. 7.34.
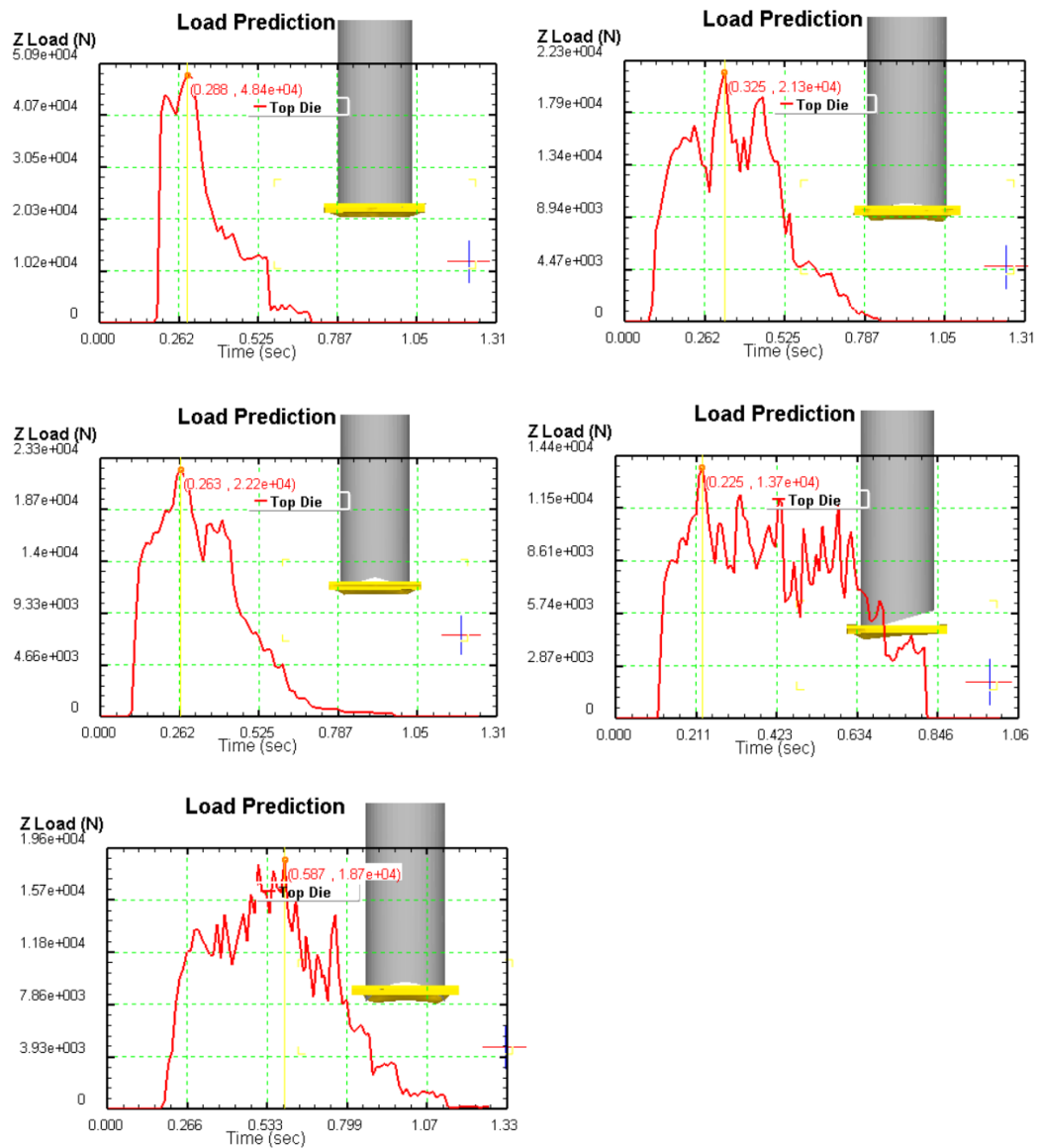
Figure 7.36. Analyses were obtained using 3D models for cutting on DP1200-Al1100 explosive welded sheet material.

Table 7.10 Compares the highest cutting forces between FEM and the real-world experimental DP1000-Al1100 explosive welded.

Table 7.10. The difference between FEM and practical experimental DP1200-Al1100 explosive welded

Punch shape	maximum cutting forces FEM	maximum cutting forces experimental	the difference %
	48436 N	47541 N	1.88%
	21275 N	20485 N	3.86%
	22204 N	21644 N	2.59%
	18706 N	18089 N	3.41%
	13673 N	13374 N	2.24%

7.5. TRYING WITH EXPLOSIVE WELDING AND UN WELDING

7.5.1. Results For Explosive Welded and Non-Welded Sheet Material In DP600-Al 1100

DP600-Al1100 sheet specimens that had been welded and had not been welded were cut to see how the welding procedure affected the cutting force. It is well known that both components get harder following the explosive welding process. The highest hardness values for these materials are close to the bonding interface, and hardness increases as the explosive ratio increases. As a result, compared to unwelded materials, the cutting force of materials combined by explosive welding was somewhat higher (Fig. 7.35).

Furthermore, it was found that slippages on the contact surfaces occurred when the non-welded sheet materials were cut together. When cutting explosively welded sheet materials, no slippage between the materials was seen (Fig. 7.36).
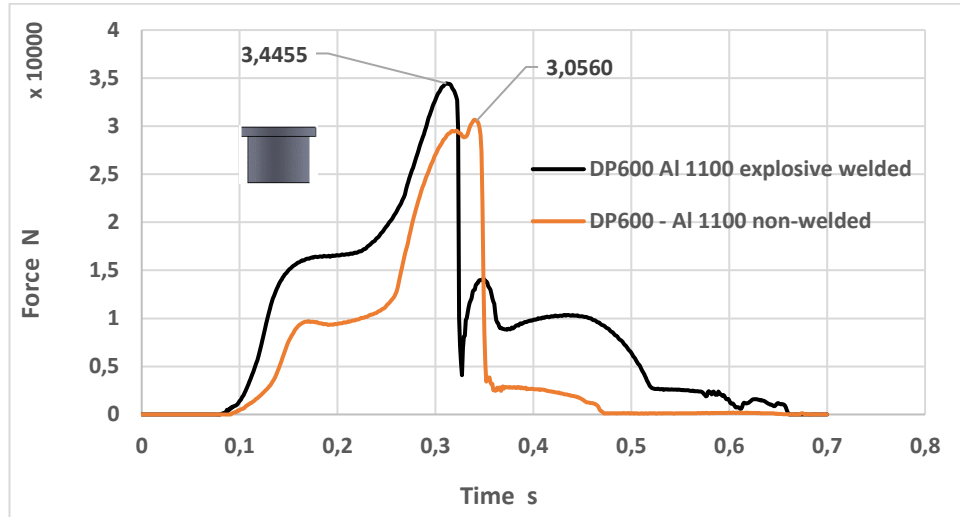
Figure 7.37. Comparison of the specimens of welded and unwelded DP600-Al1100 sheets.

| unwelded DP600-Al1100 | Welded DP600 - Al |
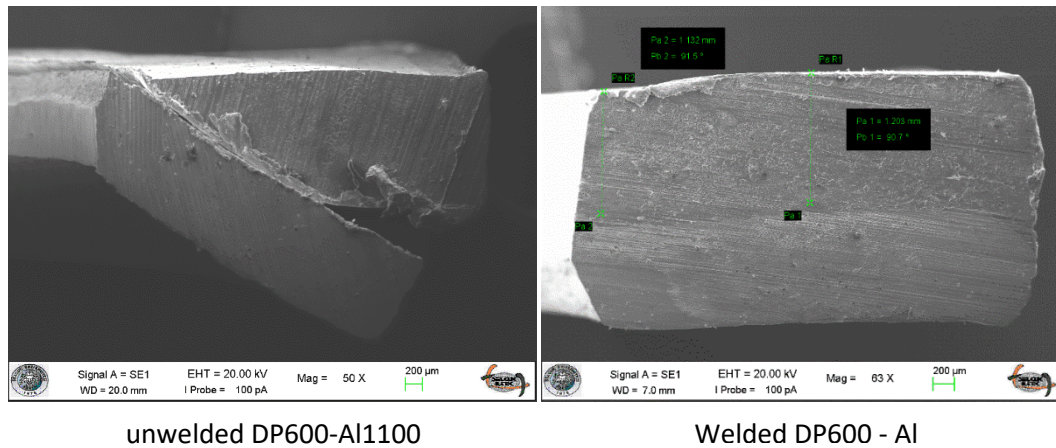
Figure 7.38. Cutting sheet materials, both welded and unwelded.

7.5.2. DP1200-Al 1100 Welded and Un-Welded Explosives Sheet Material Results

To determine how the welding process affected the shear force, DP1200-Al 1100 sheet specimens with and without welding were both punched to shear. It is well known that both components get harder following the explosive welding process.

The highest hardness values for these materials are close to the bonding interface, and hardness increases as the explosive ratio increases. As a result, compared to unwelded materials, the cutting force of materials combined by explosive welding was somewhat higher (Fig. 7.37).

Furthermore, it was found that slippages on the contact surfaces occurred when the non-welded sheet materials were cut together. When cutting explosively welded sheet materials, no slippage between the materials was seen (Fig. 7.38).
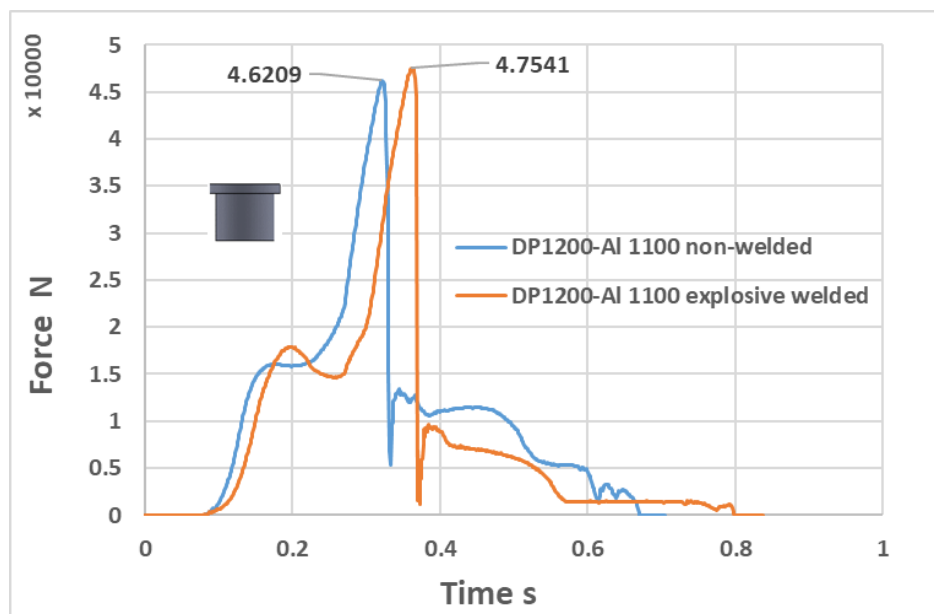
Figure 7.39. The comparison of forces vs time results from the experimental punching of DP1200 - Al 1100 pairs that were both explosively and not explosively welded.
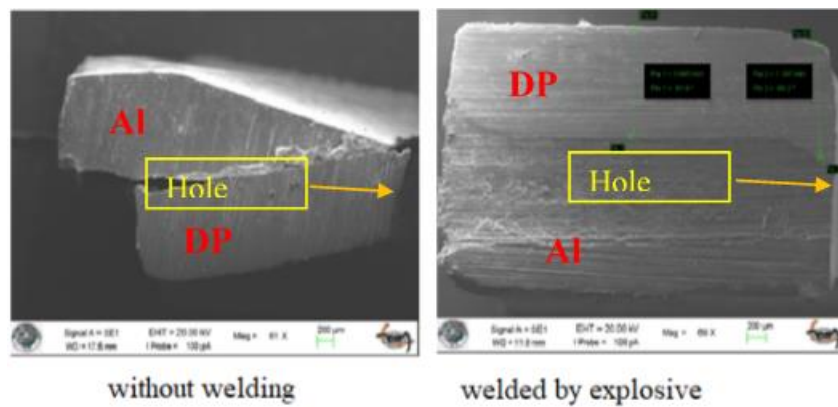
Figure 7.40. Punching Sheared part condition's images pairings of the DP1200 and Al 1100 as welds and unwelded.

125

7.6. EVALUATION OF EDGE AND SIDE PROFILE FORMS OF THE CUT PARTS

According to the experimental results, the side profile forms of the falling parts were flat where the punch "0" was used. However, the side profile forms of the falling parts for the other used punches were not flat. Therefore, it is difficult to achieve dimensional accuracy for the falling parts in the cutting processes where the other punches are used except the punch "0". Side profile forms of the blanks were obtained as planar in all punch forms used.
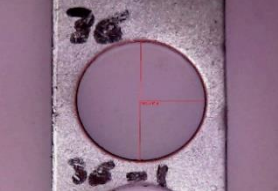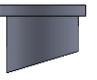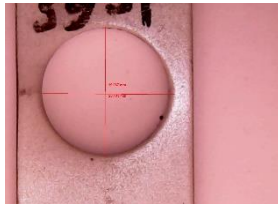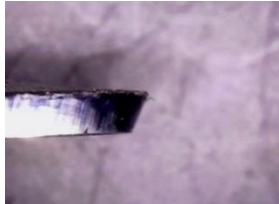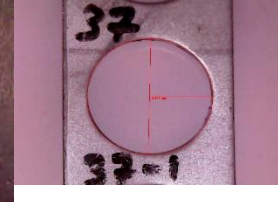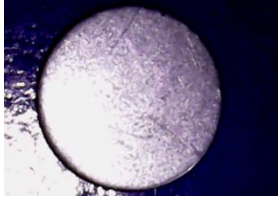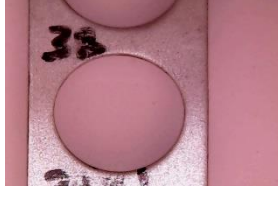
However, while using punch number 16, the cutting surfaces of both the falling and blank portions did not take on the correct shape. The measurements revealed that these cutting surfaces were angled. Following punch 16's cutting procedure, deformations appeared on the cut edges of the falling component and the blank. Additionally, the macrostructure of an explosively welded DP-Al1100 bimetal interface was studied. It was noted that when cutting forces reached their peak value during punching, the composite components did not separate from one another. Therefore, it can be claimed that the explosive welding method can create multilayer composites.

It can be concluded from experimental findings that the punch "0" is useful for both blanking and piercing processes on specimens that have been explosively fused to DP, Al1100, and DP-Al1100. Punches with concave shapes (R1 and R2) and V shapes (V16) are only suitable for piercing operations because the side form of the falling part is not flat; using these punches for the blanking process results in uncontrolled part sizes. Using punch 16 was also found to be unsuitable for both blanking and piercing processes because it permits lateral movement of the cut portion along the cutting edge. As a result, both sides' cutting surfaces are angled. Because of this, using both the blank and the falling part in manufacturing operations is inappropriate.

The following Tables show the shapes resulting from the punching process, which were taken with a microscope, in tables 7.11, 7.12, 7.13, 7.14, 7.15, 7.16, and 7.17.
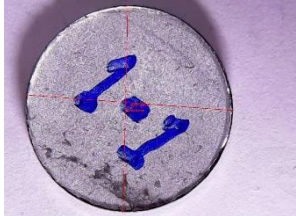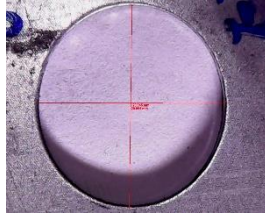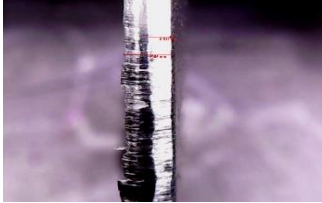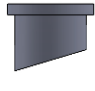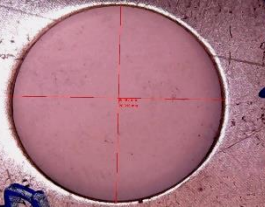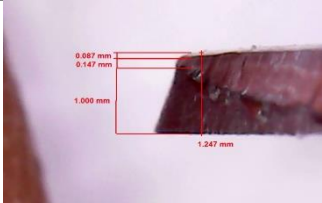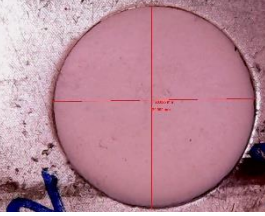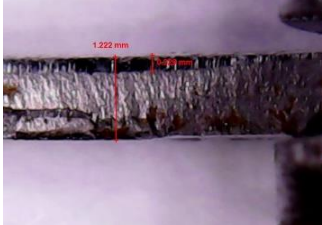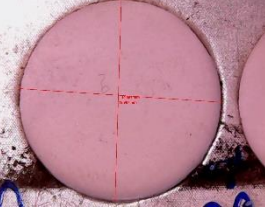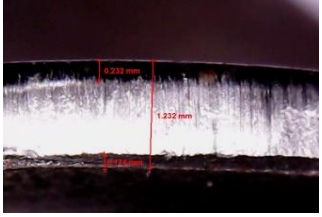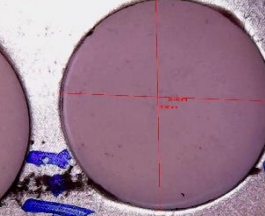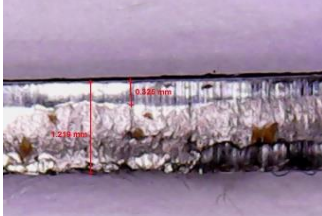
7.6.1. DP600 Analysis

Table 7.11. Punched-Sheared surface and area examinations of DP 600.

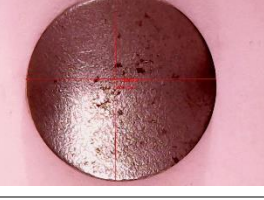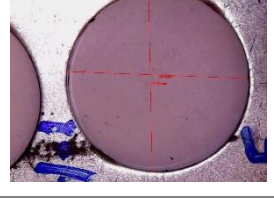| Punch shape	Blanking	Piercing	thickness
P1 (0)			
P2 (16)			
P3 (R1)			
P4 (R2)			
P5 (V16)			
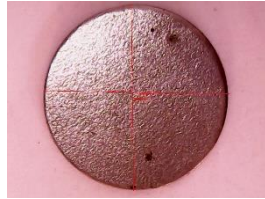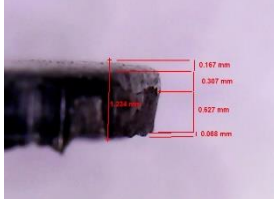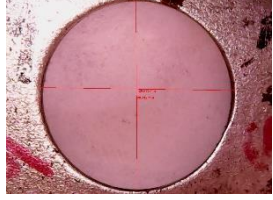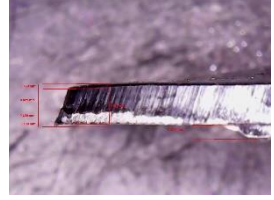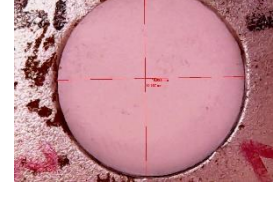
7.6.2. DP.1000

Table 7.12. Punched-Sheared surface and area examinations of DP1000.

Punch shape	Blanking	Piercing	thickness
P1 (0)			
P2 (16)			
P3 (R1)			
P4 (R2)			
P5 (V16)			
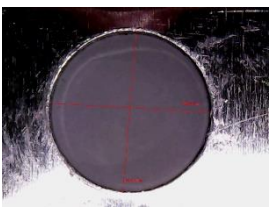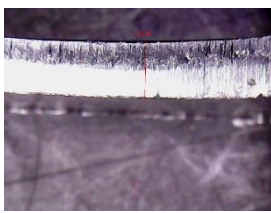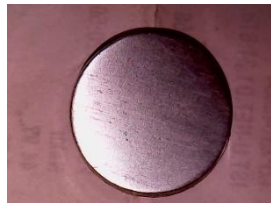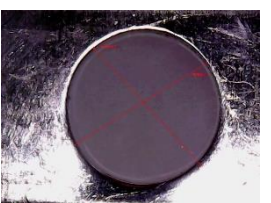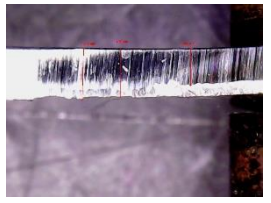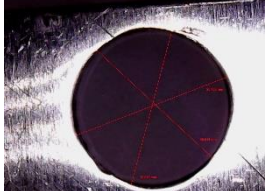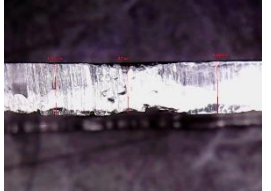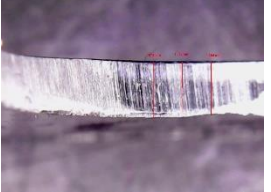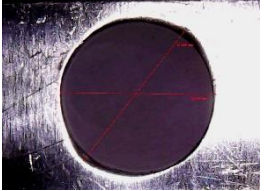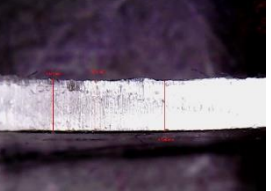
6.6.3. DP1200

Table 7.13. Punched-Sheared surface and area examinations of DP 1200.

Punch shape	Blanking	Piercing	thickness
P1 (0)			
P2 (16)			
P3 (R1)			
P4 (R2)			
P5 (V16)			
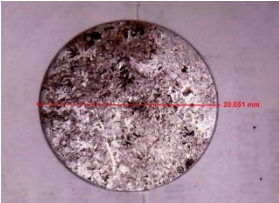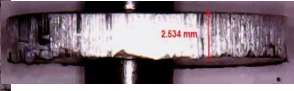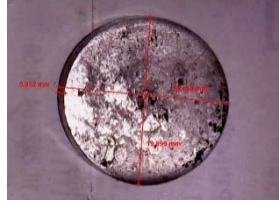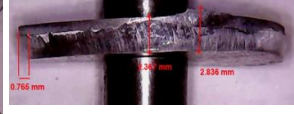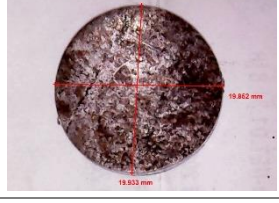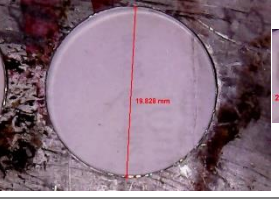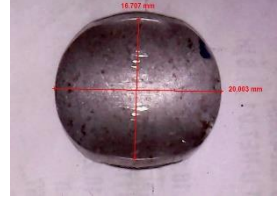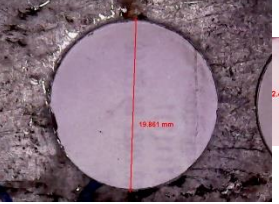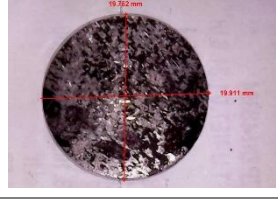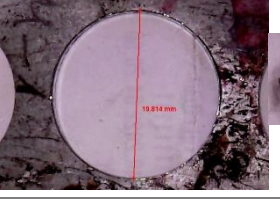
7.6.4. Al 1100 Analysis

Table 7.14. Punched-Sheared surface and area examinations of Al 1100.

Punch shape	Blanking	Piercing	thickness
P1 (0)			
P2 (16)			
P3 (R1)			
P4 (R2)			
P5 (V16)			
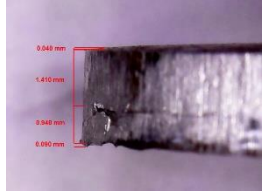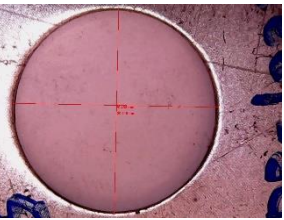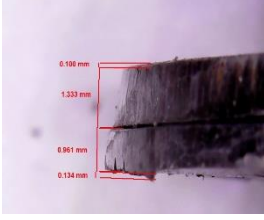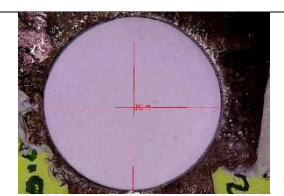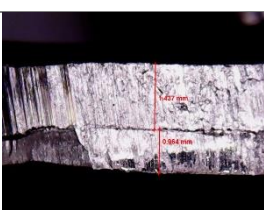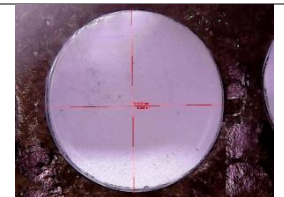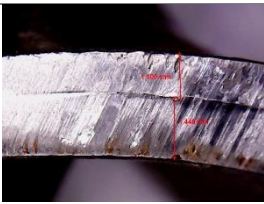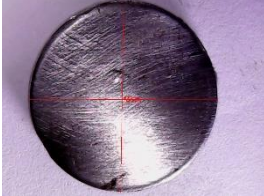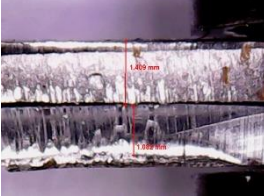
7.6.5. Explosive Welded DP600 – Al

Table 7.15. Punched-Sheared surface and area examinations of DP 600-Al explosive welded.

Punch shape	Blanking	Piercing	thickness
P1 (0)			
P2 (16)			
P3 (R1)			
P4 (R2)			
P5 (V16)			
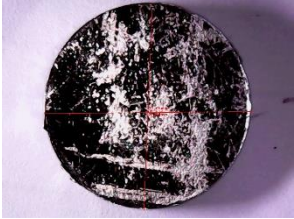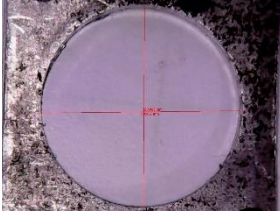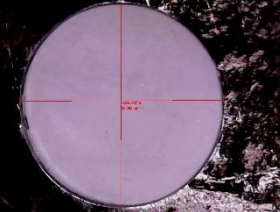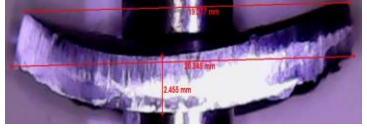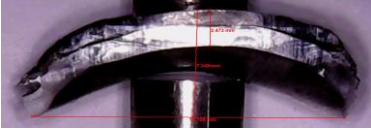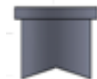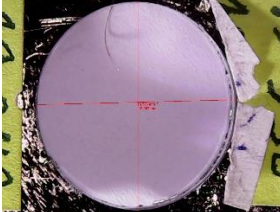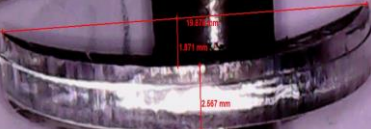
7.6.6. Explosive Welded DP1000 – Al:

Table 7.16. Punched-Sheared surface and area examinations of DP1000 -Al explosive welded.

Punch shape	Blanking	Piercing	thickness
P1 (0)			
P2 (16)			
P3 (R1)			
P4 (R2)			
P5 (V16)			

7.6.7. Explosive Welded DP1200 – Al

Table 7.17. Punched-Sheared surface and area examinations of DP1200 -Al explosive
welded.

Punch shape	Blanking	Piercing	thickness
P1 (0)			
P2 (16)			
P3 (R1)			
P4 (R2)			
P5(V16)			

7.7. SHARE SURFACES OF PUNCHING (BLANKING, PIERCING) AND AREAS EXAMINATION

One of the most crucial elements that contribute to flexibility and stretchability during expansion and flanging in the punching process is the cut surface quality. As a result, it is a key factor in the cutting process' quality approach. According to the findings of this study, four distinct regions can be examined in light of the surface texture and cutting surface described in the literature. Burr, cutting, tipping, and braking regions are the most prominently expressed in these places. A large cutting area and smaller burrs are desirable on a cutting surface of outstanding quality. Additionally, the fracture and tipping areas are preferred to be modest in the surface roughness requirement, whereas the cutting area is anticipated to be more significant. The cutting speed was held constant throughout this trial.

According to several studies, the gap influences the cutting surface characteristics. When the gap is too small, the contact of the fragmented surfaces forms the second finishing region. The shattered surfaces have been seen to touch one another in 2D numerical studies.

7.7.1. DP600
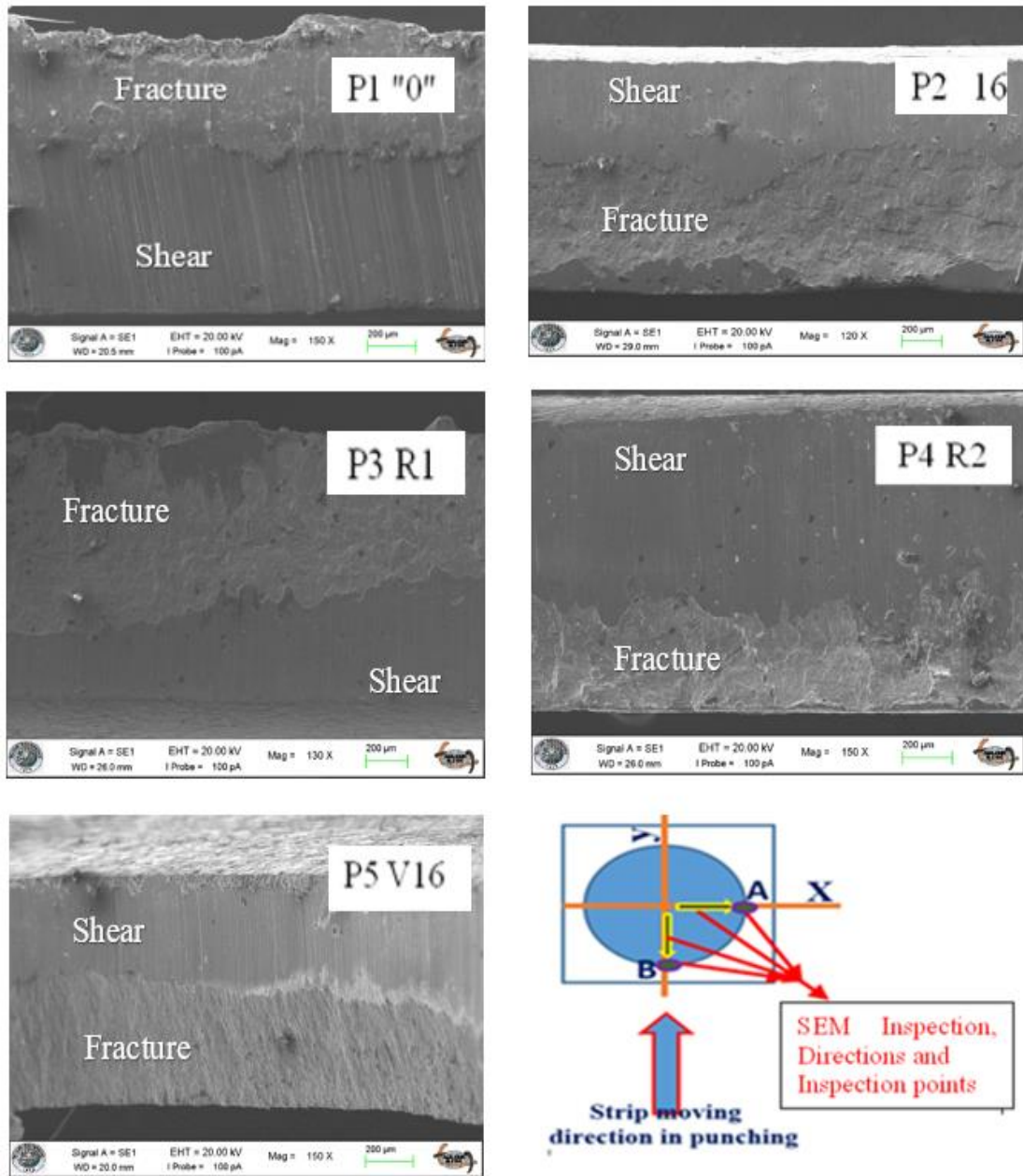
Figure 7.41. SEM images are cutting the cross-section's surface of the DP600 sheet steel.
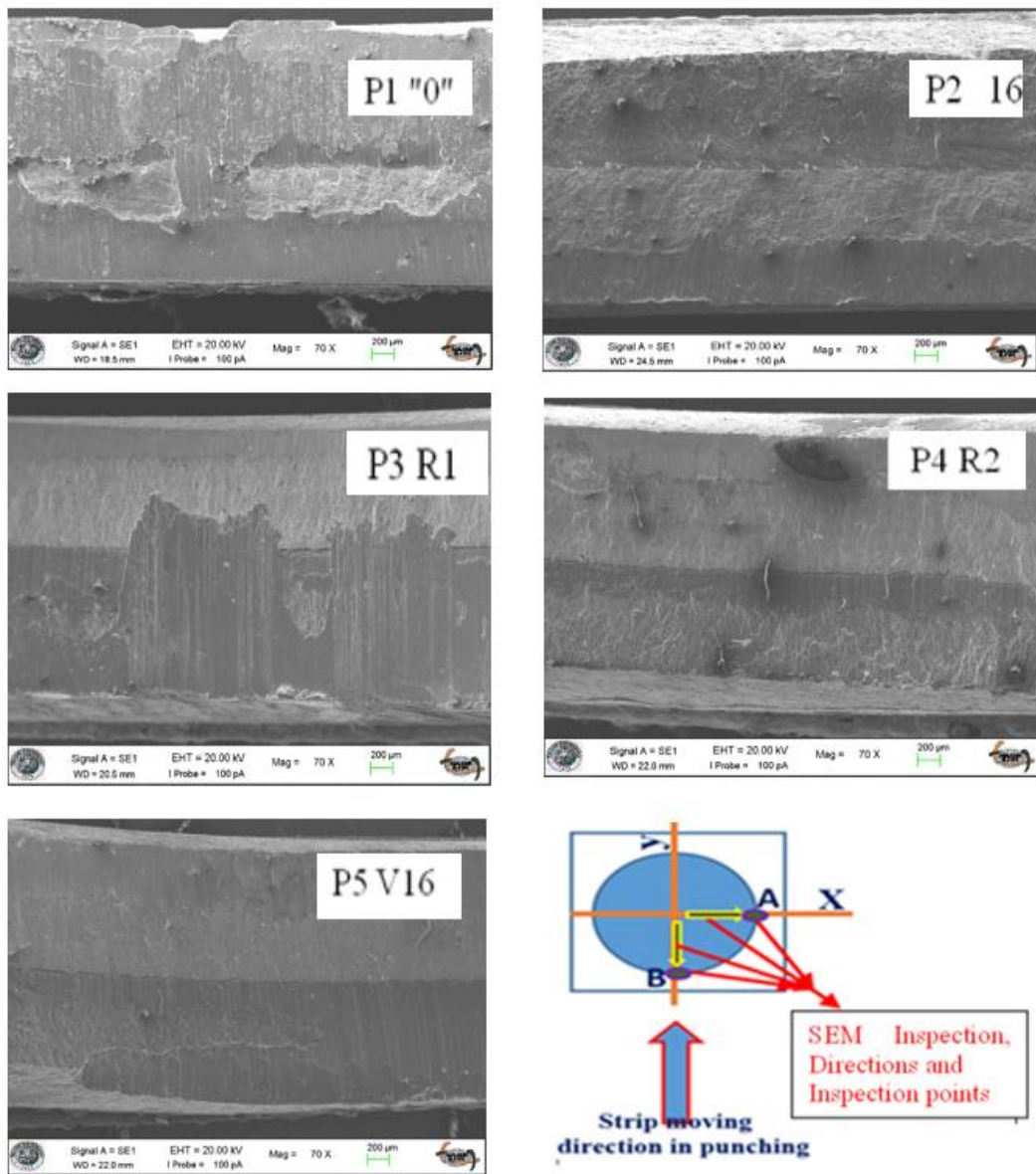
Figure 7.42. SEM photos of the DP600-Al 1100 plate composite samples' cutting
surface

7.7.2. DP1000

The cutting surface images of the pierced part taken by SEM microscopy are in Fig.
7.43 for DP1000 and Fig 7.44 for DP1000-1100 Al plate metal composite. These
figures give The macro photos and the measured status of some cutting surface
locations. It has been attained to define the rollover, shear, fracture (crack initiation
and propagation), and burr zones, commonly expressed in this image's literature, as
emphasized earlier.

Using an axe to make a hole, a picture of the view and its points (A, B) was taken.	top view X-axis point A	top view Y-axis point B
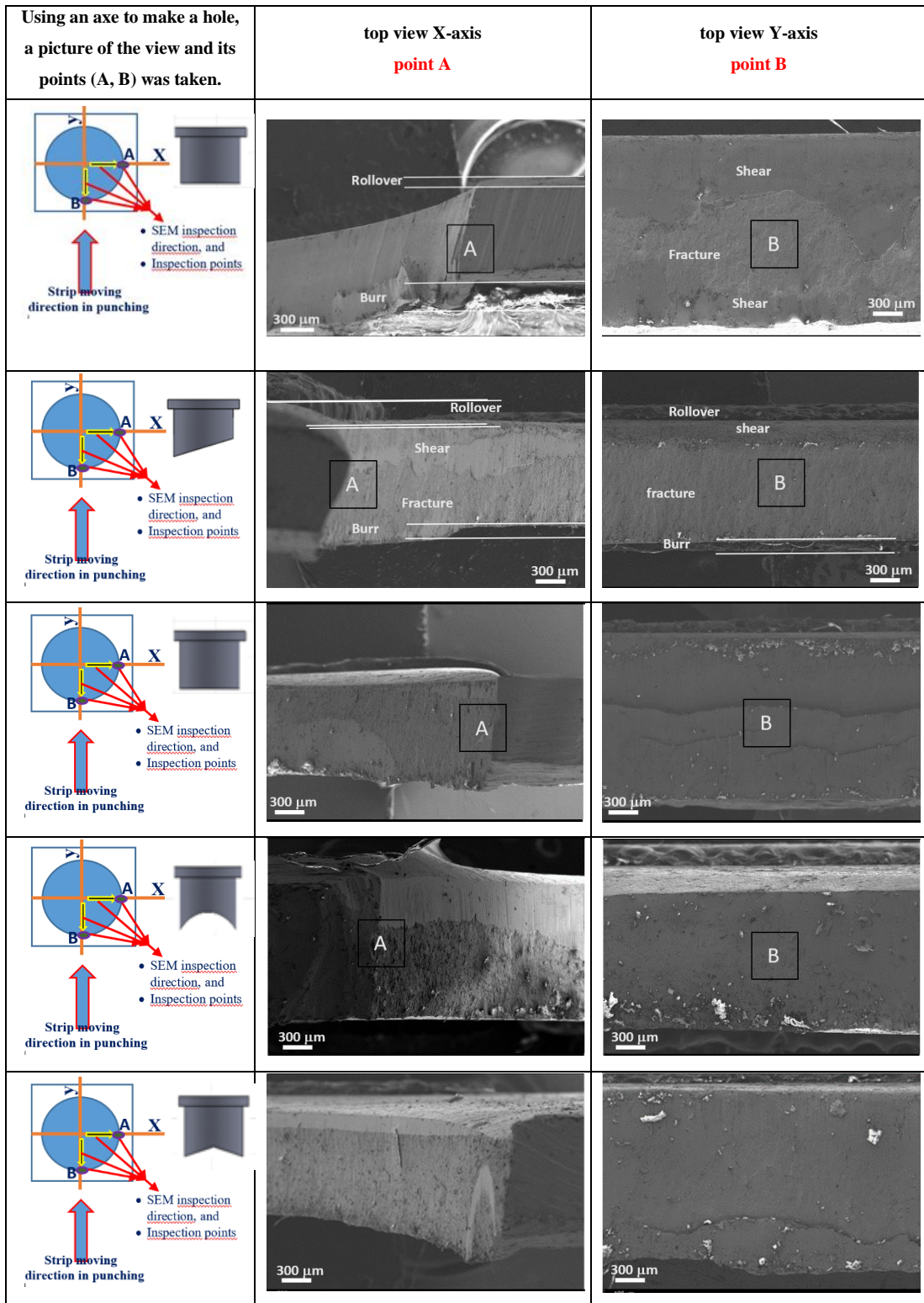
Figure 7.43. SEM images are cutting the cross surface of the DP1000 sheet steel.

Punches hole with axes, the photograph was taken a view and its points (A, B)	top view X-axis **A point**	top view Y-axis **B point**
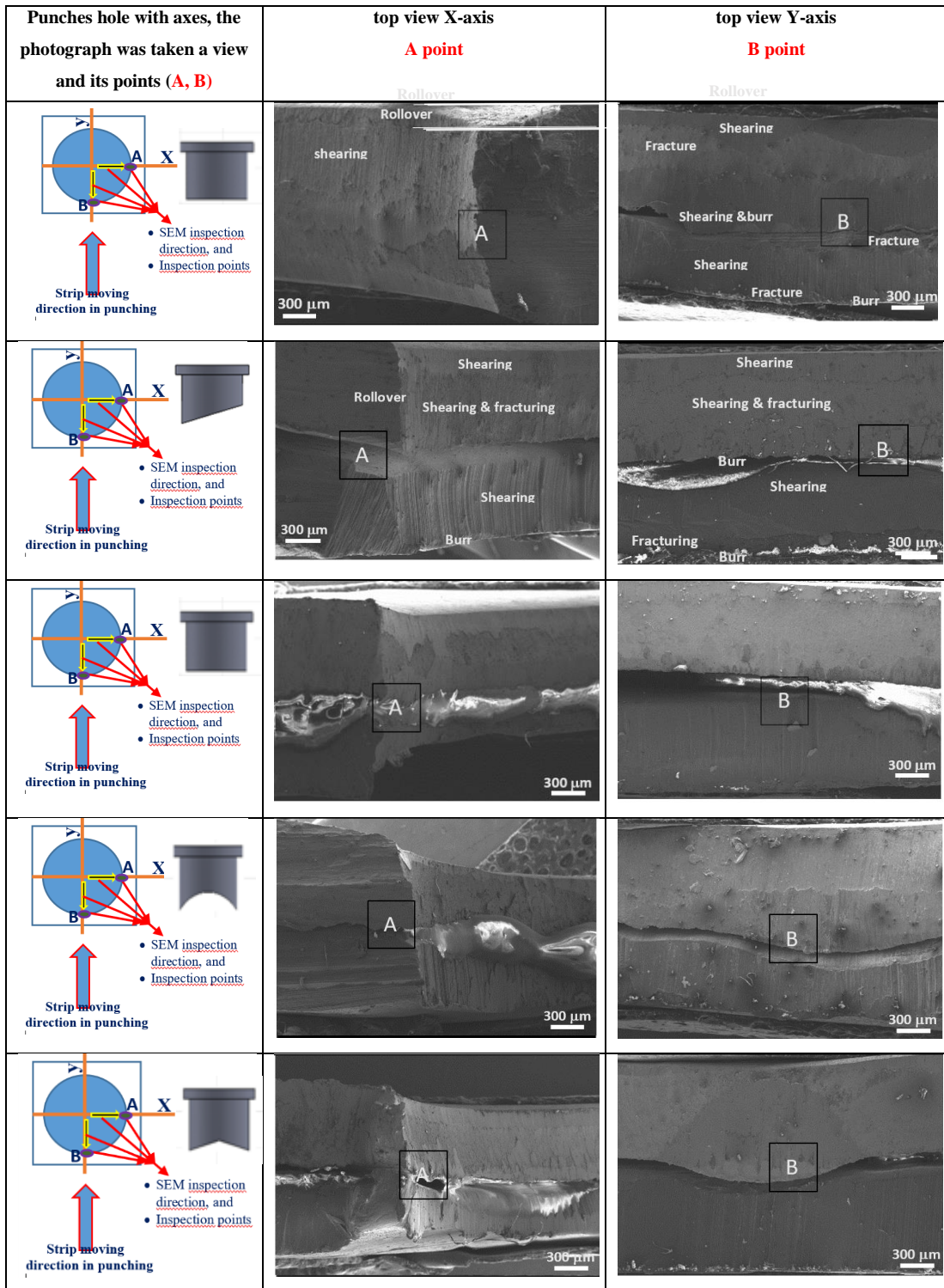
Figure 7.44. SEM photos of the DP1000-Al 1100 plate composite samples' cutting surface

7.7.3. DP1200

Figs. 7.45, 7.46, and 7.47 show the shearing-punching surface pictures of the DP1200 and DP1200-Al 1100 composites obtained for this study. The rollover, shear, fracture, and burr zones that are typically described in the literature have been defined in these pictures.

Correctly, in the case of two different materials joined with this explosion in these photographs, it is noted that these zones were almost created in both portions.

The falling part and blank shearing surfaces of punch P16 were not smooth. The measurements revealed that these shearing surfaces are angular. Figure 7.47 depicts the deformation of the falling portion and blank when punch number 16 is used.
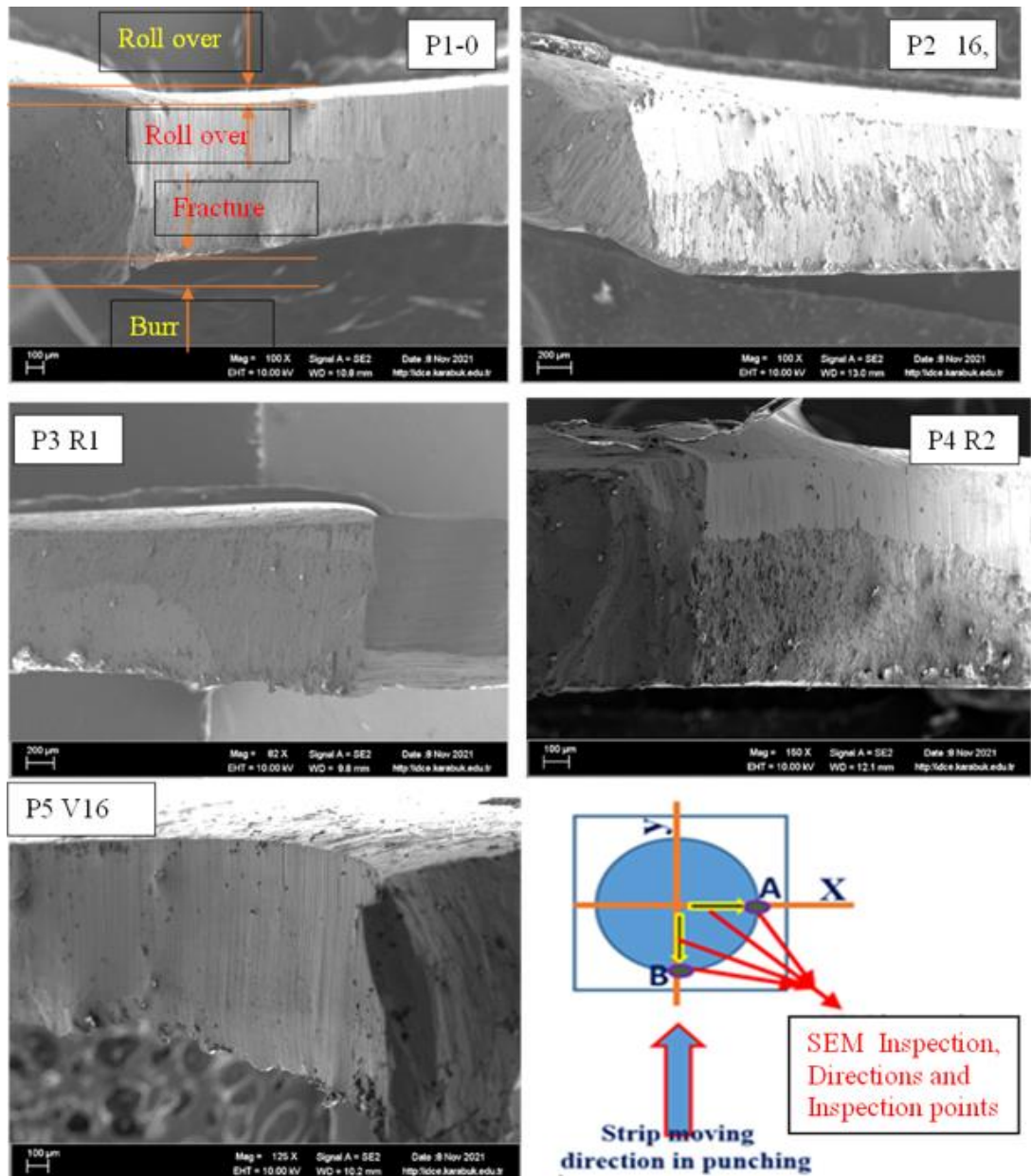
Figure 7.45. SEM photos of the DP 1200 sheet samples' shearing cross surfaces, labelled P1 (0), P2 (16), P3 (R1), P4 (R2), P5 (V16), and inspection schema, at position A.
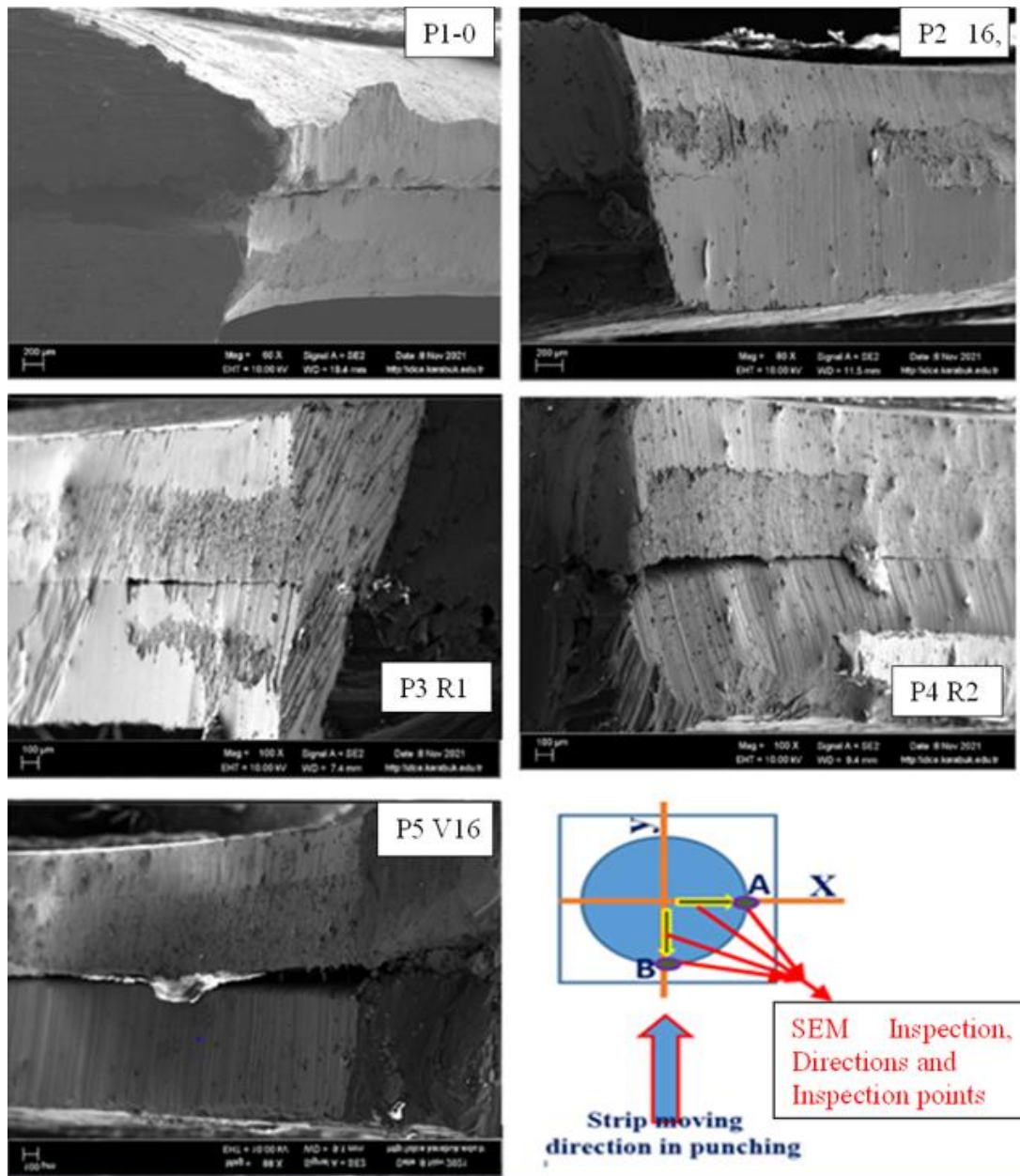
Figure 6.46. SEM photos of the DP1200–Al 1100 sheet samples' shearing cross surfaces, labelled P1 (0), P2 (16), P3 (R1), P4 (R2), P5 (V16), and inspection schema, at position A.
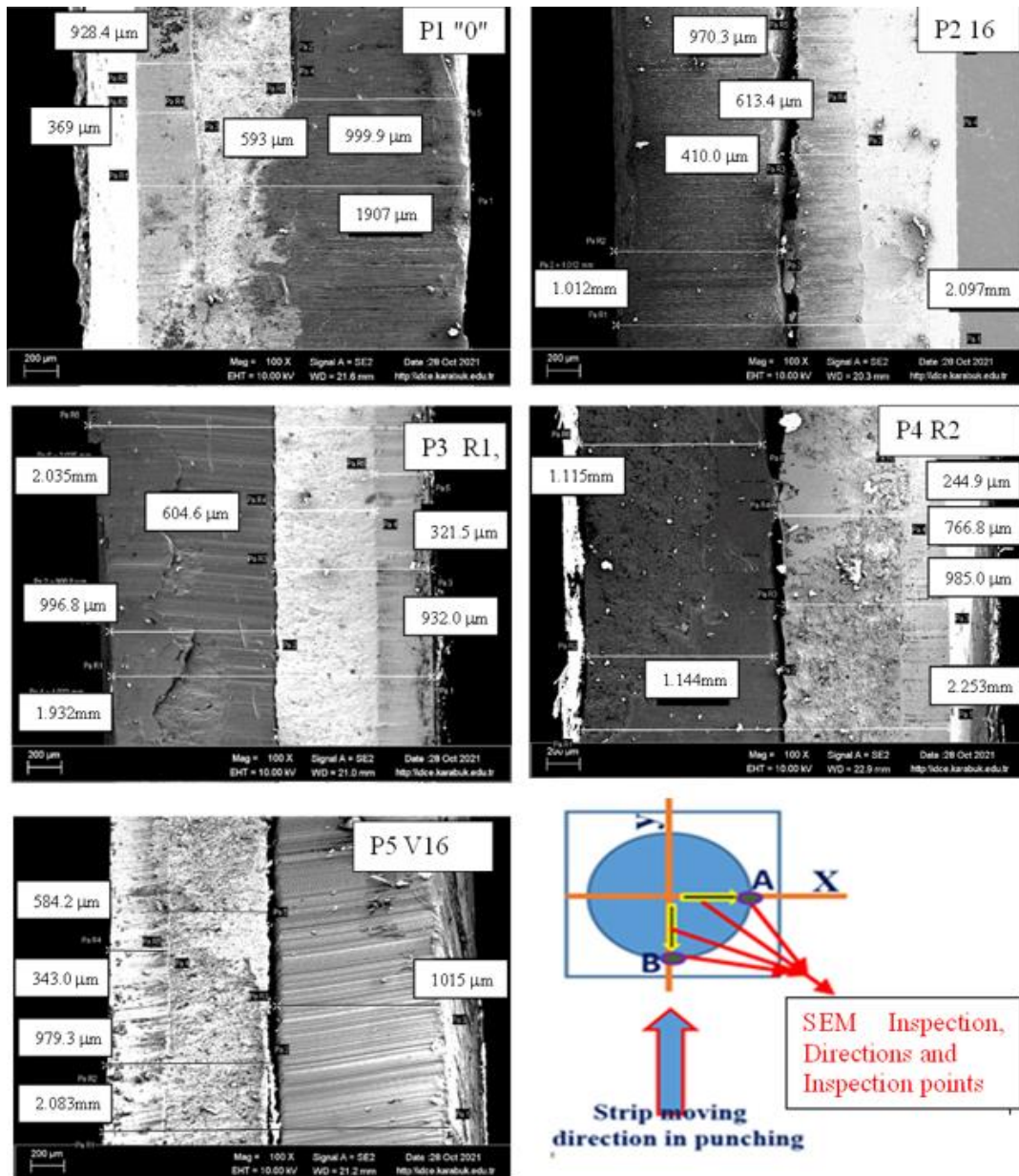
Figure 6.47. SEM-pictures (B position) measurements of the sheared surfaces of samples P1-(0), P2 (16), P3 (R1), P4 (R2), and P5, and inspection schema, in that order.

PART 8

CONCLUSIONS

This study used experimental and numerical methods to investigate the effects of several punch types (V16, R1, R2, "0," 16) on shearing forces and component quality during the blanking/piercing process. In the trials, materials such as (DP600, DP1000, DP1200, Al 1100) and (DP600-Al 1100, DP1000-Al 1100, and DP1200-Al 1100) explosive welded plate composites were employed. While the sheet materials for DP600, DP1000, DP1200, and Al 1100 were available commercially, the composite plates for DP600-Al 1100, DP1000-Al 1100, and DP1200-Al 1100 were made using explosive welding, which is a very efficient and common method for making metal composites, especially when combining different metals like steel and Al, as was the case with the specimens for this study.

It can be concluded that punch "0" should be used in punching (as blanking or piercing) operations based on the overall results of both circle and disc-shaped parts in this study, as well as the effects of experimental punch cutting and FEM modelling processes of (DP600, DP1000, DP1200, Al 1100) base metals and (DP600-Al 1100, DP1000-Al 1100, DP1200-Al 1100) explosion-welded part specimens. Only punch tips with concave shapes (punch R1 and punch R2) and punch V shapes (punch V16) are utilized for piercing. The side form of the falling piece is not straight if these punches are used for piercing or blanking; this results in uncontrolled piece sizes and shapes. Additionally, because it permits lateral movement of the component being cut along the cutting edge, punch 16 might not be the best option for blanking or piercing operations that involve falling parts, such as blanking. As a result, both sides' concave cutting surfaces are obtained at an angle. That makes it improper to use raw blanks and falling pieces in manufacture. The following inferences can be drawn as a result:

- Explosive welding might be used to join and create materials from sheet metals

143

of steel of the DP600, DP1000, and DP1200 and aluminium of the Al 1100

- The punch with the lowest shearing forces was number 16, a 16°-angled punch. However, this punch cannot be used for production since the shearing surfaces of the blank and falling portions have angular edges.

- The punch "0" (flat-ended punch, 0°) produced the largest shearing forces. When this punch was utilised, the blank and the falling bits were produced with the proper form and dimensional correctness. Punch 0's suitability for blanking and piercing operations was confirmed.

- Punch R2, V16, and R1 produced the lowest shearing forces among the other punch shapes (apart from punch "0" and punch 16). These punches can be utilized in punching operations to lessen the shearing force.

- Only punch "0" may be used in blanking processes to obtain the appropriate part form and dimensional correctness.

- It was observed that the materials slipped on top of one another, and the component shapes were not smooth during the shearing of (DP600-Al 1100, DP1000-Al 1100, and DP1200-Al 1100) sheets by stacking without welding. Explosion-welded sheets (DP600-Al 1100, DP1000-Al 1100, and DP1200-Al 1100) are sheared, and no sliding was seen between the sheet materials. It has been established that shearing sheet materials following explosive welding is practical.

- The explosively welded (DP600-Al1100, DP1000-Al1100, DP1200-Al1100) sheets sheared with larger shearing forces than the (DP600-Al1100, DP1000-Al1100, DP1200-Al1100) stacking without welding shear sheets. It is established that both components' hardness increases following the explosive welding procedure near the bonding interface.

- During punching, explosively welded (DP600- Al 1100, DP1000- Al 1100, and despite considerable shearing forces, the DP1200-Al1100 bimetal remains together.

REFERENCES

1. Matlock, D.K., et al., *Recent developments in advanced high strength sheet steels for automotive applications: an overview.* Jestech, 2012. **15**(1): p. 1-12.

2. Demir, B., M. Elitaş, and H. Karakuş, *Nokta direnç kaynağı ile birleştirilen DP600 çeliğinin çekme makaslama özelliğinin incelenmesi.* Pamukkale Üniversitesi Mühendislik Bilimleri Dergisi, 2022. **28**(4): p. 533-538.

3. DEMİR, B., M. ELİTAŞ, and H. KARAKUŞ, *Nokta direnç kaynağı ile birleştirilen DP600 çeliğinin çekme makaslama özelliğinin incelenmesi Investigation of the tensile shear property of DP600 steel combined with resistance spot welding.*

4. Matlock, D.K. and J.G. Speer, *Third generation of AHSS: microstructure design concepts*, in *Microstructure and texture in steels*. 2009, Springer. p. 185-205.

5. Hayat, F., B. Demir, and M. Acarer, *Tensile shear stress and microstructure of low-carbon dual-phase Mn-Ni steels after spot resistance welding.* Metal Science and Heat Treatment, 2007. **49**(9): p. 484-489.

6. Paetzold, I., et al. *Influence of shear cutting parameters on the fatigue behavior of a dual-phase steel*. in *Journal of physics: conference series*. 2017. IOP Publishing.

7. Davis, J.R., *Aluminum and aluminum alloys*. 1993: ASM international.

8. Santos, M.C., et al., *Machining of aluminum alloys: a review.* The International Journal of Advanced Manufacturing Technology, 2016. **86**(9): p. 3067-3080.

9. Stojanovic, B. and I. Epler, *Application of aluminum and aluminum alloys in engineering.* Applied Engineering Letters, 2018.

10. Kobayashi, T., *Strength and fracture of aluminum alloys.* Materials Science and Engineering: A, 2000. **280**(1): p. 8-16.

11. Baluch, N., Z.M. Udin, and C.S. Abdullah, *Advanced high strength steel in auto industry: an overview.* Engineering, Technology & Applied Science Research, 2014. **4**(4): p. 686-689.

12. Drexler, A., et al., *On the local evaluation of the hydrogen susceptibility of cold-formed and heat treated advanced high strength steel (AHSS) sheets.* Materials Science and Engineering: A, 2021. **800**: p. 140276.

13. Ekmekci, D. and Ö.N. Cora, *Effect of indentation loading type on the mechanical properties of advanced high strength steel grade DP 800.* Applied Physics A, 2020. **126**(11): p. 1-10.

14. Lolla, S.V.T., *Understanding Microstructure Evolution in Rapid Thermal Processing of AISI 8620 Steel.* 2009, The Ohio State University.

15. Rashid, M., *Dual phase steels.* Annual Review of Materials Science, 1981. **11**(1): p. 245-266.

16. Ji, L., et al. *On the relationship between yield ratio, uniform elongation, and strain hardening exponent of high grade pipeline steels.* in *The Seventeenth International Offshore and Polar Engineering Conference.* 2007. OnePetro.

17. Hoy, A.W., W.K. Hoy, and A.W. Hoy, *Instructional leadership: A learning-centered guide.* 2003: Allyn and Bacon Boston, MA.

18. Sahin, M., *Joining of stainless-steel and aluminium materials by friction welding.* The International Journal of Advanced Manufacturing Technology, 2009. **41**(5): p. 487-497.

19. Findik, F., *Recent developments in explosive welding.* Materials & Design, 2011. **32**(3): p. 1081-1093.

20. Mousavi, S.A., S. Al-Hassani, and A. Atkins, *Bond strength of explosively welded specimens.* Materials & Design, 2008. **29**(7): p. 1334-1352.

21. Rao, H.M., et al., *Effect of specimen configuration on fatigue properties of dissimilar aluminum to steel resistance spot welds.* International Journal of Fatigue, 2018. **116**: p. 13-21.

22. Acarer, M. and B. Demir, *An investigation of mechanical and metallurgical properties of explosive welded aluminum–dual phase steel.* Materials letters, 2008. **62**(25): p. 4158-4160.

23. Wever, D., et al., *Electrochemical and surface characterization of a nickel–titanium alloy.* Biomaterials, 1998. **19**(7-9): p. 761-769.

24. Simar, A. and M.-N. Avettand-Fènoël, *State of the art about dissimilar metal friction stir welding.* Science and Technology of Welding and Joining, 2017. **22**(5): p. 389-403.

25. Kovacs-Coskun, T., B. Volgyi, and I. Sikari-Nagl. *Investigation of aluminum-steel joint formed by explosion welding.* in *journal of physics: Conference Series.* 2015. IOP Publishing.

26. Shojaei, B., et al., *A review on the applications of polyurea in the construction industry.* Polymers for Advanced Technologies, 2021. **32**(8): p. 2797-2812.

27. Yakubovsky, O., et al. *Effect of Composition and Microstructure on the Stress-Strain Behavior of TRIP and Dual-Phase Steels.* in *Proceedings of the*

International Conference on Advanced High-Strength Sheet Steels for Automotive Applications. 2004. AIST, Warrendale, PA.

28. Boljanovic, V., *Sheet metal forming processes and die design*. 2004: Industrial Press Inc.

29. Giannakakis, T. and G. Vosniakos, *Sheet metal cutting and piercing operations planning and tools configuration by an expert system.* The International Journal of Advanced Manufacturing Technology, 2008. **36**(7): p. 658-670.

30. Gürün, H., M. Göktaş, and A. Güldaş, *Experimental examination of effects of punch angle and clearance on shearing force and estimation of shearing force using fuzzy logic.* Transactions of FAMENA, 2016. **40**(3): p. 19-28.

31. Singh, U., A. Streppel, and H. Kals, *Design study of the geometry of a punching/blanking tool.* Journal of materials processing technology, 1992. **33**(4): p. 331-345.

32. Komanduri, R., *Machining and grinding: A historical review of the classical papers.* 1993.

33. Sayyad, S., et al., *Data-driven remaining useful life estimation for milling process: sensors, algorithms, datasets, and future directions.* IEEE Access, 2021. **9**: p. 110255-110286.

34. Kang, Z., et al., *Experimental investigation of concave and convex micro-textures for improving anti-adhesion property of cutting tool in dry finish cutting.* International Journal of Precision Engineering and Manufacturing-Green Technology, 2018. **5**(5): p. 583-591.

35. Hu, J., Z. Marciniak, and J. Duncan, *Mechanics of sheet metal forming.* 2002: Elsevier.

36. Abdullah, A., et al., *Precision punching: A new method in hole-making on composite panels*, in *Hole-Making and Drilling Technology for Composites.* 2019, Elsevier. p. 115-133.

37. Liu, H., et al., *Microhole Forming and Creep Behavior of Fe-Based Nanocrystalline Alloys under Laser Dynamic Impact.* Advanced Engineering Materials, 2020. **22**(5): p. 1901361.

38. Wu, X., H. Bahmanpour, and K. Schmid, *Characterization of mechanically sheared edges of dual phase steels.* Journal of Materials Processing Technology, 2012. **212**(6): p. 1209-1224.

39. Ubhayaratne, I., et al., *Audio signal analysis for tool wear monitoring in sheet metal stamping.* Mechanical Systems and Signal Processing, 2017. **85**: p. 809-826.

40. Griffin, J.M., et al., *Application of machine learning for acoustic emissions waveform to classify galling wear on sheet metal stamping tools.* The

International Journal of Advanced Manufacturing Technology, 2021. **116**(1): p. 579-596.

41. Ali, A.K., Y. Wang, and J.L. Alvarado, *Facilitating industrial symbiosis to achieve circular economy using value-added by design: A case study in transforming the automobile industry sheet metal waste-flow into Voronoi facade systems.* Journal of cleaner production, 2019. **234**: p. 1033-1044.

42. Altan, T., B. Lilly, and Y. Yen, *Manufacturing of dies and molds.* CIRP Annals, 2001. **50**(2): p. 404-422.

43. Cui, Z. and L. Gao, *Studies on hole-flanging process using multistage incremental forming.* CIRP Journal of Manufacturing Science and Technology, 2010. **2**(2): p. 124-128.

44. Karjalainen, J.A., K. Mäntyjärvi, and M. Juuso. *Punching force reduction with wave-formed tools.* in *Key Engineering Materials.* 2007. Trans Tech Publ.

45. Park, N., et al., *Fracture-based forming limit criteria for anisotropic materials in sheet metal forming.* International journal of plasticity, 2017. **96**: p. 1-35.

46. Taupin, E., et al., *Material fracture and burr formation in blanking results of FEM simulations and comparison with experiments.* Journal of Materials processing technology, 1996. **59**(1-2): p. 68-78.

47. Koenig, W., et al., *Machining of fibre reinforced plastics.* CIRP Annals, 1985. **34**(2): p. 537-548.

48. Cheung, C.F., W.B. Lee, and W. Chiu, *An investigation of tool wear in the dam-bar cutting of integrated circuit packages.* Wear, 2000. **237**(2): p. 274-282.

49. Lee, W.B., et al., *Automatic supervision of blanking tool wear using pattern recognition analysis.* International Journal of Machine Tools and Manufacture, 1997. **37**(8): p. 1079-1095.

50. Goijaerts, A., L. Govaert, and F. Baaijens, *Evaluation of ductile fracture models for different metals in blanking.* Journal of Materials Processing Technology, 2001. **110**(3): p. 312-323.

51. Soares, J., et al., *Study of the punch–die clearance influence on the sheared edge quality of thick sheets.* The International Journal of Advanced Manufacturing Technology, 2013. **65**(1): p. 451-457.

52. Wojtkowiak, D., et al., *Estimation of the perforation force for polymer composite conveyor belts taking into consideration the shape of the piercing punch.* The International Journal of Advanced Manufacturing Technology, 2018. **98**(9): p. 2539-2561.

53. Pepelnjak, T. and B. Kaftanoglu. *Finite element analysis of non-isothermal warm deep drawing of dual phase steel.* in *MATEC Web of Conferences.* 2016. EDP Sciences.

54. KEELE, R. and M. KIMICHI, *Advanced High-Strength Steels: Application Guidelines.* World Auto Steel, 2014.

55. Choi, H.-S., B.-M. Kim, and D.-C. Ko, *Effect of clearance and inclined angle on sheared edge and tool failure in trimming of DP980 sheet.* Journal of Mechanical Science and technology, 2014. **28**(6): p. 2319-2328.

56. Montazeri, S., M. Aramesh, and S.C. Veldhuis, *Novel application of ultra-soft and lubricious materials for cutting tool protection and enhancement of machining induced surface integrity of Inconel 718.* Journal of Manufacturing Processes, 2020. **57**: p. 431-443.

57. Galán, J., et al., *Advanced high strength steels for automotive industry.* Revista de metalurgia, 2012. **48**(2): p. 118.

58. Demir, B. and M. Erdoğan, *The hardenability of austenite with different alloy content and dispersion in dual-phase steels.* Journal of materials processing technology, 2008. **208**(1-3): p. 75-84.

59. Zhao, F., et al., *The correlated impacts of fuel consumption improvements and vehicle electrification on vehicle greenhouse gas emissions in China.* Journal of Cleaner Production, 2019. **207**: p. 702-716.

60. Fayad, M., et al., *Manipulating modern diesel engine particulate emission characteristics through butanol fuel blending and fuel injection strategies for efficient diesel oxidation catalysts.* Applied Energy, 2017. **190**: p. 490-500.

61. Kuziak, R., R. Kawalla, and S. Waengler, *Advanced high strength steels for automotive industry.* Archives of civil and mechanical engineering, 2008. **8**(2): p. 103-117.

62. Wagoner, R.H. and G. Smith, *Advanced high strength steel workshop.* Arlington, Virginia, USA, 2006. **1**: p. 122.

63. Cornette, D., et al., *SAE Technical Paper of the SAE World Congress.* SAE International, Detroit, MI, 2005.

64. Hance, B.M., *Advanced high-strength steel (AHSS) performance level definitions and targets.* SAE International Journal of Materials and Manufacturing, 2018. **11**(4): p. 505-516.

65. Wu, Z.Q., et al., *Microstructural evolution and strain hardening behavior during plastic deformation of Fe–12Mn–8Al–0.8 C steel.* Materials Science and Engineering: A, 2013. **584**: p. 150-155.

66. Demeri, M.Y., *Advanced high-strength steels.* Science, Technology and applications, 2013: p. 264.

67. Khan, M., M. Kuntz, and Y. Zhou, *Effects of weld microstructure on static and impact performance of resistance spot welded joints in advanced high strength steels.* Science and Technology of Welding and Joining, 2008. **13**(3): p. 294-304.

68. Leslie, W. and A. Keh, *Mechanical working of steel II*. 1965, Gordon and Breach, New York.

69. Li, C.-C. and W. Leslie, *Effects of dynamic strain aging on the subsequent mechanical properties of carbon steels*. Metallurgical Transactions A, 1978. **9**(12): p. 1765-1775.

70. Zhang, S. and K. Findley, *Quantitative assessment of the effects of microstructure on the stability of retained austenite in TRIP steels*. Acta Materialia, 2013. **61**(6): p. 1895-1903.

71. Findley, K., et al., *Controlling the work hardening of martensite to increase the strength/ductility balance in quenched and partitioned steels*. Materials & Design, 2017. **117**: p. 248-256.

72. Cai, X.-L., J. Feng, and W. Owen, *The dependence of some tensile and fatigue properties of a dual-phase steel on its microstructure*. Metallurgical transactions A, 1985. **16**(8): p. 1405-1415.

73. Alzahougi, A., M. Elitas, and B. Demir, *RSW junctions of advanced automotive sheet steel by using different electrode pressures*. Engineering, Technology & Applied Science Research, 2018. **8**(5): p. 3492-3495.

74. Paul, S.K., *Effect of martensite volume fraction on stress triaxiality and deformation behavior of dual phase steel*. Materials & Design, 2013. **50**: p. 782-789.

75. Ramazani, A., et al., *Modelling the effect of microstructural banding on the flow curve behaviour of dual-phase (DP) steels*. Computational Materials Science, 2012. **52**(1): p. 46-54.

76. DEMİR, B., M. ELİTAŞ, and H. KARAKUŞ, *The Effects of the Electrode Type on Microstructure and Hardness of the RSW of DP600 Steel*. Nevşehir Bilim ve Teknoloji Dergisi. **9**(2): p. 181-193.

77. Xu, X., S. van der Zwaag, and W. Xu, *The effect of martensite volume fraction on the scratch and abrasion resistance of a ferrite–martensite dual phase steel*. Wear, 2016. **348**: p. 80-88.

78. Ramazani, A., et al., *Quantification of the effect of transformation-induced geometrically necessary dislocations on the flow-curve modelling of dual-phase steels*. International Journal of Plasticity, 2013. **43**: p. 128-152.

79. Elitas, M. and B. Demir, *Residual stress evaluation during RSW of DP600 sheet steel*. Materials Testing, 2020. **62**(9): p. 888-890.

80. Ramazani, A., et al., *Correlation between 2D and 3D flow curve modelling of DP steels using a microstructure-based RVE approach*. Materials Science and Engineering: A, 2013. **560**: p. 129-139.

81. Ramazani, A., et al., *Characterization and modelling of failure initiation in DP steel.* Computational materials science, 2013. **75**: p. 35-44.

82. Basantia, S.K., et al., *Influence of microstructural parameters on nanohardness of various dual-phase steels: Experiment, Finite Element simulation and Statistical analysis.* Materials Today Communications, 2022. **30**: p. 103125.

83. Pathak, N., et al., *Damage evolution in complex-phase and dual-phase steels during edge stretching.* Materials, 2017. **10**(4): p. 346.

84. Maggi, S. and M. Murgia, *Introduction to the metallurgic characteristics of advanced high-strength steels for automobile applications.* Welding International, 2008. **22**(9): p. 610-618.

85. Zhao, D., et al., *Modeling and process analysis of resistance spot welded DP600 joints based on regression analysis.* Materials & Design, 2016. **110**: p. 676-684.

86. Pushkareva, I., et al., *Relationship between microstructure, mechanical properties and damage mechanisms in high martensite fraction dual phase steels.* ISIJ international, 2015: p. ISIJINT-2015-186.

87. Bracke, L., et al., *Microstructure and texture evolution during cold rolling and annealing of a high Mn TWIP steel.* Acta Materialia, 2009. **57**(5): p. 1512-1524.

88. Roth, R., J. Clark, and A. Kelkar, *Automobile bodies: can aluminum be an economical alternative to steel?* Jom, 2001. **53**(8): p. 28-32.

89. Tasan, C.C., et al., *An overview of dual-phase steels: advances in microstructure-oriented processing and micromechanically guided design.* Annual Review of Materials Research, 2015. **45**: p. 391-431.

90. Pouranvari, M., *Critical assessment 27: dissimilar resistance spot welding of aluminium/steel: challenges and opportunities.* Materials science and technology, 2017. **33**(15): p. 1705-1712.

91. Zuidema, B.K., *Bridging the design–manufacturing–materials data gap: material properties for optimum design and manufacturing performance in light vehicle steel-intensive body structures.* JOM, 2012. **64**(9): p. 1039-1047.

92. ELİTAŞ, M. and B. DEMİR, *Elektrod Basıncının Nokta Direnç Kaynaklı DP600 Çeliğinin Mikroyapı ve Sertliğine Etkileri.* Nevşehir Bilim ve Teknoloji Dergisi. **7**(2): p. 194-205.

93. MI, K., et al., *Microstructure and mechanical properties of resistance spot welded advanced high strength steels.* Materials Transactions, 2008: p. 0805260435-0805260435.

94. Long, X. and S.K. Khanna, *Fatigue properties and failure characterization of spot welded high strength steel sheet.* International journal of fatigue, 2007. **29**(5): p. 879-886.

95. Ma, C., et al., *Microstructure and fracture characteristics of spot-welded DP600 steel.* Materials Science and Engineering: A, 2008. **485**(1-2): p. 334-346.

96. Lindgren, C., J. Sperle, and M. Jonsson, *Fatigue strength of spot welded beams in high strength steels.* WELDING IN THE WORLD-LONDON-, 1996. **37**: p. 90-104.

97. Holovenko, O., et al., *Microstructural and mechanical characterization of welded joints on innovative high-strength steels.* La Metallurgia Italiana, 2013.

98. Pal, T.K. and K. Bhowmick, *Resistance spot welding characteristics and high cycle fatigue behavior of DP 780 steel sheet.* Journal of Materials Engineering and Performance, 2012. **21**(2): p. 280-285.

99. Ghaheri, A., A. Shafyei, and M. Honarmand, *Effects of inter-critical temperatures on martensite morphology, volume fraction and mechanical properties of dual-phase steels obtained from direct and continuous annealing cycles.* Materials & Design (1980-2015), 2014. **62**: p. 305-319.

100. Farabi, N., D. Chen, and Y. Zhou, *Fatigue properties of laser welded dual-phase steel joints.* Procedia Engineering, 2010. **2**(1): p. 835-843.

101. Sarwar, M. and R. Priestner, *Influence of ferrite-martensite microstructural morphology on tensile properties of dual-phase steel.* Journal of materials science, 1996. **31**(8): p. 2091-2095.

102. Erden, M.A., *The effect of the sintering temperature and addition of niobium and vanadium on the microstructure and mechanical properties of microalloyed PM steels.* Metals, 2017. **7**(9): p. 329.

103. Mazaheri, Y., et al., *Effects of initial microstructure and thermomechanical processing parameters on microstructures and mechanical properties of ultrafine grained dual phase steels.* Materials Science and Engineering: A, 2014. **612**: p. 54-62.

104. Sodjit, S. and V. Uthaisangsuk, *A micromechanical flow curve model for dual phase steels.* Journal of Metals, Materials and Minerals, 2012. **22**(1).

105. Kuang, S., et al., *Effect of continuous annealing parameters on the mechanical properties and microstructures of a cold rolled dual phase steel.* International Journal of Minerals, Metallurgy and Materials, 2009. **16**(2): p. 159-164.

106. RAHMAH, M.M.M., *FARKLI TİPTE ZIMBA KULLANILARAK DP600 OTOMOTİV SAC ÇELİĞİNİN PRESTE DELME İŞLEMİNİN, TEORİK VE DENEYSEL İNCELENMESİ.* 2021.

107. Calcagnotto, M., D. Ponge, and D. Raabe, *Microstructure control during fabrication of ultrafine grained dual-phase steel: characterization and effect of intercritical annealing parameters.* ISIJ international, 2012. **52**(5): p. 874-883.

108. Chang, C., *Correlation between the microstructure of dual phase steel and industrial tube bending performance.* 2010.

109. Kuang, S., et al. *Simulation of Intercritical austenization of a C-Mn cold rolled dual phase steel.* in *Materials Science Forum.* 2008. Trans Tech Publ.

110. Alzahougi, A.R.O., *Investigation and simulation of resistance spot welding using dp600 steel in automotive industry.* 2020.

111. Dai, Q., et al., *Structural parameters of the martensite transformation for austenitic steels.* Materials characterization, 2002. **49**(4): p. 367-371.

112. Hayat, F. and B. Demir, *The effect of the weld time on dept intensity factor and strength at RSW junctions of commercial DP600 sheet steel, 5.* Uluslararası İleri Teknolojiler Sempozyumu (IATS'09), Karabük, Türkiye, 2009: p. 13-15.

113. Elitas, M. and B. Demir, *The effects of the welding parameters on tensile properties of RSW junctions of DP1000 sheet steel.* Engineering, Technology & Applied Science Research, 2018. **8**(4): p. 3116-3120.

114. Amirthalingam, K., *Women's rights, international norms, and domestic violence: Asian perspectives.* Human Rights Quarterly, 2005: p. 683-708.

115. Waterschoot, T., L. Kestens, and B.C. De Cooman, *Hot rolling texture development in CMnCrSi dual-phase steels.* Metallurgical and Materials Transactions A, 2002. **33**(4): p. 1091-1102.

116. Amirthalingam, M., *Microstructural development during welding of TRIP steels.* 2010.

117. Garrido, F., V. Illera, and M. Garcia-Gonzalez, *Effect of the addition of gypsum- and lime-rich industrial by-products on Cd, Cu and Pb availability and leachability in metal-spiked acid soils.* Applied Geochemistry, 2005. **20**(2): p. 397-408.

118. Meng, Q., et al., *Effect of water quenching process on microstructure and tensile properties of low alloy cold rolled dual-phase steel.* Materials & Design, 2009. **30**(7): p. 2379-2385.

119. Park, K., et al., *Effect of the martensite distribution on the strain hardening and ductile fracture behaviors in dual-phase steel.* Materials Science and Engineering: A, 2014. **604**: p. 135-141.

120. Avramovic-Cingara, G., et al., *Effect of martensite distribution on damage behaviour in DP600 dual phase steels.* Materials Science and Engineering: A, 2009. **516**(1-2): p. 7-16.

121. Mazinani, M. and W. Poole, *Effect of martensite plasticity on the deformation behavior of a low-carbon dual-phase steel.* Metallurgical and materials transactions A, 2007. **38**(2): p. 328-339.

122. Peng-Heng, C. and A. Preban, *The effect of ferrite grain size and martensite volume fraction on the tensile properties of dual phase steel.* Acta Metallurgica, 1985. **33**(5): p. 897-903.

123. Ramazani, A., et al., *Characterisation of microstructure and modelling of flow behaviour of bainite-aided dual-phase steel.* Computational materials science, 2013. **80**: p. 134-141.

124. Jiang, Z., Z. Guan, and J. Lian, *Effects of microstructural variables on the deformation behaviour of dual-phase steel.* Materials Science and Engineering: A, 1995. **190**(1-2): p. 55-64.

125. Calcagnotto, M., D. Ponge, and D. Raabe, *Effect of grain refinement to 1 μm on strength and toughness of dual-phase steels.* Materials Science and Engineering: A, 2010. **527**(29-30): p. 7832-7840.

126. Calcagnotto, M., et al., *Deformation and fracture mechanisms in fine-and ultrafine-grained ferrite/martensite dual-phase steels and the effect of aging.* Acta Materialia, 2011. **59**(2): p. 658-670.

127. Speich, G., *Physical metallurgy of dual-phase steels.* Fundamentals of dual-phase steels, 1981: p. 3-45.

128. Morais, W.A.d. and H.C. Borges, *Condições técnico-econômicas para viabilizar o emprego de aços planos de elevada resistência mecânica em aplicações práticas.* Tecnologia em Metalurgia, Materiais e Mineração, 2013. **6**(1): p. 1-6.

129. Pouranvari, M. and S. Marashi, *Failure mode transition in AHSS resistance spot welds. Part I. Controlling factors.* Materials Science and Engineering: A, 2011. **528**(29-30): p. 8337-8343.

130. Chung, J. and O. Kwon. *Development of high performance auto steels at Posco steels.* in *Proc. of the 9th ICTP Conference, Gjeongjyu-Korea.* 2008.

131. Yoshida, F., M. Urabe, and V. Toropov, *Identification of material parameters in constitutive model for sheet metals from cyclic bending tests.* International journal of mechanical sciences, 1998. **40**(2-3): p. 237-249.

132. Keeler, S. and M. Kimchi, *Advanced high-strength steels application guidelines V5.* 2015: WorldAutoSteel.

133. Hasegawa, K., et al., *Effects of microstructure on stretch-flange-formability of 980 MPa grade cold-rolled ultra high strength steel sheets.* ISIJ international, 2004. **44**(3): p. 603-609.

134. Huang, K., et al., *The double-edge effect of second-phase particles on the recrystallization behaviour and associated mechanical properties of metallic materials.* Progress in Materials Science, 2018. **92**: p. 284-359.

135. Crane, E., *What happens in shearing metal.* Machinery, 1927. **30**(763): p. 225-230.

136. Oldenburg, P., *Study in shearing.* Mach. Tool Blue Book, 1980. **75**(7): p. 77-90.

137. Hambli, R., A. Potiron, and A. Kobi, *Application of design of experiment technique for metal blanking processes optimization.* Mécanique & industries, 2003. **4**(3): p. 175-180.

138. Gustafsson, E., M. Oldenburg, and A. Jansson, *Design and validation of a sheet metal shearing experimental procedure.* Journal of Materials Processing Technology, 2014. **214**(11): p. 2468-2477.

139. Suchy, I., *Handbook of die design.* Vol. 1998. 2006: McGraw-Hill New York.

140. Chatterjee, S., S.S. Mahapatra, and K. Abhishek, *Simulation and optimization of machining parameters in drilling of titanium alloys.* Simulation Modelling Practice and Theory, 2016. **62**: p. 31-48.

141. Lange, K., *Handbook of metal forming.* McGraw-Hill Book Company, 1985, 1985: p. 1216.

142. Totre, A., R. Nishad, and S. Bodke, *An overview of factors affecting in blanking processes.* International Journal of Emerging Technology and Advanced Engineering (IJETAE), 2013. **3**(3): p. 390-395.

143. Choy, C. and R. Balendra. *Experimental analysis of parameters influencing sheared-edge profiles.* in *Proceedings of the Fourth International Conference on Sheet Metal, Twente.* 1996.

144. Hambli, R., *Etude expérimentale, numérique et théorique du découpage des tôles en vue de l'optimisation du procédé.* 1996, ENSAM.

145. Hambli, R. and F. Guerin, *Application of a neural network for optimum clearance prediction in sheet metal blanking processes.* Finite Elements in Analysis and Design, 2003. **39**(11): p. 1039-1052.

146. Arslan, Y., et al., *An investigation of the hole diameter and circulirty on the stainless steel sheet perforated via by deep cryogenically treated cold work tool steel punches.* Journal of Engineering Research and Applied Science, 2016. **5**(1): p. 378-390.

147. Makich, H., et al., *Metrology of the burr amount-correlation with blanking operation parameters (blanked material–wear of the punch).* International Journal of Material Forming, 2008. **1**(1): p. 1243-1246.

148. Hernández, J., et al., *Modelling and experimental analysis of the effects of tool wear on form errors in stainless steel blanking.* Journal of Materials Processing Technology, 2006. **180**(1-3): p. 143-150.

149. Marcondes, P., et al., *A smart stamping tool for punching and broaching combination.* Journal of Materials Processing Technology, 2008. **206**(1-3): p. 184-193.

150. Singh, U. and H. STREPPEL. *Computer aided design study of a die-set for punching/blanking.* in *Machine Tool Design and Research: International Conference Proceedings.* 2016. Macmillan International Higher Education.

151. Suchy, I., *Handbook of die design.* 2006: McGraw-Hill Education.

152. Levy, B. and C. Van Tyne, *Review of the shearing process for sheet steels and its effect on sheared-edge stretching.* Journal of materials engineering and performance, 2012. **21**(7): p. 1205-1213.

153. Shivpuri, R., et al., *Energy release rate based approach for the wear of punches in precision blanking of high strength steel.* CIRP annals, 2011. **60**(1): p. 307-310.

154. Mackensen, A., et al., *Experimental investigation of the cutting force reduction during the blanking operation of AHSS sheet materials.* CIRP annals, 2010. **59**(1): p. 283-286.

155. Murakawa, M., et al., *Precision piercing and blanking of ultrahigh-strength steel sheets.* Procedia Engineering, 2014. **81**: p. 1114-1120.

156. Thipprakmas, S. and A. Sontamino, *Fabrication of clean cut surface on high strength steel using a new shaving die design.* Journal of Mechanical Science and Technology, 2020. **34**(1): p. 301-317.

157. Matsuno, T., et al., *Synergy effect of shear angle and anisotropic material ductility on hole-expansion ratio of high-strength steels.* Journal of Materials Processing Technology, 2016. **230**: p. 167-176.

158. Mori, K.-i., Y. Abe, and Y. Suzui, *Improvement of stretch flangeability of ultra high strength steel sheet by smoothing of sheared edge.* Journal of Materials Processing Technology, 2010. **210**(4): p. 653-659.

159. Casellas, D., et al., *Fracture toughness to understand stretch-flangeability and edge cracking resistance in AHSS.* Metallurgical and Materials Transactions A, 2017. **48**(1): p. 86-94.

160. ISO, D., *16630: Metallic materials–Method of hole expanding test.* Deutsches Institut für Normung eV, 2003.

161. Larour, P., et al. *Evaluation of alternative stretch flangeability testing methods to ISO16630 standard.* in *IDDRG 2014 Conference, Paris, France.* 2014.

162. Larour, P., et al. *Edge crack simulation with the modular "smiley" forming tool.".* in *Proceedings of International Deep Drawing Research Group 2016 conference.* 2016.

163. Dykeman, J., et al., *Characterization of edge fracture in various types of advanced high strength steel.* SAE Technical Paper, 2011: p. 01-1058.

164. Watanabe, K., et al., *Simple Prediction Method for the Edge Fracture of Steel Sheet During Vehicle Collision–Evaluation of Fracture Limit from the Edge Using Small-Sized Test Pieces*. LS-Dyna Anwenderforum, Ulm, Deutschland, 2006.

165. Frómeta, D., et al. *Evaluation of edge formability in high strength sheets through a fracture mechanics approach*. in *AIP Conference Proceedings*. 2019. AIP Publishing LLC.

166. Mori, K.-i., *Review of shearing processes of high strength steel sheets*. Journal of Manufacturing and Materials Processing, 2020. **4**(2): p. 54.

167. Nakada, N., et al., *Quantification of large deformation with punching in dual phase steel and change of its microstructure–part II: local strain mapping of dual phase steel by a combination technique of electron backscatter diffraction and digital image correlation methods*. isij international, 2016. **56**(11): p. 2077-2083.

168. Yokoi, T., et al., *Quantification of large deformation with punching in dual phase steel and change of its microstructure–Part I: Proposal of the quantification technique of the punching damage of the dual phase steel*. isij international, 2016. **56**(11): p. 2068-2076.

169. Mucha, J., *An experimental analysis of effects of various material tool's wear on burr during generator sheets blanking*. The International Journal of Advanced Manufacturing Technology, 2010. **50**(5): p. 495-507.

170. Luo, S., *Studies on the wear conditions and the sheared edges in punching*. Wear, 1997. **208**(1-2): p. 81-90.

171. Luo, S., *Effect of the geometry and the surface treatment of punching tools on the tool life and wear conditions in the piercing of thick steel plate*. Journal of Materials Processing Technology, 1999. **88**(1-3): p. 122-133.

172. Tekiner, Z., M. Nalbant, and H. Gürün, *An experimental study for the effect of different clearances on burr, smooth-sheared and blanking force on aluminium sheet metal*. Materials & design, 2006. **27**(10): p. 1134-1138.

173. Kwak, T., Y. Kim, and W. Bae, *Finite element analysis on the effect of die clearance on shear planes in fine blanking*. Journal of Materials Processing Technology, 2002. **130**: p. 462-468.

174. Hu, X., et al., *Edge fracture prediction of traditional and advanced trimming processes for AA6111-T4 sheets*. Journal of Manufacturing Science and Engineering, 2014. **136**(2).

175. Akyürek, F., K. Yaman, and Z. Tekiner, *An experimental work on tool wear affected by die clearance and punch hardness*. Arabian Journal for Science and Engineering, 2017. **42**(11): p. 4683-4692.

176. Lin, Y., M.-S. Chen, and J. Zhong, *Numerical simulation for stress/strain distribution and microstructural evolution in 42CrMo steel during hot upsetting process.* Computational Materials Science, 2008. **43**(4): p. 1117-1122.

177. Lin, Y., et al., *Constitutive descriptions for hot compressed 2124-T851 aluminum alloy over a wide range of temperature and strain rate.* Computational Materials Science, 2010. **50**(1): p. 227-233.

178. Yang, C.-C. and X.-Y. Lin, *The forming analysis of two-stage extrusion for 1010 fastener.* Journal of Mechanical Engineering and Automation, 2016. **6**(3): p. 43-50.

179. Mehtonen, S., L. Karjalainen, and D. Porter, *Hot deformation behavior and microstructure evolution of a stabilized high-Cr ferritic stainless steel.* Materials Science and Engineering: A, 2013. **571**: p. 1-12.

180. Liu, X., et al., *Study on hot deformation behaviour of 316LN austenitic stainless steel based on hot processing map.* Materials Science and Technology, 2013. **29**(1): p. 24-29.

181. Sun, S.L., M.G. Zhang, and W.W. He. *Hot deformation behavior and hot processing map of P92 steel.* in *Advanced Materials Research.* 2010. Trans Tech Publ.

182. Maarefdoust, M., *Simulation of finite volume of hot forging process of industrial gear.* International Proceedings of Computer Science and Information Technology, 2012. **57**: p. 111.

183. Lin, Y., M.-S. Chen, and J. Zhong, *Effects of deformation temperatures on stress/strain distribution and microstructural evolution of deformed 42CrMo steel.* Materials & Design, 2009. **30**(3): p. 908-913.

184. Evans, R. and P. Scharning, *Axisymmetric compression test and hot working properties of alloys.* Materials science and technology, 2001. **17**(8): p. 995-1004.

185. Oh, S., et al., *Capabilities and applications of FEM code DEFORM: the perspective of the developer.* Journal of Materials Processing Technology, 1991. **27**(1-3): p. 25-42.

186. Zhang, Z., et al., *Simulation of 42CrMo steel billet upsetting and its defects analyses during forming process based on the software DEFORM-3D.* Materials Science and Engineering: A, 2009. **499**(1-2): p. 49-52.

187. Maiti, S., et al., *Assessment of influence of some process parameters on sheet metal blanking.* Journal of Materials Processing Technology, 2000. **102**(1-3): p. 249-256.

188. Maiti, S., *A numerical study on the edge-profile during shearing of bars using the principles of linear elastic fracture mechanics.* 1982.

189. McClintock, F.A., *A criterion for ductile fracture by the growth of holes.* 1968.

190. Chadwick, M. and P. Jackson, *Explosive welding in planar geometries.* Explosive Welding, Forming and Compaction, 1983: p. 219-287.

191. Carpenter, S. and R. Wittman, *Explosion welding.* Annual review of materials science, 1975. **5**(1): p. 177-199.

192. Linse, V., R. Wittman, and R. Carlson, *Explosive Bonding.* Vol. 225. 1967: Battelle Memorial Institute, Defense Metals Information Center.

193. Acarer, M., et al., *Microstructure, mechanical properties, and corrosion resistance of an explosively welded Mg–Al composite.* Journal of Magnesium and Alloys, 2022. **10**(4): p. 1086-1095.

194. Birkhoff, G., et al., *Explosives with lined cavities.* Journal of Applied Physics, 1948. **19**(6): p. 563-582.

195. Ezra, A.A., *Principles and practice of explosive metalworking.* Industrial Newspapers, 1973. **150**.

196. Walsh, J., R. Shreffler, and F. Willig, *Limiting conditions for jet formation in high velocity collisions.* Journal of Applied Physics, 1953. **24**(3): p. 349-359.

197. Cowan, G.R. and A.H. Holtzman, *Flow configurations in colliding plates: explosive bonding.* Journal of applied physics, 1963. **34**(4): p. 928-939.

198. Abrahamson, G.R., *Permanent periodic surface deformations due to a traveling jet.* 1961.

199. Hunt, J., *Wave formation in explosive welding.* The Philosophical Magazine: A Journal of Theoretical Experimental and Applied Physics, 1968. **17**(148): p. 669-680.

200. Robinson, J., *The inviscid nonlinear instability of parallel shear flows.* Journal of Fluid Mechanics, 1974. **63**(4): p. 723-752.

201. Carpenter, S.H., *Explosion Welding: A Review.* Shock Waves and High-Strain-Rate Phenomena in Metals: Concepts and Applications, 1981: p. 941-959.

202. Fiala, A.D., *Determination of the Mass of Jupiter from a Study of the Motion of (57) Mnemosyne.* 1968: Yale University.

203. Bahr, G., E. Zeitler, and K. Kobayashi, *High-Voltage Electron Microscopy.* Journal of Applied Physics, 1966. **37**(7): p. 2900-2907.

204. Nagarkar, M.D., *A STUDY OF DIFFUSION IN EXPLOSION WELDED METALS.* 1974: University of Denver.

205. Bergmann, O., G. Cowan, and A. Holtzman, *Experimental evidence of jet formation during explosion cladding.* AIME MET SOC TRANS, 1966. **236**(5): p. 646-653.

206. Carpenter, S., R. Wittman, and R. Carlson. *Relationships of explosive welding parameters to material properties and geometry factors*. in *Proc first int conf of the center for high energy forming, University of Denver*. 1967.

207. Groschopp, J., V. Heyne, and B. Hofmann, *Explosively clad titanium steel composite*. Welding International, 1987. **1**(9): p. 879-883.

208. Gurney, R.W., *The initial velocities of fragments from bombs, shell and grenades*. 1943, Army Ballistic Research Lab Aberdeen Proving Ground Md.

209. Kennedy, J., *EXPLOSIVE OUTPUT FOR DRIVING METAL*. 1972, Sandia Labs., Albuquerque, N. Mex.

210. Committee, A.I.H., *ASM Handbook, Vol. 6, Welding, brazing, and soldering*. ASM International, Materials Park, Ohio, 1997: p. 88.

211. Fabin, M. and T. Jarosz, *Improving ANFO: Effect of Additives and Ammonium Nitrate Morphology on Detonation Parameters*. Materials, 2021. **14**(19): p. 5745.

212. Acarer, M., B. Gülenç, and F. Findik, *Investigation of explosive welding parameters and their effects on microhardness and shear strength*. Materials & design, 2003. **24**(8): p. 659-664.

213. Chao, R., J. Yang, and S. Lay, *Interfacial toughness for the shipboard aluminum/steel structural transition joint*. Marine structures, 1997. **10**(5): p. 353-362.

214. SCHAEPER, T.J., *THE FRENCH COUNCIL OF COMMERCE, 1700-1715: AN ADMINISTRATIVE STUDY OF MERCANTILISM AFTER COLBERT*. 1977: The Ohio State University.

215. DEMİR, B., *AnInvestigationontheProductionofDual-PhaseSteelfromAISI4140 andItsImpactStrengthatDifferentMartensiteVolumeFractions*. 2007.

216. Bayram, A., A. Uğuz, and M. Ula, *Effects of microstructure and notches on the mechanical properties of dual-phase steels*. Materials characterization, 1999. **43**(4): p. 259-269.

217. Elitas, M., et al., *Finite element modelling of the fatigue damage in an explosive welded Al-dual-phase steel*. Materials Testing, 2023. **65**(5): p. 787-801.

218. Gram, M.D. and R. Wagoner, *Fineblanking of high strength steels: Control of material properties for tool life*. Journal of Materials Processing Technology, 2011. **211**(4): p. 717-728.

219. Wojtkowiak, D., K. Talaśka, and D. Wilczyński, *Evaluation of the belt punching process efficiency based on the resistance force of the compressed material*. The International Journal of Advanced Manufacturing Technology, 2020. **110**(3): p. 717-727.

220. Canales, C., P. Bussetta, and J.-P. Ponthot, *On the numerical simulation of sheet metal blanking process.* International Journal of Material Forming, 2017. **10**(1): p. 55-71.

221. Shi, C.-g., et al., *Detonation mechanism in double vertical explosive welding of stainless steel/steel.* Journal of Iron and Steel Research, International, 2015. **22**(10): p. 949-953.

222. Shi, C.-g., et al., *Lower limit law of welding windows for explosive welding of dissimilar metals.* Journal of Iron and Steel Research International, 2017. **24**(8): p. 852-857.

223. Fronczek, D., et al., *Growth kinetics of TiAl3 phase in annealed Al/Ti/Al explosively welded clads.* Materials Letters, 2017. **198**: p. 160-163.

224. Han, J.H., J.P. Ahn, and M.C. Shin, *Effect of interlayer thickness on shear deformation behavior of AA5083 aluminum alloy/SS41 steel plates manufactured by explosive welding.* Journal of Materials Science, 2003. **38**(1): p. 13-18.

225. Mudali, U.K., et al., *Corrosion and microstructural aspects of dissimilar joints of titanium and type 304L stainless steel.* Journal of Nuclear Materials, 2003. **321**(1): p. 40-48.

226. Manikandan, P., et al., *Control of energetic conditions by employing interlayer of different thickness for explosive welding of titanium/304 stainless steel.* Journal of materials processing technology, 2008. **195**(1-3): p. 232-240.

227. Carvalho, G., et al., *Formation of intermetallic structures at the interface of steel-to-aluminium explosive welds.* Materials Characterization, 2018. **142**: p. 432-442.

228. Bataev, I., et al., *High cooling rates and metastable phases at the interfaces of explosively welded materials.* Acta materialia, 2017. **135**: p. 277-289.

229. Basariya, M.I.R. and N.K. Mukhopadhyay, *Structural and mechanical behaviour of Al-Fe intermetallics.* Intermetallic compounds–formation and applications. Rijeka: IntechOpen, 2018: p. 97-122.

230. Gulenc, B., *Investigation of interface properties and weldability of aluminum and copper plates by explosive welding method.* Materials & Design, 2008. **29**(1): p. 275-278.

231. Raghukandan, K., K. Hokamoto, and P. Manikandan, *Optimization of process parameters in explosive cladding of mild steel and aluminum.* Metals and Materials International, 2004. **10**(2): p. 193-197.

232. Biro, E., et al., *Predicting transient softening in the sub-critical heat-affected zone of dual-phase and martensitic steel welds.* ISIJ international, 2013. **53**(1): p. 110-118.

233. Demir, B., M. Elitaş, and H. Karakuş, *Investigation of the tensile shear property of DP600 steel combined with resistance spot welding.* Pamukkale University Journal of Engineering Sciences. **1000**(1000): p. 0-0.

234. Xia, M., et al., *Effects of heat input and martensite on HAZ softening in laser welding of dual phase steels.* ISIJ international, 2008. **48**(6): p. 809-814.

235. Song, J., et al., *Hierarchical microstructure of explosive joints: Example of titanium to steel cladding.* Materials Science and Engineering: A, 2011. **528**(6): p. 2641-2647.

236. Ramazani, A., et al., *Transformation-induced, geometrically necessary, dislocation-based flow curve modeling of dual-phase steels: effect of grain size.* Metallurgical and Materials Transactions A, 2012. **43**(10): p. 3850-3869.

237. Demir, B., *An investigation on the production of dual-phase steel from AISI 4140 and its impact strength at different martensite volume fractions.* Metallofizika I Noveishie Tekhnologii, 2007. **29**(9): p. 1159-1166.

RESUME

Khalil Abubaker BELRAS ALI he lived in the city of Misrata and finished his university studies there, then he started a master's program at the University of Tripoli in machine design. he started working for the Engineering Technologies Company In 2004.

In 2014, he started working as a teaching member at the College of Industrial Technology.

In 2018 he moved to Karabük University, Technology Faculty, Department of Manufacturing Engineering to study Ph.D. program.